SURFACE INTERACTIONS OF Cs^{+} AND Co^{2+} WITH BENTONITE AND PERLITE

by

ÖMER ÖZSOY

B.S. in Chemistry, Bogazici University, 2004

Submitted to the Institute of Environmental Sciences in partial fulfillment of the requirements for the degree of

Master of Science

in

Environmental Sciences

Bogazici University

2014

Dedicated to my parents, wife and kids…

ACKNOWLEDGEMENTS

Firstly, I would like to express my sincere gratitude to my supervisor Prof. Dr. Miray BEKBÖLET, Institute of environmental Sciences, Bogazici University, for her patience, useful comments, remarks and engagement and immense knowledge through the learning process of this master thesis. She also provided me with many oppurtinities for valuable scientific and personal experiences.

I would also like to express my appreciation to the members of my thesis jury; Prof. Dr. Zekiye Çınar and Assoc. Prof. Dr. Burak DEMİREL for their valuable time and comment.

My sincere thanks also go to Dr. Seval BAYÜLKEN and Dr. Yusuf Ziya YILMAZ for her patience and support during working at laboratory and writing my thesis.

I am very grateful to Tamer YILDIZ and İlker ÖZDEMİR for SEM analysis, to Dr. Sevgi Akbal for BET analysis and to Dr. Asiye Başsarı for XRF analysis.

Last but not least, I would like to thank my parents, wife and kids for their never-ending support and love throughout my life.

SURFACE INTERACTIONS OF Cs^{+} AND Co^{2+} WITH BENTONITE AND PERLITE

During nuclear weapon tests, any accidents in the nuclear power plants or nuclear fuel cycle generating, considerable amounts of radioactive waste can release very hazardous radionuclides such as ^{137}Cs and ^{60}Co to the geosphere. Both ^{137}Cs and ^{60}Co have long half- lives as 30.2 and 5.27 years, respectively, and these radiotoxic elements can give hazards to biota or human being in the environment. The isolation of radiotoxic elements from environment is efficiently and low-costly achieved by the adsorption of these radionuclides onto the clay or oxide surfaces. In this study, bentonite and perlite was used as adsorbents for the removal of Cs^{+} and Co^{2+} from aqueous solution. In this concern, the adsorption behavior of Cs^{+} and Co^{2+} onto either bentonite or perlite as a function of pH, time, initial metal concentration, temperature, ionic strength and humic acid (HA) concentration was studied by batch adsorption technique.

The adsorption isotherm data were interpreted by Langmuir, Freundlich and Dubinin-Radushkevich (D-R) isotherm models. Bentonite attained maximum adsorption capacity for Cs^{+} as 83.3 mgg^{-1} and for Co^{2+} mgg^{-1} as 15.9 whereas perlite attained capacity values for Cs^{+} as 1.22 mgg^{-1} and for Co^{2+} as 1.83 mgg^{-1}. HA had little influence on adsorption capacity of bentonite for Cs^{+}, but it greatly affected the adsorption capacity of perlite for Cs^{+}. Furthermore, HA increased the adsorption capacity of bentonite for Co^{2+}, whereas it decreased adsorption capacity of perlite for Co^{2+}. Thermodynamic parameters, standard enthalpy (ΔH^{o}), standard entropy (ΔS^{o}) and standard free energy (ΔG^{o}), for the adsorption of Cs^{+} and Co^{2+} were determined at four different temperatures of 288 K, 298 K, 318 K and 338 K. All adsorption processes, except Cs^{+} adsorption onto bentonite, showed the endothermic nature with the positive ΔH^{o} values. The negative values of ΔG^{o} and the positive values of ΔS^{o} indicated the feasibility and spontaneous nature for all adsorption processes and more disordered form after adsorption.

Cs^{+} ve Co^{2+} NİN BENTONİT VE PERLİT İLE YÜZEY ETKİLEŞİMLERİ

Nükleer silah denemeleri, nükleer güç santrallerindeki herhangi kazalar veya yüksek miktarda radyoaktif atık üreten nükleer yakıt dönüşümleri yeryüzüne ^{137}Cs ve ^{60}Co gibi çok tehlikeli radyonüklitleri salabilir. Sırasıyla 30.2 ve 5.27 yıl gibi uzun yarı ömürlere sahip ^{137}Cs ve ^{60}Co, çevredeki insan ve biotaya zarar verebilir. Radiotoksik elementlerin çevreden izolasyonu bu elementlerin kil veya oksitlerin yüzeylerine adsorpsiyonu ile kolayca ve düşük maliyetle başarılabilir. Bu çalışmada bentonit ve perlit, Cs^{+} ve Co^{2+} nin sulu çözeltilerden uzaklaştırılmada adsorban olarak kullanıldı. Bu ilgi içinde, Cs^{+} ve Co^{2+} nin adsorpsiyon davranışlarının pH, zaman, sıcaklık, iyonik kuvvet ve humik asit konsantrasyonuna göre değişimleri kesikli adsorpsiyon yöntemi ile incelendi. Adsorpsiyon izoterm dataları Langmuir, Freundlich ve Dubinin-Radushkevich (D-R) izoterm modelleri ile izah edildi. Bentonit maksimum adsorpsiyon kapasitesi olarak Cs^{+} için 83.3 mgg^{-1} ve Co^{2+} için 15.9' a ulaşırken, perlit daha düşük maksimum adsorpsiyon kapasitesine, Cs^{+} için 1.22 mgg^{-1} ve Co^{2+} için 1.83' e ulaştı. HA' in bentonitin Cs^{+} için adsorpsiyon kapasitesinin üzerinde düşük etkiye sahiptir, fakat o perlitin Cs^{+} için adsorpsiyon kapasitesini fazlaca etkiledi. Ayrıca, HA bentonitin Co^{2+} için adsorpsiyon kapasitesini yükseltirken, perlitin Co^{2+} için adsorpsiyon kapasitesini düşürdü. Cs^{+} ve Co^{2+} nin adsorpsiyonlarının termodinamik parametreleri (standart entalpi (ΔH^{o}), standart entropi (ΔS^{o}) ve standart serbest enerji (ΔG^{o})) dört farklı sıcaklık değeri için (288 K, 298 K, 318 K and 338 K) belirlendi. Cs^{+} nın bentonite üzerine adsorpsiyonu haricinde bütün adsorpsiyon prosesleri endotermik yapı gösterdi. Bütün adsorpsiyon proseslerinde ΔG^{o} değerleri negative iken ΔS^{o} değerleri positiftir ki, bu durum adsorpsiyon proseslerinin olabilirliliğini, kendiliğinden gerçekleşme doğasını ve adsorpsiyondan sonra daha düzensiz forma girdiğini gösterdi.

TABLE OF CONTENTS

LIST OF FIGURES

LIST OF TABLES

LIST OF SYMBOLS/ABBREVATIONS

Symbol	Explanation	Unit used
AES	Atomic Emission Spectroscopy	
CEC	Cation Exchange Capacity	
C_e	Equilibrium Concentration of Adsorbate	mgL^{-1}
C_i	Initial Concentration of Adsorbate	mgL^{-1}
C_s	Amount of Adsorbate Adsorbed on Adsorbent	mgL^{-1}
D-R	Dubinin-Radushkevich Isotherm Model	
E	Mean Free Energy	$kJmol^{-1}$
EP	Expanded Perlite	
HA	Humic Acid	
HLW	High Level Waste	
IAEA	International Atomic Energy Agency	
ICP-OES	Inductively Coupled Plasma-Optical Emission Spectroscopy	
K	Kelvin	
Ka	Langmuir Adsorption Constant	
K_d	Distribution Coefficient	
K_F	Freundlich Adsorption Capacity Constant	Lg^{-1}
LILW	Low and Intermediate Level Waste	
NOM	Natural Organic Matter	
1/n	Freundlich Adsorption Intensity Constant	
q_A	Adsorbed Amount per Unit Weight of Adsorbent	mgg^{-1}
q_{max}	Maximum Adsorption Capacity	mgg^{-1}
R	Ideal Gase Constant	$Jmol^{-1}K^{-1}$
R^2	Regression Coefficient	
SEM	Scanning Electron Micrograph	
WDXRF	Wavelength Dispersive X-Ray Fluorescence	
β	Activity Coefficient Related with Adsorption Energy	mol^2kJ^{-2}
ΔH_{hyd}	Hydration Enthalpy	
ΔH_{int}	Intrinsic Enthalpy Change	
ΔH^o	Standard Enthalpy	

ΔG^o	Standard Gibs's Free Energy
ΔS^o	Standard Entropy
ε	Polanyi Potential

1. INTRODUCTION

Environmental pollution arising from released radionuclides from nuclear weapon tests or from the accidents of nuclear power plants and from toxic heavy metal caused by the effluents of a wide range of industrial applications has obviously great importance in terms of protection of public health. Removal of pollutants, especially radionuclide ones, from the natural or potable water sources has been achieved by traditional methods such as solvent extraction, chemical precipitation, reverse osmosis, ion-exchange and adsorption etc (Ozeroglu et al., 2011). Ion exchange and adsorption mechanism generally proceed with together when an adsorbent is used for removal of toxic or radioactive metals from aqueous solutions (Kraepiel, 1999; Metwally et al., 2007).

During nuclear weapon tests, any accidents in the nuclear power plants or nuclear fuel cycle generating considerable amounts of radioactive waste can release very hazardous radionuclides such as ^{137}Cs, ^{134}Cs, ^{131}I, ^{60}Co, $^{239+240}Pu$ and ^{90}Sr etc. to the geosphere. Both ^{137}Cs and ^{60}Co have long half- life, 30.2 and 5.27 years, respectively, and they can affect the contaminated area for long years and give hazards to biota or human being in the environment (Khan, 2003). For the protection of environment, nuclear waste could be disposed of geological repository in which clay minerals have been proposed as suitable backfilling materials because of their ability in retarding or delaying the migration of radionuclide to the biosphere (Yıldız, 2007).

Nuclear energy recently gains more interest in Turkish energy market. Turkish energy policy- makers have decided to get nuclear power plants construct in Akkuyu, Mersin and Sinop until 2023. Therefore, adsorption of radiotoxic metals derived from nuclear waste of nuclear power plant or by-products of recycling of spent nuclear fuel onto natural adsorbents (e.g. bentonite and perlite) received wide attention among Turkish researchers in the past decades (Kubilay et al., 2007; Bayulken et al., 2011; Alkan and Dogan, 2001; Talip et al., 2009). Bentonite and perlite were selected as adsorbents because Turkey has large bentonite and perlite reserves and their cost is quite low in Turkish market. In spite of lots of studies related with metal adsorption onto bentonite or perlite in the worldwide, there is still a need for investigation of Turkish bentonite or

perlite because adsorption characteristics of bentonite and perlite may change according to their mining places. (Galambos et al., 2010). Co^{2+} and Cs^{+} were selected as adsorbates because $^{137}Cs^{+}$ and ^{60}Co are among the most common radiotoxic metals emitted from an accident of a nuclear power plant or leaked from liquid nuclear waste to the aqueous or terrestrial environment (Lima et al., 1998; Yu et al., 2006).

Adsorption characteristics of Cs^{+} and Co^{2+} on natural bentonite and expanded perlite extracted from Turkish mines should be investigated due to proposing a sufficient backfill material for using in a multibarrier engineered geological repository and revealing potential usage as decontaminant material for wastewater or liquid radiowaste. The effect of pH, initial metal concentration, time, temperature and ionic strength on the adsorption of ions onto bentonite and perlite has been investigated. Cesium and cobalt were selected in their stable form, ^{133}Cs and ^{59}Co, as chloride salt solution because they have the same chemical properties with their active form, i.e. ^{137}Cs and ^{60}Co. The equilibrium data was interpreted in terms of Langmuir, Freundlich and Dubinin-Radushkevich adsorption isotherm models. Moreover, thermodynamic parameters of the adsorption processes were calculated.

Considering the natural environmental systems, the role of natural organic matter (NOM) should also be investigated. Therefore, humic acid was used as the model compound of NOM and its role effect on the adsorption of selected metals onto selected adsorbents.

2. THEORETICAL BACKGROUND

2.1. Management of Radioactive Waste

Radioactive materials are extensively used in industrial, medical, agricultural and environmental applications and in research activities. During the production and use of these materials, radioactive waste will inevitably arise. Because of the wide variety of nuclear applications, the amounts, types and even physical forms of radioactive wastes vary considerably. Some wastes can remain radioactive for hundreds or thousands of years, while others may require storage for only a short decay period prior to conventional disposal.

International Atomic Energy Agency (IAEA) classifies the radioactive waste into three principal classes that include exempt waste, low and intermediate level waste, and high level waste (IAEA, 1994).

Exempt Waste: It means that the waste has very low level radioactive material such that the waste can be excluded from the nuclear regulatory control because of negligible hazards.

Low and Intermediate Level Waste: (LILW) contains enough radioactive material that it requires actions to ensure the protection of workers and the public for short or extended periods of time. LILW is generated from operation and maintenance of nuclear reactors, mining and milling of nuclear fuel, and recycling the spent nuclear fuel. In general, such radioactive waste contains a variety of radionuclides that are fission byproducts generated from above process (Singh et al., 2008). Among the byproducts, Co^{2+}, Sr^{2+} and Cs^{+} are considered as the most dangerous radionuclides to human health due to their high transferability, high solubility, long half-lives and easy assimilation in living organisms (Ma et al., 2011).

Treatment of liquid LILW is needed to concentrate the radionuclides to decrease its volume and convert the liquid form to more stable solid form (Chen and Wang, 2012). Several technologies such as chemical precipitation, conventional coagulation, reverse osmosis, ion exchange and adsorption have been developed for the removal of radionuclides present in the liquid radioactive waste (Corami et al., 2008).

Furthermore, the adsorption of radionuclides on clay minerals is widely accepted to be an important process for the treatment of liquid LILW because the natural availability of clays in large quantities that causes low cost, their relatively good adsorption properties, their low permeability and their stability compared to organic adsorbents make the clays very useful in controlling radionuclides concentrations in liquid LILW (Omar et al., 2009). Bentonite, kaolinite and sepiolite are the main clays in Turkey with fairly large reserves (Kubilay et al., 2007). Some scientists studied the radioactive metal adsorption characteristics of these clays for determining the possible use as decontaminant for liquid nuclear waste and as backfill material in multiple engineering barrier system in deep geological repository (Kubilay et al., 2007; Bayulken et al., 2011; Shahwan et al., 2006).

High Level Waste: High-level waste (HLW) arises from the 'burning' of uranium fuel in a nuclear reactor. HLW contains the fission products and transuranic elements generated in the reactor core. The fission of uranium and plutonium in a nuclear reactor produces numerous fission products having varying half-lives. Their percentage yield depends on the mode of fission under specific nuclear reactor conditions. As the process of fission continues, more and more fission products are produced and accumulated. After some time, the fission efficiency of the nuclear fuel becomes low and requires reprocessing, because of the accumulation of fission products. The spent fuel is processed generally by using solvent extraction procedures to separate the unused fuels from the fission products, radionuclides formed through nuclear reactions and their decay products. The chemical processing of burnt up nuclear fuel yields wastewater effluents containing various radionuclides (Khan, 2003).

HLW has both long-lived and short-lived components, depending on the length of time it will take for the radioactivity of particular radionuclides to decrease to levels that are considered no longer hazardous for people and the surrounding environment. If

generally short-lived fission products can be separated from long-lived actinides, this distinction becomes important in management and disposal of HLW.

To isolate radioactive wastes from the environment effectively, a repository facility based on the multibarrier concept is applied. The multibarrier concept involves placing the radioactive wastes into canisters, which are further surrounded by barrier layers including buffer or backfill materials (clays), cement or concrete and isolating geological substances. Should nuclides leach out, they are expected to be retarded by these sorbents, and as a result the possibility of radioactive contamination of the environment can be greatly reduced (Wang et al., 2011).

It is vital to select proper backfill and barrier material and to engineer them in the most appropriate manner to backfill, seal and cover the disposal facilities. The selection of proper backfill materials for the nuclear waste disposal repository has been derived from a much data on adsorption behavior of radionuclides on several natural clays or synthetic materials. Due to their ion exchange capacities, low permeability and swelling capacities clay minerals and some synthetic materials are candidate backfill materials for radioactive waste repository located in a variety of geological environment (Ibrahim et al., 2008).

The study of adsorption behavior of candidate of backfill material or buffer is an inseparable step for creating a migration model for radionuclides in deep geological repository. The model preparation of potential sites suited for a deep repository includes the study of interaction between the host environment and engineering barrier. The possible changes of host rock and engineering barriers caused by the expected geochemical processes as well as mineralogical composition of geological barriers should be studied (Galambos et al., 2010).

Another significant area studied while planning a repository is stability and adsorption properties of potential backfill materials. There are various factors occurring in the area of deposited HLW in deep geological conditions. The radiation, temperature, microbial stability, pH of environment, influence of competitive ions and presence of complex forming natural and synthetic organic chelating agents can be cited as several factors (Galambos et al., 2010).

In conclusion, the main objective in managing and disposing of several types of radioactive waste is to protect people and the environment. Management of radioactive waste means isolating or diluting the waste so that the rate or concentration of any radionuclides returned to the biosphere is harmless.

2.2. Adsorption

Sposito (2004) defines the adsorption as a process through which a chemical substance accumulates at the common boundary of two contiguous phases. If one of the contiguous phases involved is solid and the other fluid, the solid phase is termed the adsorbent and the matter which accumulates at its surface is an adsorbate. The interaction between adsorbate and the surface of the adsorbent could be specific or nonspecific. While chemical adsorption and inner-sphere surface complex forming are the examples of specific interaction, outer-sphere surface complex forming and physical adsorption are the examples of nonspecific interaction.

In the physical adsorption, there are weak forces of attraction or vander Waals' forces between molecules and it is reversible. It is predominant at low temperature, and is characterized by a relatively low energy of adsorption while adsorbed molecule is free to move about over the adsorbent surface. In the chemical adsorption, adsorbed molecules form a layer on the surface. There are much stronger forces between the molecules, so it is rarely reversible. Hence, in order to remove the adsorbed materials, the adsorbent must be heated to higher temperatures.

Adsorption is directly related with surface area of the adsorbent, pore size distribution, as well as the characteristic of the adsorbed molecules. Higher surface area of adsorbent generally provides with higher potential sites for adsorption. Diffusion coefficients decrease as molecular size of adsorbate increases and thus longer times is required to remove large molecules size of adsorbate than are needed for the low molecular size of adsorbate. Moreover, adsorbent particle size is also important because it affects the time needed for the transport within the pore to available adsorption sites (Snoeyink and Summers, 1999).

There are other factors that affect the adsorption like pH and temperature. Generally many organics form negative ions at high pH, positive ions at low pH, and neutral species in intermediate pH ranges. Adsorption normally increases at pH ranges where the species is neutral in charge (Suphandag, 2006**)**. Moreover, pH affects the charge on the surface of the adsorbent altering the ability to adsorb materials. For instance, metal adsorption onto oxides or clays is governed by pH change in two types. In one type, pH decrease cause the metal oxide or clay surface more positive and thus electrostatic repulsion between metal cation and the surface increases hindering adsorption. In other type, pH increase makes the surface of metal oxide or clay more negative and electrostatic attraction occurs between metal cation and the surface improving the adsorption. But, when pH increase continues towards higher pH value that may cause the change the species of the metal cation to the anionic complex form, negative surface of adsorbent and negative species of the metal at high pH repel each other by decreasing adsorption. As for explanation of temperature effect on the adsorption, adsorption reactions normally occur as exothermic therefore the extent of adsorption generally increases with decreasing temperature.

The adsorption of the metal ions onto clay or metal oxides can also be influenced by other ion species in aqueous environment. Many scientists have studied the effect of ionic strength of a solution upon adsorption of metal ions on several types of adsorbents (Yu et al., 2006; Xu et al., 2008; Alkan and Doğan, 2001). Competitive interactions between ions from adsorbate and background electrolyte can be resulted from addition of background electrolytes. Ionic strength effects on metal adsorption may occur by changing adsorbate activity or diffuse electrical double layer thickness. These effects depend on the concentration, composition, and charge of the ionic species in solution (Fike, 2001).

Olu-Owulabi and colleagues studied the effects of type of background electrolyte and change of concentration of background electrolyte on the adsorption of Cu^{2+} and Cd^{2+} on the bentonite. It was stated that using $NaNO_3$ as electrolytes gives higher result for adsorption efficiency than using KNO_3 as electrolyte. Furthermore, ionic strength of the electrolyte solution was changed by changing the concentration of $NaNO_3$ and adsorption capacity of bentonite increased for both ions when decreasing $NaNO_3$ concentration. It was suggested that strong ionic strength dependence indicates that outher sphere complexes are formed on the surface of the bentonite (Olu-Owulabi et al., 2010).

Surface complexation models have been utilized to obtain information about the nature of metal complexes adsorbed at solid surfaces (Fike, 2001). Surface complexes forming during adsorption can be classified as outer-sphere surface complexes and inner-sphere surface complexes which were introduced by Sposito (1981). Sposito (2004) describes that outer sphere surface complex has at least one water molecule interposed between the adsorbate species and the adsorbent site to which it is bound to form an adsorption complex. Thus, an outer-sphere surface complex contains a solvated adsorbate species.

Figure 2.1 depicts the structure of the outer-sphere surface complex formed between Na^+ and a surface site on the basal plane of the clay mineral, montmorillonite. The Na^+ ions that are the balancing ions for the negative structural charge developed as a result of isomorphic substitutions within the clay mineral layer tend to adsorb as solvated species on the basal plane. This mode of adsorption occurs as a result of the strong solvating characteristics of Na^+ and the physical impediment to direct contact between Na^+ and the site of negative charge posed by the layer structure itself.

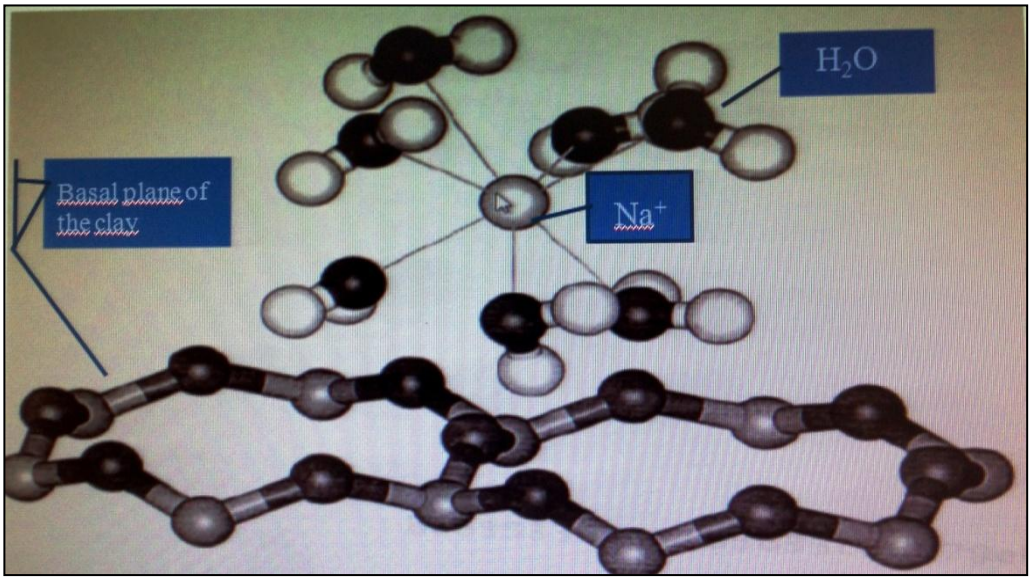

Figure 2.1.The illustration of outer surface complex formation between Na^+ and surface site in montmorillionite. The salvation shell comprises seven water molecules coordinated to Na^+(Sposito, 2004).

An inner-sphere surface complex, by contrast, has no water molecule interposed between the adsorbate species and the adsorbent site that binds it. Therefore, the formation of the complex involves a desolvated adsorbate species although the latter may be partially solvated by water molecules that do not intervene in the bond to the adsorbent site.

Figure 2.2 illustrates an inner sphere complex between Cd^{2+} and a hydroxylated surface site on the plane in goethite. This plane features reactive OH groups bound to just a single Fe^{3+}, which allows them to protonate. Adsorbed Cd^{2+} can bind to a pair of OH groups after their protons are dissociated, thereby linking them to corners of two adjacent $FeO_3(OH)_3$ octahedra in the mineral structure.

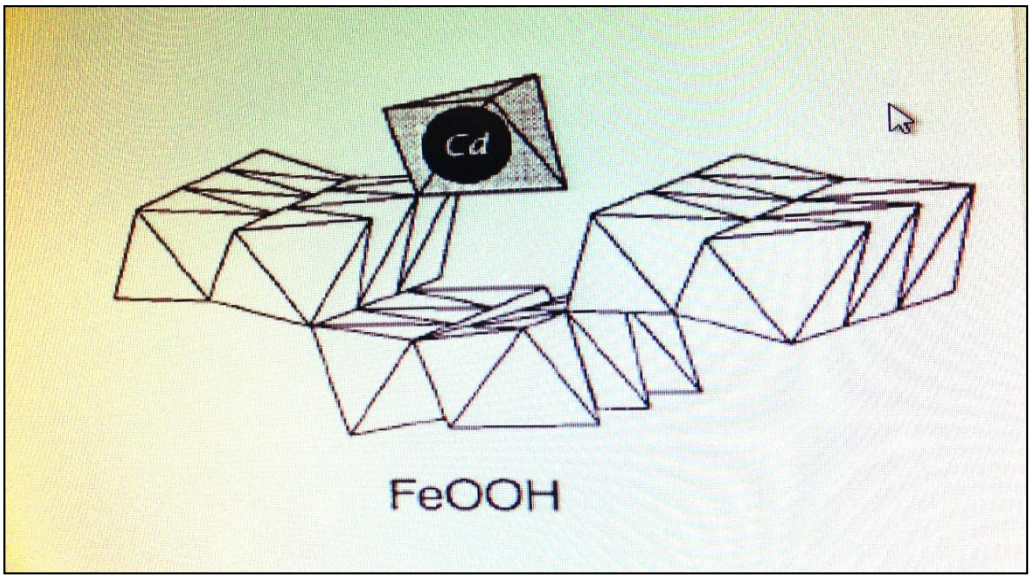

Figure 2.2. An example of inner surface complex formed between Cd^{2+} and a pair of ionized surface OH groups in the plane in goethite. The cation is coordinated to six oxygen atoms, two of which are on the goethite surface in neighboring $FeO_3(OH)_3$ octahedra (Sposito, 2004).

Changes in metal adsorption as a function of ionic strength could serve as a method to distinguish between inner and outer sphere complexes (Fike, 2001). Using the Triple Layer Model in which the model specifically focus on potential and surface conductivity in evaluating electrokinetic properties of clay-water interface (Leroy and Revil, 2004), Pb^{2+} and Cd^{2+} adsorption were tested against ionic strength at the goethite- water interface

(Hayes and Leckie, 1987). Their research indicated that Pb^{2+} and Cd^{2+} adsorption were relatively unaffected by changing ionic strength and thus this observation showed that Pb^{2+} and Cd^{2+} adsorption as a function of ionic strength were best modeled as inner sphere surface reaction.

Bostick and coworkers studied cesium adsorption on the clays. On the basis of the influence of Cs^{+} loadings and exchangeability on the structural arrangement, either outher sphere or inner sphere complexes could be recognized. The shorter Cs-O bond distance belongs to outer sphere complexes typical of hydrated ions. In inner sphere complexes partially or fully dehydrated cesium coordinates directly to siloxane groups of clay minerals forming longer Cs-O bonds. It was also claimed that the inner sphere adsorption complexes may have occurred within interlayer or at frayed edge sites and were less extractable than outer sphere adsorption complexes (Bostick et al., 2002).

2.2.1. Adsorption Isotherms

The constant-temperature equilibrium relationship between the quantity of adsorbate per unit of adsorbent q_A and its equilibrium solution concentration C_e is called the adsorption isotherm. Adsorption isotherms relate the adsorbate or solute concentration in the bulk liquid to the concentration of the adsorbent on the solid phase at equilibrium.

Adsorption isotherms can be termed their shapes resembling the letters, such as “L” type, “S” type, “C” type, etc. and they are characterized to their initial slope. (Giles et al., 1960). The four main classes, which are shown in Figure 2.1, are briefly described in Sposito (2004).

The S-curve isotherm is characterized by initially small slope that increases with adsorptive concentration. This indicates that the affinity of the adsorbent for the adsorbate is less than that of the aqueous solution. It may also suggest the presence of cooperative interactions such that increasing surface coverage increases the solute's affinity for the surface. The S-curve isotherm is the result of cooperative interactions among the adsorbed molecules. These interactions cause the adsorbate to become stabilized on a solid surface

and, thus produce an enhanced affinity of the surface for the adsorbate as its concentration increases.

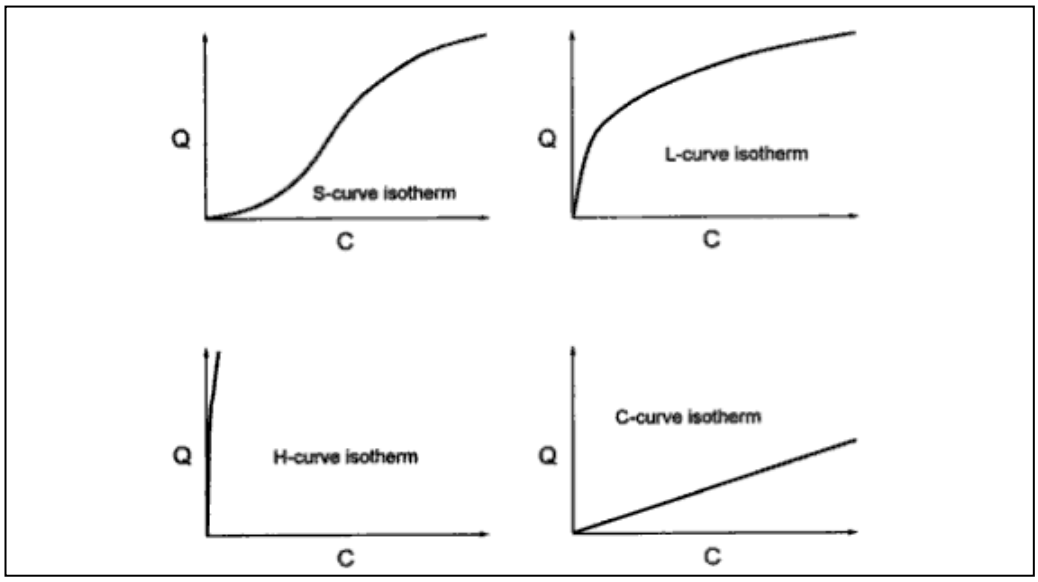

Figure 2.3. Four different shapes of adsorption isotherm (Sposito, 2004).

L curve isotherm which typically concave to the concentration axis, is generally characterized by an initial slope that does not increase with the concentration of adsorbate in the solution. This type of isotherm is the resultant effect of a high relative affinity of the adsorbent particles for the adsorbate at low concentration. In addition, as the concentration of the adsorbate increases, the amount of the remaining adsorbing surface is decreased.

The C-curve isotherm shows an initial slope that remains independent of adsorptive concentration until the maximum possible adsorption is achieved. This type of isotherm is produced either by a constant partitioning of a substance between the interfacial region and the soil solution or by a proportionate increase in the amount of adsorbing surface as the concentration of an adsorbate increases.

The H-curve isotherm is an extreme version of the L-curve isotherm. It is characterized by a large initial slope suggesting a very high relative affinity of the adsorbent for an adsorbate which is caused either by very specific interactions between the solid phases and the adsorbate (inner-sphere surface complexation) or by significant van

der Waals interactions in the adsorption process. It is illustrate that the observed H-curve isotherm is the result of specific adsorption. Large organic molecules and inorganic polymers (e.g., aluminum hydroxyl polymers) provide examples of H-curve isotherms resulting from van der Waals interactions.

In addition to shape-based classification of adsorption isotherm, mathematical relations or models have been widely used to describe adsorption isotherms. Some of them are given below.

Adsorption on a homogeneous surface can easily be modeled by means of Langmuir equation given as at the following;

$$q_A = q_{max}K_aC_e/1+K_aC_e \quad (2.1)$$

where q_A is the adsorbed amount of adsorbate per unit weight of adsorbent at equilibrium, q_{max} is the maximum capacity of the adsorbent for adsorbed ion, K_a represents an empirical constant, which is called as the binding constant. The equation can be linearized by;

$$1/q_A = 1/q_{max} + 1/q_{max}K_aC_e \quad (2.2)$$

The linear plot of the $1/q_A$ as a function of $1/C_e$ would yield the slope as $1/q_{max}$ K_a and the intercept is $1/q_{max}$. The reciprocal of the intercept is q_{max} and the intercept to slope ratio is equal to K_a.

The Freundlich equation of adsorption on heterogeneous surface is given by;

$$q_A = K_F C_e^{1/n} \quad (2.3)$$

where q_A and C_e have the same meanings as in the Langmuir equation and K_F and 1/n are Freundlich parameters. 1/n is unitless and indicates the strength of adsorption while K_F is primarily related with adsorption capacity. The equation can be linearized by taking logarithmic function of right and left side as the following;

$$\log q_A = \log K_F + 1/n \log C_e \quad (2.4)$$

The linear plot of the $\log q_A$ against $\log C_e$ would give the slope as 1/n and intercept as $\log K_F$.

Dubinin-Radushkevic (D-R) isotherm is generally applied at low concentration and can be utilized to describe the adsorption on both heterogeneous and homogeneous surfaces (Shahwan and Erten, 2004). The equation for the D-R isotherm model is given by;

$$q_A = q_{max} e^{-\beta \varepsilon 2} \quad (2.5)$$

or in the linear form ;

$$\ln q_A = \ln q_{max} - \beta \varepsilon^2 \quad (2.6)$$

where β is the activity coefficient related to mean adsorption energy (mol^2kJ^{-2}) and ε is the Polanyi potential which equals to

$$\varepsilon = RT\ln(1+1/Ce) \quad (2.7)$$

where R is the ideal gas constant (8.3145 $Jmol^{-1}K^{-1}$) and T is the absolute temperature in Kelvin (K). q_A and C_e have the same meanings as in the Langmuir model, but q_{max} has little difference from that in the Langmuir model because it represents the total specific micropore volume of the adsorbent. The value of β is related to the adsorption free energy, E ($kJmol^{-1}$), which is defined as the free energy change required to transfer 1 mol of ions from solution to the solid surfaces (Aksoyoglu, 1989). The relation is as the following;

$$E = 1/\beta^{1/2} \quad (2.8)$$

The magnitude of E is useful for estimating the mechanism of the adsorption reaction. If E is in the range of 8-16 $kJmol^{-1}$, adsorption is governed by chemical ion exchange. In the case of E is below 8 $kJmol^{-1}$, physical forces may affect the adsorption.

On the other hand, adsorption may be dominated by particle diffusion if E is higher than 16 $kJmol^{-1}$ (Donat et al., 2005; Özcan et al., 2006).

Adsorption efficiency which is the percentage of the adsorption can be also used to evaluate the equilibrium data obtained from batch adsorption experiments.

$$\text{Efficiency} = C_s/C_i*100 \quad (2.9)$$

Here, C_i is the initial concentration of the material adsorbate, and C_s is the concentration of the adsorbed material on the adsorbent.

2.2.2. Thermodynamic Parameters

Adsorption studies of metal ions have been conducted to calculate the distribution coefficient, K_d, which is regarded as a standard parameter in the assessment of the physicochemical behavior of metal ions between solid and liquid phases. It is calculated by the following equation (Xu et al., 2008).

$$K_d = (C_i-C_e)/C_e*(V/m) \quad (2.10)$$

where C_i is the initial concentration of the adsorbate, C_e is the concentration of the adsorbate at equilibrium, V is the volume of the solution and m is the mass of the adsorbent.

The distribution coefficient can be related with Gibbs free energy, ΔG, as

$$\Delta G = \Delta G^o + RTlnK_d \quad (2.11)$$

where ΔG^o is the standard Gibbs free energy change, R is the ideal gas constant (8.3145 $Jmol^{-1}K^{-1}$), and T is the absolute temperature. At the equilibrium the equation transforms to

$$\Delta G^o = -RTlnK_d \quad (2.12)$$

Gibbs free energy change can also be written in terms of enthalpy change, ΔH^o, and the entropy change, ΔS^o, as given below

$$\Delta G^o = \Delta H^o - T\Delta S^o \quad (2.13)$$

Combining equation 2.12 and 2.13 the expression below is obtained

$$\ln K_d = (\Delta S^o/R)-(\Delta H^o/RT) \quad (2.14)$$

It is possible to determine the value of ΔH^o of adsorption process from the slope and ΔS^o of the adsorption from the intercept of the linear fits obtained by plotting lnKd against 1/T.

2.3. Adsorbents

Bentonite and perlite were previously studied as adsorbent during various metal adsorption experiments by some researchers in order to elucidate the potential usage as decontaminant or backfill material (Galambos et al., 2010; Khan, 2003; Yu et al., 2006; Xu et al., 2008; Mostaedi et al., 2010; Ghassabzadeh et al., 2010). Turkey has large reserves for bentonite and perlite. The 75 % and 20 % of worldwide known reserves of perlite and bentonite respectively are in Turkey (Tubitak, 2009). Therefore, the cost of bentonite and perlite as adsorbent can be evaluated as very low in Turkish market. Furthermore, to become readily available and environmental friendly urged some scientists to work on bentonite and perlite to reveal their potential usage as adsorbent during metal adsorption experiments in Turkey (Kubilay et al., 2007; Bayulken et al., 2011; Alkan and Dogan, 2001; Talip et al., 2009). The adsorption characteristics of the perlite or bentonite may differ with respect to the place of mine (Galambos et al., 2010).

2.3.2. Bentonite

Bentonite forms mainly from the alteration of volcanoclastic or glassy rocks and is composed of primarily montmorillonite from the smectite group. Bentonite may be formed as deposit any of the following three mechanisms (Christidis and Huff, 2009)

Diagenetic alteration of volcanic glass in aqueous environment
Hydrothermal alteration of volcanic glass
Formation of smectite-rich sediments in salt lakes and sabkha environments.

Bentonite is a clay mineral particle with two silica tetrahedral sheets and one aluminum octahedral sheet and has a dominant element attached to tetrahedral sheet (Figure 2.4). Bentonite is named with respect to that element. Two basic types of bentonite are Ca-bentonite and Na-bentonite. Bentonite has permanent negative charge on the basal plane and pH-dependent charge on the edge surfaces (Chang and Sposito, 1996). Its permanent negative charge is resulted from the isomorphous substitution of Al^{3+} for Si^{4+} in the tetrahedral layer and Mg^{2+} for Al^{3+} in the octahedral layer. This charge imbalance is offset by exchangeable cations, such as Ca^{2+} and Na^{+} at the bentonite surface (Doulia et al., 2009).

In aqueous medium, bentonite absorbs large amount of water and swells. Water molecules interact with dominant cations at the bentonite and removes them from the basal surface of the bentonite by leaving the surface negative (Figure 2.4). The negatively charged surface may adsorb the low-level metal cations. Ca-bentonite, which has Ca^{2+} as the dominant exchangeable cation, is characterized by its low water absorption and swelling capabilities and its inability to stay suspended in water. Na-bentonite is characterized by its ability to absorb large amounts of water and form viscous suspensions. In addition, Na-bentonite has higher cation exchange capacity, better swelling property, and larger specific surface area than Ca-bentonite (Doulia et al., 2009).

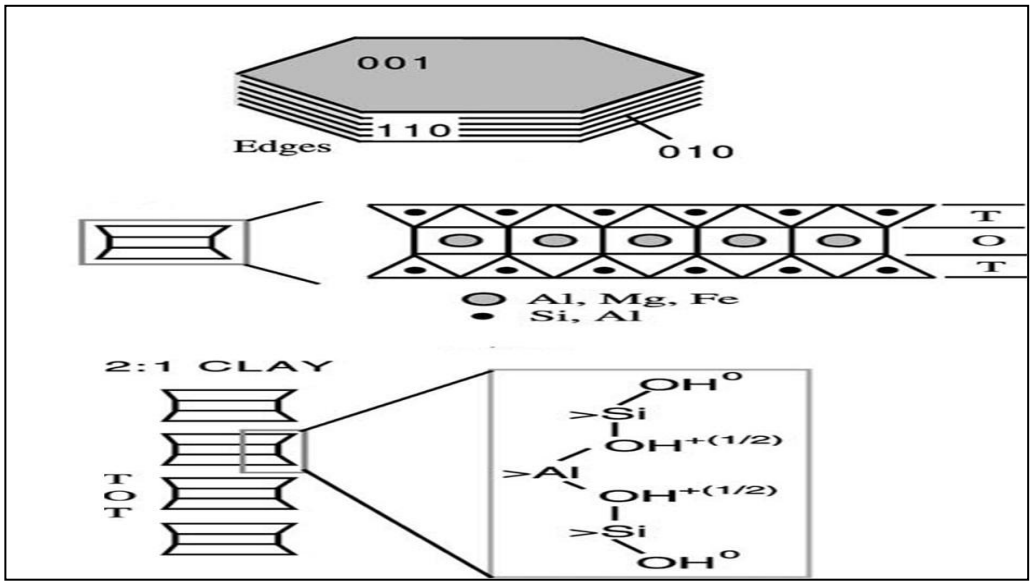

Figure 2.4. The active surface sites of bentonite (T: Tetrahedral sheet, O: Octahedral sheet) (Leroy and Revil, 2004).

As a result of the above explanations, it can be stated that Na-bentonite is more convenient for metal adsorption than Ca bentonite, but worldwide bentonite reserve is 2.5 billion tons, more than 80 % of which is Ca-bentonite. Therefore, conversion of Ca-bentonite to Na-bentonite is of vital significance in terms of adsorption applications on the treatment of wastewater or nuclear wastewater effluents.

The isolation of radiotoxic elements from environment is efficiently achieved by the help of the system of multiple engineering and natural sealing barriers in a deep repository. An important segment in a multibarrier system is clay rocks, of which bentonite seems to be the most suitable clay material because of its properties that determine their use in a multibarrier system of deep geological repository. These properties can be cited as low permeability, high swelling capacity, adsorption and retardation ability of fission products such as ^{137}Cs, ^{90}Sr, ^{241}Am known their high migration ability, heat conductivity and long term stability in barrier system (Galambos et al., 2010).

The property of swelling makes Na-bentonite useful as a sealant, especially for the sealing of subsurface disposal systems for spent nuclear fuel and for quarantining metal pollutants of groundwater. Similar uses include making slurry walls, waterproofing of

below-grade walls, and forming other impermeable barriers, for example, to seal off the annulus of a water well, to plug old wells, or to line the base of landfills to prevent migration of leachate.

2.3.2. Perlite

Perlite is a naturally occurring amorphous volcanic glassy rock. It has high amount of water trapped at inner structure. When it is rapidly heated to 800 -1100 ^{o}C, it expands to 8-20 times its orginal volumes due to vaporization of trapped water. The processed perlite is called expanded perlite (EP). Raw perlite has a density around 1.1 gcm^{-3}, while EP has a bulk density of about 0.03 gcm^{-3}. The heating process changes not only density but also structure from amorphous to crystalline, and color from black to white (Figure 2.5).

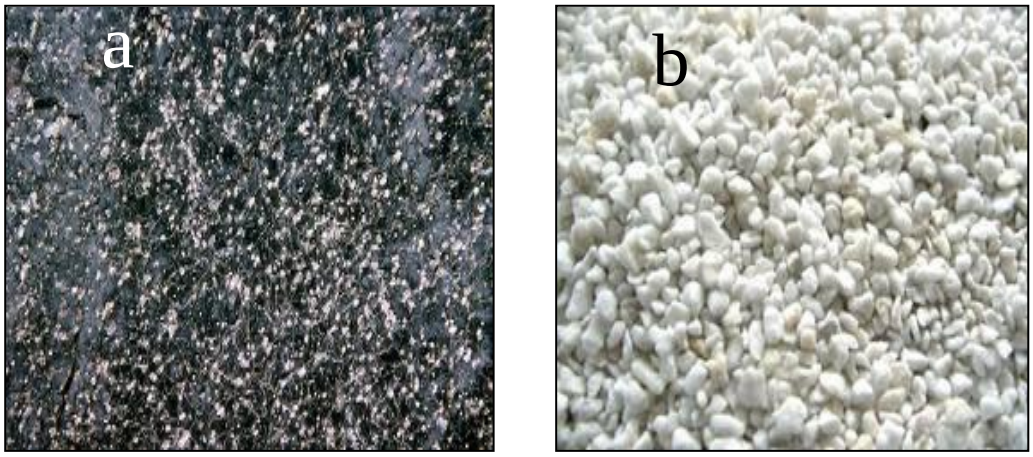

Figure 0.5.Thermal treatment changes the color of raw perlite from black (a) to white (b).

In addition, both cation exchange capacity (CEC) and specific surface area of raw perlite increase in pretty much amount by thermal treatment. EP becomes industrial mineral and a commercial product useful for its light weight and adsorption properties after processing. In the surface hydroxyl groups, the silicon atoms at the surface tend to maintain their tetrahedral coordination with oxygen. They complete their coordination at room temperature by attachment to monovalent hydroxyl groups, forming silanol groups. The different types of silanol groups and aluminas' hydrous oxide surface groups in expanded perlite are shown in Figure 2.6 (Dogan et al., 2000).

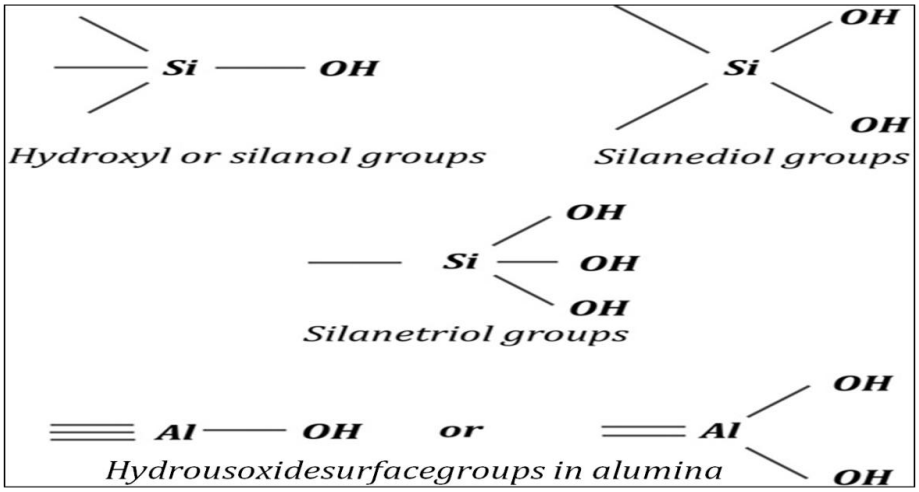

Figure 0.6. Types of the silanol groups and hydrous oxide surface groups in alumina (Talip et al., 2009).

Doğan and co-workers studied the electrokinetic properties of the natural perlite and expanded perlite. Both perlite samples yields no isoelectric point in the pH range of 3 to 11 and both perlite samples remained negative at the same pH range (Doğan et al., 1997). Furthermore, it was stated that expanded perlite has a more negatively charged surface than unexpanded perlite, presumably due to increasing the broken edges during the heating to produce the expanded perlite.

There is extensive worldwide production and consumption of perlite. The leading countries producing perlite include United States, China, Greece, Japan, Hungary, Armenia, Italy, Mexico, Philippines, and Turkey. About the 70 % of the world's known perlite reserve are present along the Aegean Coast of Turkey (Dogan et al., 2000). Perlite is very economic and easily available mineral for Turkish market. High cation exchange capacity, large specific surface area, and silanol and aluminol groups on the surface, furthermore quite economic and becoming chemically inert give impressive adsorption property to the expanded perlite. Therefore, EP may be used as low-cost adsorbent during treatment of industrial and nuclear wastewater.

During the last decades, research interest was directed to the use of perlite as an efficient adsorbent. Selected literature findings (2010-) are compiled and presented in below given Table 2.1. Perlite was used as adsorbent in native form, modified form and as

a modified nanomaterial. In addition to the cationic native elements, radioactive elements are also used as adsorbates. Moreover, selected organic substrates are also presented.

Table 2.1. Use of perlite as an adsorbent.

Substrate	Perlite type	Reference
Metals		
Sb(III)	Perlite/Mn-Modified Perlite	Sari et al., 2012
Ag, Cu and Hg	Natural perlite	Ghassabzadeh et al., 2010a
Co (II) and Pb (II)	Natural perlite	Ghassabzadeh et al., 2010b
Arsenate	Iron oxide/Perlite, NP	Mostafa et al., 2011
Zn	Natural perlite	Silber et al., 2012
Pb and Cd	Natural perlite	Malakootian et al., 2011
Cd and Ni	Expanded perlite	Torab-Mostaedi et al., 2010
UO_2^{2+} and Th^{4+}	P(HEMA)-EP	Akkaya, 2013b
Rare earth ions, Tb^{3+}	Polyacrylamide-EP	Akkaya, 2012
Pb	Natural perlite	Irani et al, 2011
Tl^{+}, Ra^{2+}, Bi^{3+}, Ac^{3+} and Pb^{2+}	P(HEMA)-expanded Perlite	Akkaya, 2013a
As(V)	γ-Fe_2O_3/ α-MnO_2 Perlite	Thanh et al., 2011
Organic compounds		
Fungicide, Vapam	Soil modified perlite	Azizi and Asemi, 2012
Green Malachite Dye	Perlite	Bedii et al., 2011
Cationic-PAM	Perlite	Tekin et al., 2010
Crude oil	Natural perlite	Alihosseini et al., 2010
Green Malachite Dye	$FeCl_2$/$FeCl_3$ Perlite, NP	Heydartaemech et al., 2014
Petroleum Hydrocarbon	Natural perlite	Moussavi and Bagheri, 2012
Methylene blue	Perlite	Rafatullah et al., 2010
Rhodamine B	Natural perlite	Vijayakumar et al., 2012

In addition to usage as adsorbent, EP acts as an excellent insulator , both thermal and acoustical, resists fire and is classified as ultra-light weight material. EP is also an excellent filter aid and filler in various processes such as paint enamals, glazes, plastics and resins (Sarı et al., 2007). Besides diverse applications of perlite in construction and chemical industries, perlite has become important in the horticultural industry, as a soilless growth medium and in potting mixes (Papadopoulos et al., 2008).

2.4. Adsorbates

Cesium and cobalt were chosen as adsorbate for this study because they may represent possible dangerous contaminants during a nuclear accident, a nuclear leakage in a deep repository or some nuclear applications like recycling of spent nuclear fuel. The adsorption characteristics of cesium and cobalt onto bentonite have extensively been studied at different experimental conditions but there are still very little studies on the adsorption of cesium and cobalt onto perlite in spite of cost effective in Turkish markets.

2.4.1. Cesium

Cesium is a very soft, ductile, silvery-white alkali metal. The melting and boiling point for cesium are 28.4 and 641 ^{o}C, respectively. Therefore, it is in liquid form at warm room temperature. It has a density of 1.93 gcm^{-3}. Cesium occurs primarily as the mineral pollucite, $CsAlSi_2O_6$ in nature. Pure cesium is obtained from this mineral ore as ^{133}Cs, only stable and natural isotope of cesium. Cesium also has 22 artificial isotopes that their mass numbers change in the range from 123 to 144.

The chemistry of cesium is similar to that of other alkali metals, but is more closely similar to that of rubidium, the element above cesium in the periodic table (Greenwood and Earnshaw, 1984). It is the most electropositive and reactive of the alkali metals and forms compounds with a variety of anions and alloys with the other alkali metals and with gold (Butterman, et al., 2005). It reacts with easily oxygen to produce orange color of cesium oxide (Reaction 2.16) at even room temperature and with water or ice explosively to produce CsOH (Reaction 2.15), the most powerful base that easily attack the glass.

$$2Cs + 2H_2O \rightarrow 2CsOH + H_2 \quad (2.15)$$

$$4Cs + O_2 \rightarrow 2Cs_2O \quad (2.16)$$

While cesium forms water soluable salts (Reaction 2.17) with some common ions such as acetate, sulfate, halides and nitrate, it produce water-insoluble double salts (Reaction 2.18) with antimony, bismuth, cadmium, copper, iron, and lead.

$$2Cs + Cl_2 \rightarrow 2CsCl \quad (2.17)$$

$$2Cs + 2Pb + 3Cl_2 \rightarrow 2CsPbCl_3 \quad (2.18)$$

Like all metal cations, Cs^+ forms complexes with Lewis bases in solution. Because of its large size, Cs^+ usually adopts coordination numbers greater than six-coordination, which is typical for the lighter alkali metal cations. This trend is already apparent by the 8-coordination in CsCl. Its high coordination number and softness (tendency to form covalent bonds) are the basis of the separation of Cs^+ from other cations, as is practiced in the remediation of nuclear wastes, where $^{137}Cs^+$ is separated from large amounts of non-radioactive K^+ (Moyer et al., 2005).

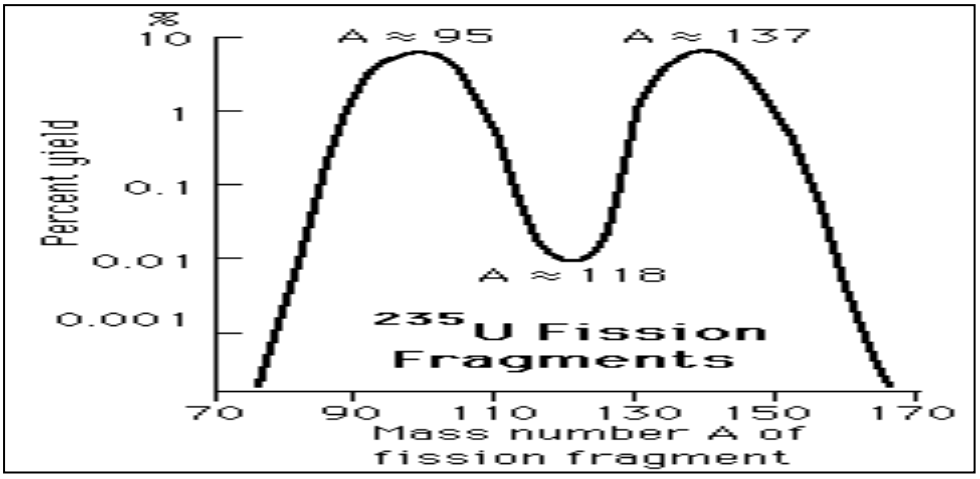

Figure 2.7. The change of percent yield of atoms with respect to mass number of atoms resulting from the fission of uranium (Okumura, 2003).

When uranium and plutonium absorb neutron, they undergo fission which produces numerous fragments (Figure 2.7). The fission process is the splitting of nucleus of a large atom. The fission process occurs in nuclear reactor or nuclear weapon facilities. There are many of possible fission fragments produced corresponding to different mass numbers, but the largest yields occur at mass numbers 95 and 137 (Figure 2.7). Therefore, ^{137}Cs is considered one of the major fission byproducts and remains in spent nuclear fuel (Okumura, 2003).

^{137}Cs naturally disappears by radioactive decay by emitting beta particles and gamma radiations and ultimate decay product becomes ^{137}Ba. As seen in Figure 2.8, 100 unit of mass of ^{137}Cs decrease nearly to half of amount in almost 30 years, and one unit of mass remains nearly after 200 years (Okumura, 2003).

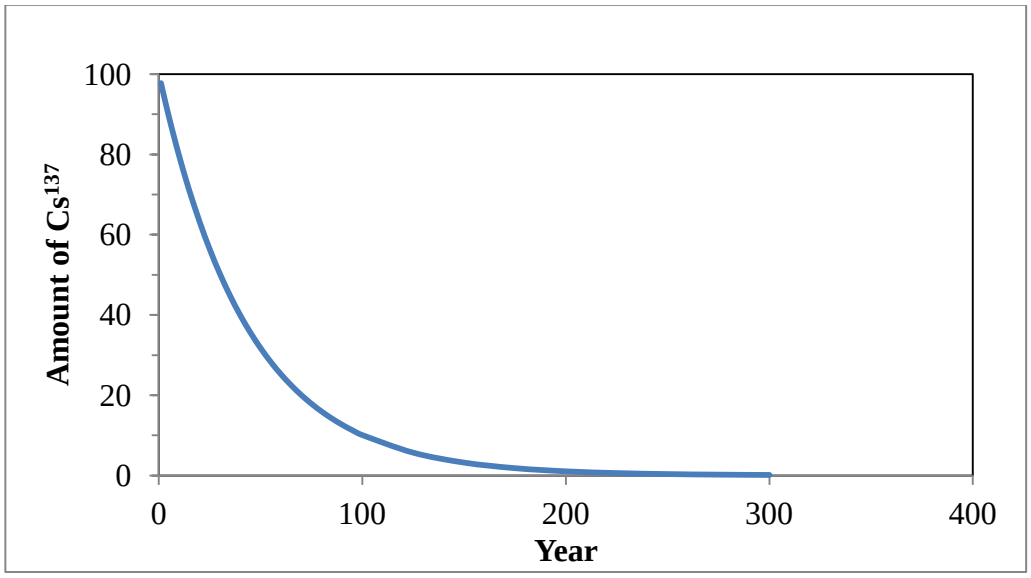

Figure 2.8. Change of mass of ^{137}Cs by years with radioactive decay

^{137}Cs is used in many industrial applications. It is used as moisture and density gauges in construction industry, as leveling gauges to detect liquid flows in pipes and tanks, as thickness gauges to measure thickness of sheet of metal, film, paper and many other products. ^{137}Cs is also used as a powerful gamma emitter in medical devises during cancer treatment.

^{137}Cs may enter the environment in various ways. The large portion comes from nuclear weapon tests in the 1950s and 1960s which dispersed and deposited ^{137}Cs worldwide. But much of the testing ^{137}Cs has decayed up to the present. The other large portion of ^{137}Cs comes from nuclear reactor accidents such as Chernobyl and Fukushima nuclear accidents. Spent nuclear fuel reprocessing plant waste may introduce small portion of ^{137}Cs to the environment (EPA, 2011).

2.4.2. Cobalt

Pure cobalt is not found in nature. It is mostly present as a mixture in arsenic, copper, nickel ore. Cobalt can be separated from other elements and impurities by several steps that involve the flotation, roasting, and acid leaching. Cobalt is a member of a group of first transition element that has very grey color, density of 8.9 gcm^{-3} at 20 ^{o}C and the melting point of 1493 ^{o}C. The solubility of ultrafine cobalt powder in water is at 1.1 mgL^{-1}.

Cobalt occurs in the 0, +2, and +3 valance states. Cobalt (II) is more stable than cobalt (III), which is a powerful oxidizing agent that can oxidize water and liberate oxygen. Metallic cobalt occurs in two allotropic forms, hexagonal and cubic, which are stable at room temperature.

The dissolution of Co(II) in dilute acid gives the pink aqua ion, $[Co(H_2O)_6]^{2+}$, which forms many hydrated salts. Addition of excess Cl^- to pink solutions of the aqua ion readily gives the blue tetrahedral species.

$$[Co(H_2O)_6]^{2+} + 4Cl^- \rightarrow [CoCl_4]^{2-} + 6H_2O \qquad 2.19$$

Addition of OH^- to Co^{2+} gives the hydroxide ion which may be blue or pink depending on the conditions; it is weakly amphoteric dissolving in very concentrated OH^- to give a blue solution containing the $[Co(OH)_4]^{2-}$ ion (Cotton, et al., 1995). In the absence of complexing agent, the oxidation of $[Co(H_2O)_6]^{2+}$ is unfavorable and Co^{3+} is reduced with water. In the presence of complexing agents, such as NH_3, the stability of Co^{3+} is greatly improved, forming $[Co(NH_3)_6]^{3+}$ ion. N donor ligands make strong contribution to forming stable complex ion of Co^{3+}, which produces complex ion in octahedral form.

As apparent from Figure 2.9, the Co^{2+} species remains dominant until pH of about 8 and then decreases sharply, $Co(OH)^+$ species exhibits a maximum around 9 with a decrease gradually above it. In other words, above pH 8, the Co^{2+} in solution decreases and the other hydroxyl species in various forms and concentrations e.g. $Co(OH)^+$, $Co(OH)_{2aq}$, and $Co(OH)_3^-$ appear. The $Co(OH)_{2aq}$ takes over and eventually precipitates as $Co(OH)_{2s}$ (Yuzer et al., 2008).

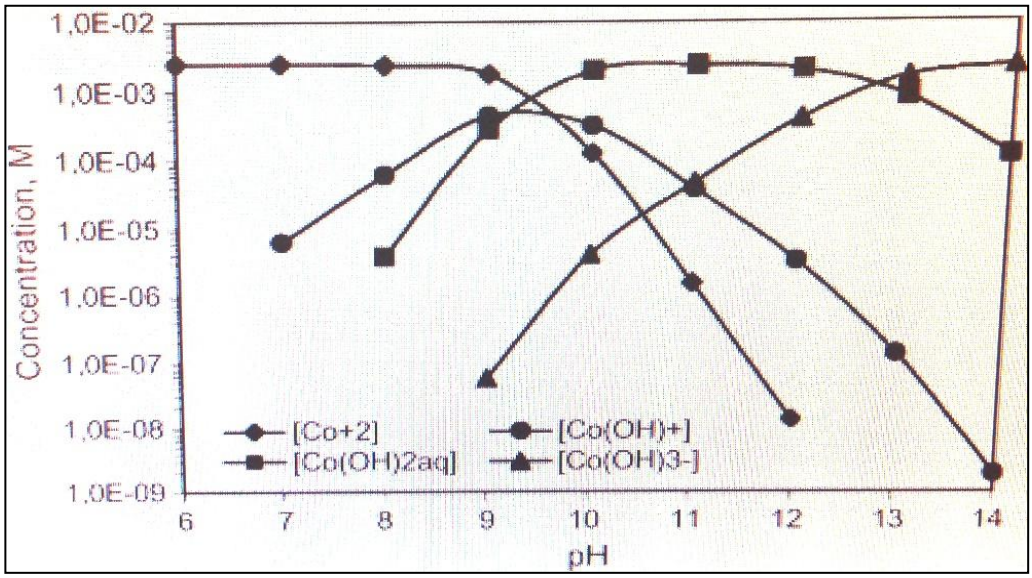

Figure 2.9. pH- Concentration diagram for cobalt species at initial concentration of almost 150 mgL^{-1} (Yuzer et al., 2008).

As apparent from Figure 2.9, the Co^{2+} species remains dominant until pH of about 8 and then decreases sharply, $Co(OH)^{+}$ species exhibits a maximum around 9 with a decrease gradually above it. In other words, above pH 8, the Co^{2+} in solution decreases and the other hydroxyl species in various forms and concentrations e.g. $Co(OH)^{+}$, $Co(OH)_{2aq}$, and $Co(OH)_3^{-}$ appear. The $Co(OH)_{2aq}$ takes over and eventually precipitates as $Co(OH)_{2s}$ (Yuzer et al., 2008).

Cobalt containing compounds have several applications in industry. The main application of cobalt is as metal in alloy production. Cobalt is used as an essential component of lithium ion or nickel-cadmium batteries. Furthermore, some cobalt compounds can catalysis some chemical reaction, such as cobalt carboxylates used as drying agent in paints and varnishes. Some cobalt compounds have been also used as pigments since ancient times.

Cobalt is an element occurring naturally and having one stable and a number of radioactive isotopes. The stable cobalt is ^{59}Co, and radioisotopes are ranged in atomic weight from 50 to 73. ^{60}Co and ^{58}Co are moderately short-lived, manufactured radioactive isotopes that are produced in nuclear reactors. Although these isotopes are not produced by

nuclear fission, small amounts of these radioisotopes are also produced by the neutron interaction with the structural materials found in the reactor of nuclear plants, and are produced during the routine operation of nuclear plants. Small amounts may be released to the environment as contaminants in cooling water or in radioactive waste. Since these isotopes are not fission products (Figure 2.7), they are not produced in nuclear weapons testing and are not associated with nuclear fallout. ^{60}Co undergoes radioactive decay with the emission beta particles and strong gamma radiation. It ultimately decays to non radioactive nickel. ^{60}Co has a half-life of 5.27 years. As seen in Figure 2.10, 100 unit of mass of ^{60}Co decrease nearly to half of amount in almost 5 years, and one unit of mass remains nearly after 30 years. 30 years are short enough to make isolation in a useful treatment strategy for contaminated area with ^{60}Co.

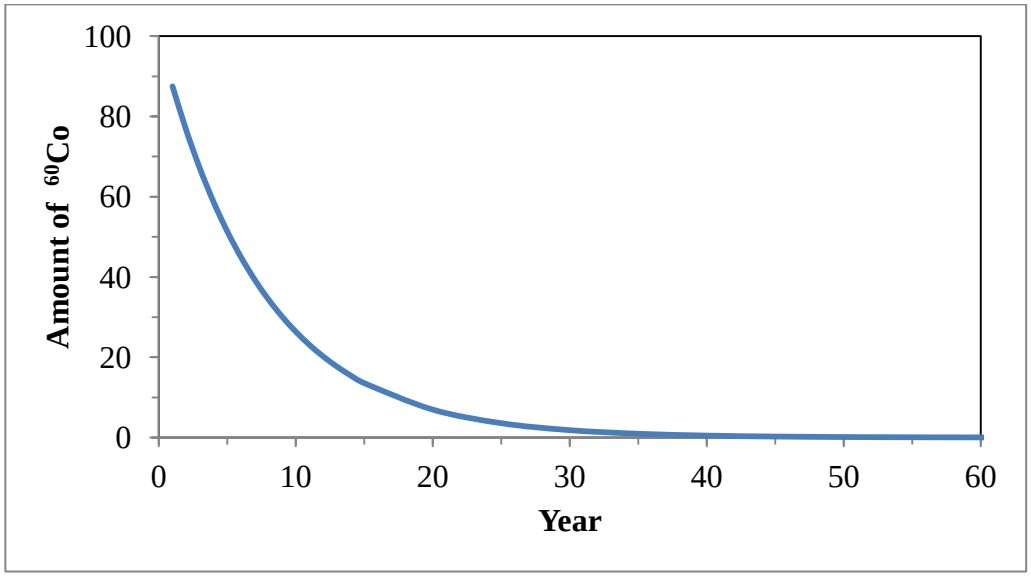

Figure 2.10. Change of mass of ^{60}Co by years with radioactive decay.

^{60}Co is produced for commercial use in linear acceleration and also as a by-product of nuclear reactor operations when structural materials, such as steel, exposed to neutron radiation. ^{60}Co is used in many common industrial applications such as leveling devices and thickness gauges and in radiotherapy in hospitals. Large sources of ^{60}Co are increasingly used for sterilization of certain foods. The powerful gamma rays emitted from ^{60}Co kill the bacteria and other pathogens without damaging the product. The process is

called as cold pasteurization. ^{60}Co is also used for industrial radiography to detect the structural flaws in metal (EPA, 2011).

Anthropogenic usage of cobalt as in above applications release cobalt to the environment. Therefore, cobalt can be present in wastewater of livestock or nuclear effluents. The permissible limit of cobalt in livestock wastewater and irrigation water is 0.05 ppm and 0.1 ppm, respectively. The acute cobalt poisoning in humans may cause serious health effects e.g. asthma like allergy, damage to heart, damage to thyroid and liver. Cobalt may cause mutations in living cells (Ghassabzadeh et al., 2010). In addition, radioactive cobalt source may give serious damage if sufficient precaution is not taken when working with the radioactive source and maybe cause fatal disease as cancer.

2.5. Review of Literature

Sorption has been most widely used for the removal of the radionuclides because it is simple and cost effective with low cost sorbents (Ma et al., 2011). Adsorption of metal ions from aqueous solution on oxides, clays mineral and clays has been a subject of interest in chemistry as well as in other research areas. It is considered that the adsorption of heavy metal and radioactive ions on clay minerals occurs as a result of ion exchange, surface complexation, hydrophobic interaction, and electrostatic interaction. (Nowack and Sigg, 1996; Krapiel et al., 1999).

Clay minerals have high sorption, ion exchange and expansion properties. They are widely used to adsorb heavy metals and radionuclides from large volumes of radioactive or industrial wastewater. Giannakopoulou and co-workers studied the interaction of Cs^+ with different soils and clays by combining microscopic and macroscopic techniques (Giannakopoulou et al., 2007). Among different soils and under all medium pH conditions, the decrease of distribution coefficient of the Cs, followed the sequence of the soils as sandyloam>loam>clayloam>clay, indicating that the particle size fractions and especially the clay contents played predominant role on the sorption of Cs^+ to soils. Similarly, the kinetics of Ce^{3+} sorption-desorption on four soils were also investigated by using batch adsorption technique with radionuclide ^{141}Ce as radiotracer (Li et al., 2001). Abollino and

colleagues studied the sorption of metal ions of Cd, Cr, Cu, Mn, Ni, Pb and Zn on Na-montmorillonite and found that Na-montmorillonite was a good adsorbent towards all examined metal ions (Abollino et al., 2003).

Except for researches on the natural minerals, many researches were focused on modified minerals. There have been various attempts to improve the quality and characteristic of the clays by modifying them with different techniques (Zhao et al., 2011). Abollino and co-workers studied the sorption of Pb^{2+} and Cd^{2+} from aqueous solutions onto sodium tetraborate modified kaolinite clay and increase in adsorption capacity by rising the cation exchange capacity was observed after modification (Abollino et al., 2003). Christidis and colleagues also reported that treatment of bentonite with hydrochloric acid leaded to an increase of surface area as compared to the raw bentonite by as much as five times and so enhanced the sorption capacity in the removal of heavy metal ions from aqueous solutions (Christidis et al., 1997) .

The certain metal oxides are also used as adsorbent such as Mn-oxides, Fe-oxides, Al-oxides and titanium oxide. Debnath and co-worker applied nanostructured hydrous titanium oxide to adsorb Ni^{2+} from natural and industrial wastewater and found that the Fe^{3+} ion showed a strong negative influence (Debnath and Ghosh, 2009). O'Reilly and Hochella measured and compared the Pb^{2+} sorption on a number of natural and synthetic Mn- and Fe-oxides using a flow-through reactor, and found that Pb^{2+} sorption on different oxides was dominated by different mechanisms (O'Reilly and Hochella, 2003). The sorption and complexation of Eu^{3+} on alumina as a function of pH, ionic strength and humic acid were investigated by using batch techniques, and the results showed that sorption was dominated by ion exchange at low pH and by strong surface complexation at high pH values (Wang et al., 2006).

Chemical precipitation is considered to be a simple technique. Rao and colleagues applied chemical treatment method to remove Sr^{2+} and Cs^{+} from radioactive wastewater Rao et al., 2000). Makrlik and co-workers extracted Sr^{2+} ions into nitrobenzene by using synergistic mixture of hydrogen dicarbollylcobaltate and polyethylene glycol PEG1000 Makrlik et al., 2010). Valsala and colleagues studied the separation of Sr^{2+} ions from

radioactive waste solutions using hydrous manganese dioxide composite materials (Valsala et al., 2010).

Khan studied the sorption of long-lived radionuclides Cs, Sr and Co on bentonite (Khan, 2003). The equilibrium time, optimum pH, effect of initial metal concentration and adsorbent dosage were determined for all studied radionuclides. 30- minutes shaking time for Cs and Sr and 4-hour of shaking time for Co were selected as equilibrium time. Optimum pH was found as 7.3 for each radionuclides. The effect of adsorbent concentration on the sorption percentage was studied by varying the amount of bentonite from 0.05 to 1 g, while keeping metal concentration in aqueous solution constant. Optimum amount of sorbent was selected as 0.5 g for each radionuclides. On the basis of these foundings it could be concluded that a good quality bentonite can very effectively be used for decontamination of nuclear wastewater effluents containing low concentrations of the radionuclides Cs, Sr and Co.

Omar and colleagues examined on the adsorption of Co radionuclides from the aqueous solution by raw and modified bentonite (Omar et al., 2009). The adsorption of Co^{+2} ions onto bentonite and formaldehyde modified form followed pseudo-second-order rate model. The adsorption isotherms were more accurately described by Langmuir model. Adsorption studies were also performed at different temperatures. The numerical value of ΔG^o decreased with an increase in temperature , indicating that the adsorption was more favorable at higher temperature. The positive value of ΔH^o corresponds to the endothermic nature of the process. Furthermore, the adsorption capacity of modified form of bentonite is higher than raw bentonite.

Karakaya and co-workers studied the some properties and potentials applications of Na-and Ca- bentonite of Ordu in Turkey (Karakaya et al., 2011). They drew a conclusion that the physical and chemical properties of Ordu region bentonite indicate that they may be suitable as raw material for several industrial applications such as coating, filler additives and a filtering agent.

Vejsada investigated the uncertainties associated with the application of batch technique for distribution coefficients determination in a model case of Cs radionuclide

adsorption onto four different bentonite (Vejsada, 2006). Ca-Mg bentonite as natural Czech bentonite used for potential barrier material of spent nuclear fuel repository, Na-bentonite as industrial sorbent and two standart and comparative bentonite as Ca-bentonite and Na-bentonite were selected. Experiments confirmed that the batch technique contains various sources of uncertainty and brings relevant uncertainty to determined adsorption parameters. The mineral heterogeneity is generally an important source of uncertainty. In the case of centrifugation following adsorption, for coarse particles, the high-speed centrifugation has been found as a sufficient removing method, but for fine particles it is not sufficient. Ultrafiltration has been applied by using Millipore centrifugal filter devices with 30 kDa membranes as the second step. The results were not satisfactory for removing bentonite colloids for each types of bentonite. Vejsada also studied the types of tubes used during batch experiment. The polypropylene and high-transparent polypropylene tubes were selected. The results showed that there is no significant difference between two types of tubes.

Galambos and colleagues studied the influence of chemical natrification of bentonite on adsorption of Cs and Sr with regards to utilization of bentonite for depositing high-level radioactive waste and spent nuclear fuel (Galambos et al., 2010). Bentonite samples from three Slovak deposits natural and natrified forms, which a part of the natural exchangeable cations is substituted for a Na^+ cation, have been investigated. When comparing the Na-bentonite and their natural analogues, the highest adsorbed Cs and Sr amounts were reached on the natrified samples. Furthermore, natrification as a technological process of bentonite quality improvement cannot be applied when constructing a long-term repository for high-level radioactive waste and spent nuclear fuel. The main problem of natrification is a technological process which leads to a significant pH increase because of that alkali environment damages the adsorption quality of bentonite.

Sarı and co-workers studied the adsorption characteristics of Cu and Pb onto expanded perlite from aqueous solution with respects to the changes in pH of solution, adsorbent dosage, contact time and temperature of solution (Sarı et al., 2007). For the adsorption of both metal ions, the Langmuir isotherm model is fitted to equilibrium data better than Freundlich isotherm model. Using the Langmuir model equation, the monolayer adsorption capacity of expanded perlite was found to be 8.62 and 13.39 mgg^{-1} for Cu^{2+} and

Pb^{2+} ions, respectively. Thermodynamic functions, the change of free energy (ΔG^o), entalpy (ΔH^o), and entropy (ΔS^o) of adsorption were also calculated and the parameters showed that adsorption of Cu^{2+} and Pb^{2+} ions onto expanded perlite was feasible, spontaneous and exothermic at 20-50 ^oC. Experimental data were also evaluated in terms of kinetic characteristics of adsorption and it was found that adsorption process for both metal ions followed well pseudo-second order kinetics.

Talip and colleagues studied the adsorption of thorium onto expanded perlite from aqueous solution by batch technique under different experimental conditions (Talip et al., 2009). They reported that adsorption varied strongly by pH and thorium initial concentration. Temperature had a minor effect on the adsorption. The application of the Langmuir and Freundlich models to experimental results showed that the adsorption equilibrium data fitted very well to Langmuir models in the studied concentrations. The thermodynamic parameters were evaluated as well, and showed that the process is spontaneous and exothermic.

Irani and co-workers compared the lead sorption onto natural perlite, dolomite and diatomite. The equilibrium adsorption data were tested with Langmuir and Freundlich models Irani et al., 2011). It was observed that the maximum lead adsorption capacity of natural clays the followed the order of diatomite (25.01 mgg^{-1}), dolomite (19.69 mgg^{-1}) and perlite (8.91 mgg^{-1}). The calculated thermodynamic parameters showed that lead sorption by studied adsorbents was spontaneous and feasible.

Ghassabzadeh and co-workers investigated the characterization of adsorption of Co and Pb onto expanded perlite with respects to changes in pH, adsorbent dosage, and contact time (Ghassabzadeh et al., 2010). The adsorption of Co and Pb onto expanded perlite approached their equilibrium value at 150 and 90 min, respectively. The optimum pH for adsorption of both metal ions was found to be around 6.5. Isotherm analysis of equilibrium data followed well Langmuir isotherm model and the calculated maximum adsorption capacity by this model was 1.05 and 6.27 mgg^{-1} for Co^{2+} and Pb^{2+} ions, respectively. The pseudo-second order rate equation described best the kinetic data of metal ions.

Mostaedi and co-workers examined the adsorption characteristics of cadmium and nickel onto expanded perlite from aqueous solution with respect to changes in pH of solution, adsorbent dosage, contact time and temperature of the solution (Mostaedi et al., 2010). The maximum removal efficiency of Cd is 88.8 % at pH 6 and exposure to 10 gL^{-1} expanded perlite, while for Ni, it is 93.3 % at the same pH and exposure to 8 gL^{-1} adsorbent. For the adsorption of both metals, the Freundlich isotherm model fitted the equilibrium data better than the Langmuir isotherm model. Experimental data are also evaluated in terms of kinetic characteristics of adsorption and it was found that the adsorption process for both metal ions follows well pseudo-second-order kinetics. Thermodynamic functions, the change of free energy (ΔG°), enthalpy (ΔH°) and entropy (ΔS°) of adsorption are also calculated for each metal ion. The results show that the adsorption of these metal ions on expanded perlite is feasible and exothermic at 20-50°C.

3. MATERIALS AND METHODS

3.1. Materials

3.1.1. Adsorbents

3.1.1.1. Bentonite. Bentonite samples originated from Sabanozu, Cankırı were supplied by MTA. Bentonite powder was pulverized to pass through a 125 μm sieve, washed with distilled water, dried at 373 K, and stored in tightly stoppered bottle. 50 mg of bentonite sample was used as adsorbent for each adsorption experiment in this study.

3.1.1.2. Perlite. Perlite samples mined from Yuntdağı, Manisa were supplied by Pertaş Metal Perlite and Natural Stone LTD as expanded perlite. Expanded perlite was used as adsorbent throughout the whole adsorption experiments in this study. It should be in mind that the results of this study are related with expanded perlite, not natural perlite. 125 μm sieve was used to sieve and after that perlite particles under 125 μm were washed with distilled water, dried at 373 K and stored in tightly stoppered bottle for further experiments. 50 mg of expanded perlite was used as adsorbent for each adsorption experiment.

3.1.2. Adsorbates

3.1.2.1. Cesium. Cesium containing solutions were prepared from CsCl which was of analytical grade and procured from Merck. 1.2731 g of CsCl was dissolved in 1 L of ultra pure distilled water in order to prepare 1000 $mgCs^{+}L^{-1}$ stock solution. For each adsorption experiments, cesium solutions were prepared by diluting stock solution to produce various concentrations ranging from 5 mgL^{-1} to 600 mgL^{-1}. The pH was adjusted to the required value by adding 0.1 M NaOH or 0.1 M HCl solution, respectively, to each solution

3.1.2.2. Cobalt. $CoCl_2.6H_2O$ which was of analytical grade and procured from Merck was used for preparing cobalt solution. 4.0372 g of $CoCl_2.6H_2O$ was dissolved in 1 L of ultra pure distilled water in order to prepare 1000 mgL^{-1} Co^{2+} stock solution. Dilution of stock solution in order to get required value of concentration ranging from 5 mgL^{-1} to 300 mgL^{-1} was made. 0.1 M NaOH or 0.1 M HCl solution was added to obtain required value of pH of the solution

3.1.3. Ultra Pure Distilled Water

Ultra pure distilled water obtained from ELGA PURELAB Option Q 15BP model device was used to prepare metal solution throughout this study. The value of conductivity of ultra pure distilled water was 0.055 μScm^{-1}.

3.1.4. Other Chemicals

HCl and NaOH, which were analytical grade from Merck, were used to adjust pH of the metal solutions. 1 $molL^{-1}$ of HCl was prepared by dissolving 8.28 mL of concentrated HCl in 100 mL ultra pure distilled water and diluted to 0.1 $molL^{-1}$ of concentrations. In the same manner, 1 $molL^{-1}$ of NaOH were prepared by dissolving 3.99 g of NaOH granule in 100 ml of ultra pure distilled water and diluted to 0.1 $molL^{-1}$ of concentrations. NaCl, which was analytical grade from Merck, was used to adjust the desired background electrolyte concentration of the metal solution and to change ionic strength of the metal solution. 1 $molL^{-1}$ of NaCl were prepared by dissolving 5.84 g of NaCl in 100 mL of ultra pure distilled water.

3.2. Methods

3.2.1. Characterization Experiments

Adsorbents (i.e. bentonite and perlite) were ground by a grinder type Fritsch Pulverisette 2 then sieved through Fritsch Spartan sieve to obtain particle size less than 125

μm. Particle size of the adsorbents was measured and particle size distribution graphs were obtained by the instrument of the Malvern Instruments Mastersizer using the technique of laser diffraction. In this technique, as a laser beam passes through a dispersed particulate sample, intensity of the light scattered is measured. The data obtained is then analyzed to measure the size of the particles.

Surface areas of adsorbents were determined by using Standard Volumetric Method by nitrogen adsorption at 77 K and the application of multipoint BET equation by means of Quantachrome Instrument Absorber-1type instrument. Surface area was expressed as m^2 per g of adsorbent (m^2g^{-1}).

Elemental analysis of the adsorbents was made with the method of wavelength dispersive XRF (WDXRF) by using PANalytical Axios WDXRF instrument. In this method, polychromatic beam emerging from a sample surface is dispersed into its monochromatic constituent by the use of diffracting crystal and a detector that are placed in positions according to Bragg's law. The wavelength of any measured line is computed from knowledge of crystal parameters and diffraction angle. Some amounts of adsorbents and 1-2 g cellulose were mixed to produce pellets under the force of 25 tones. After preparing the pellets, they were given to instruments (WDXRF) for making elemental analysis.

The morphological structures of the raw and either Cs^+ or Co^{2+} loaded adsorbents were obtained by using scanning electron micrograph (SEM). The SEM and energy dispersive spectroscopy (EDS) analysis was started by sprinkling the solid samples onto adhesive carbon taps supported by circular metallic disk. The samples were then analyzed using a JEOL JSM 639OVL type SEM instrument.

3.2.2. Batch Adsorption Experiment

Adsorption experiments were conducted in a 50 mL of polyethylene tube filled with 20 mL of metal solution. 50 mg of adsorbent was added to tube in order to provide the ratio of mass of adsorbent to the volume of the solution as 2.5 gL^{-1}. This ratio was kept

constant for all experiments. The suspension was then shaken for the desired contact time in an electrically thermostatic shaker produced by Memmert at maximum rate at 298 K temperature. After adsorption equilibrium was reached, the suspension was filtered by 0.45μm Millipore syringe driven membrane filter. The filtrate was analyzed in order to measure Cs^{+} or Co^{2+} concentration by ICP-OES or AES, respectively.

3.2.3. Effects of Operational Parameters on Adsorption

Several experiments were carried out to elucidate the effect of pH, contact time, initial metal concentration, temperature, ionic strength and humic acid (HA) in the manner mentioned above. Initial solution pH adjustment was made by using HACH HQ11d model of pH meter by adding 0.1 M NaOH or 0.1 M HCl solution to obtain the value of pH: 2, 4, 6, 8, 10 and 12. The time intervals of 5, 15, 30, 60, 120, 180, 240 and 360 min were chosen to determine the optimum value of contact time. Initial metal concentration effect on the adsorption isotherm was investigated at different concentrations previously prepared from the respective stock metal solution by keeping the pH, contact time and temperature as constant. Furthermore, the effect of temperature on the adsorption process was studied at 288, 298, 318 and 338 K. The procedure was similar to that noted above.

Similar experiments were conducted in order to determine the effect of ionic strength on the adsorption of Cs^{+} and Co^{2+} onto bentonite and perlite. 1.0 M of NaCl solution previously prepared was added to the metal solution for making NaCl concentration 0.001 M, 0.01M and 0.1 M. 50 mg of adsorbent was added to these solutions at constant initial metal concentration, pH and temperature and the mixture was shaken for 30 min. 100 mgL^{-1} concentration of HA was prepared from 1000 mgL^{-1} of HA and HA concentration in metal solution was adjusted as 20 mgL^{-1} when preparing Cs^{+} and Co^{2+} solutions at varying concentrations. Afterwards, several initial concentrations of Cs^{+} and Co^{2+} solutions with 20 mgL^{-1} of HA were mixed 50 mg of bentonite or perlite in order to investigate the effect of HA on the interactions of above mentioned metals with the surface of bentonite and perlite.

3.2.4. Analytical Methods

3.2.4.1. Flame AES Measurement. The concentration of Cs^+ in the sample was determined with Varian SpectraAA-200 device (Figure 3.2). When the acetylene was used as fuel gas, air was used as oxidant for flame. The sample was sprayed to flame by means of a nebulizer. This flame provided the atomization of the sample at the temperature between 3323 and 3423 K. Emitted radiation from excited atoms was converted to an emission signal by a detector. For the determination of cesium concentration, the wavelength and slit width were chosen as 852.1 and 0.1 nm, respectively.

Figure 3.1. Varian Spectra AA-200 model of flame atomic emission spectroscopy.

Calibration standard solutions of Cs^+ were prepared from stock primary standard solution and a calibration curve with a correlation coefficient of 0.9999 was constructed with the three working standards in the range of 0.5 mgL^{-1} and 3.0 mgL^{-1}. Ultra pure distilled water acidified with suprapure nitric acid was used as calibration blank. Blank and working standards and samples were kept under the 2 % acidic condition in volume. For preventing ionization of excited atoms, KCl used as an ionization suppressor was added to blank, sample and working standards in a way that its concentration becomes 1000 mgL^{-1} in the solution.

3.2.4.2. ICP-OES Measurement. PerkinElmer Optima 7000 DV ICP-Optical Emission Spectrometer, as shown in Figure 3.1, equipped with WinLab 32 for ICP Version 4.0 software, was used for measurement of Co^{2+} concentration. The sample-introduction unit includes a cyclonic spray chamber concentric glass nebulizer. The cyclonic spray chamber was used to provide both high sample transfer into the ICP and very fast sample rinse-in and rinse-out times, which improved productivity. The concentric nebulizer provided excellent sensitivity and precision for aqueous solutions and is well suited for the analysis of water samples.

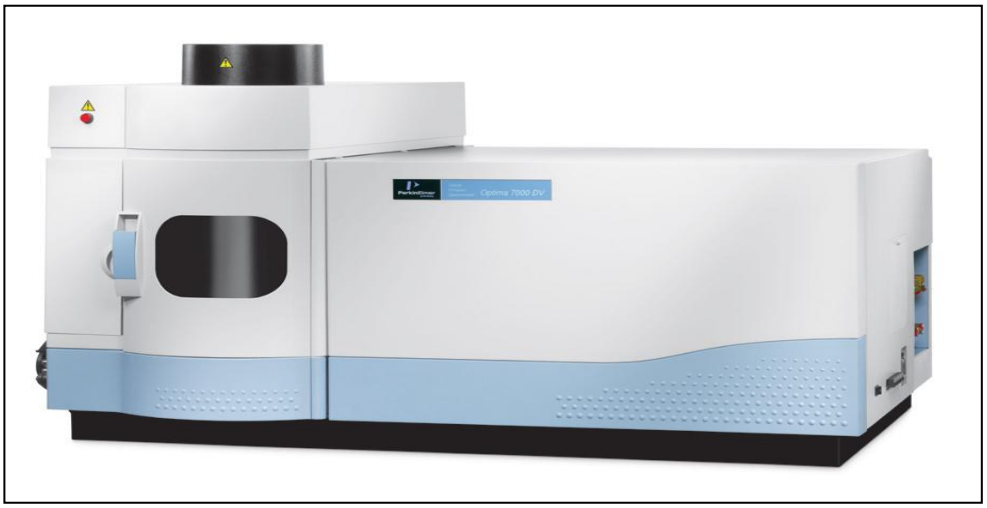

Figure 0.1. Perkin Elmer Optima 7000DV ICP-OES.

Calibration standard solutions of Co^{2+} were prepared from stock primary standard solution and a calibration curve with a correlation coefficient of 0.9999 was constructed with the three working standards in the range of 0.5 mgL^{-1} and 3.0 mgL^{-1}. Ultra pure distilled water acidified with suprapure nitric acid was used as calibration blank. Blank and working standards and samples were kept under the 2% acidic condition in volume.

4. RESULTS AND DISCUSSION

4.1. Characterization of the Adsorbents

Inorganic adsorbents used in the experimental studies are bentonite from Çankırı, Şabanozu and perlite from Manisa, Yuntdağı . The chemical composition of the adsorbents was determined by the technique of wavelength dispersion X-Ray Fluorescence (WDXRF) and related results were given in Table. 4.1. Samples were used as is without any further purification.

Table 4.1.Chemical composition of the adsorbents used in adsorption studies.

Sample	Chemical composition, %									
	SiO_2	Al_2O_3	Fe_2O_3	CaO	MgO	Na_2O	K_2O	TiO_2	P_2O_5	MnO
Bentonite	58	18	9.3	5.5	2.0	3.1	2.2	0.60	0.13	0.22
Perlite	68	13	1.7	1.4	0.09	4.3	9.9	0.16	0.02	0.12

Bentonite has montmorillonite as a major constituent mineral and its aluminum octahedral sheet has a permanent negative surface charge due to isomorphic substitution of Mg or Fe with Al or Si. The value of Fe content of bentonite (Table 4.1) shows that substitutions are resulted mainly from Fe atoms. Ca and Na content of the bentonite (Table 4.1) are similar to each other. This also exhibited that bentonite type is a mixing bentonite. Exchangeable cations between layers may come from Na and Ca atoms during the absorption of water in aqueous medium (Sposito, 2004). The chemical composition of perlite was also given in Table 4.1. The major constituents are silicate as 68 % and aluminum oxide as 13 % which are consistent with the expression that basic functional groups on the surface of perlite are silanol and aluminol groups. The Figure 4.1 indicates the particle size distribution graphs of both bentonite and perlite. With respect to graphs, particles of both of the adsorbents collected after sieving displayed diameters which are mostly less than 125 μm and bentonite has smaller particles than perlite. While bentonite had the peak at about 5 μm, perlite had the peak at about 10 μm (Figure 4.1).

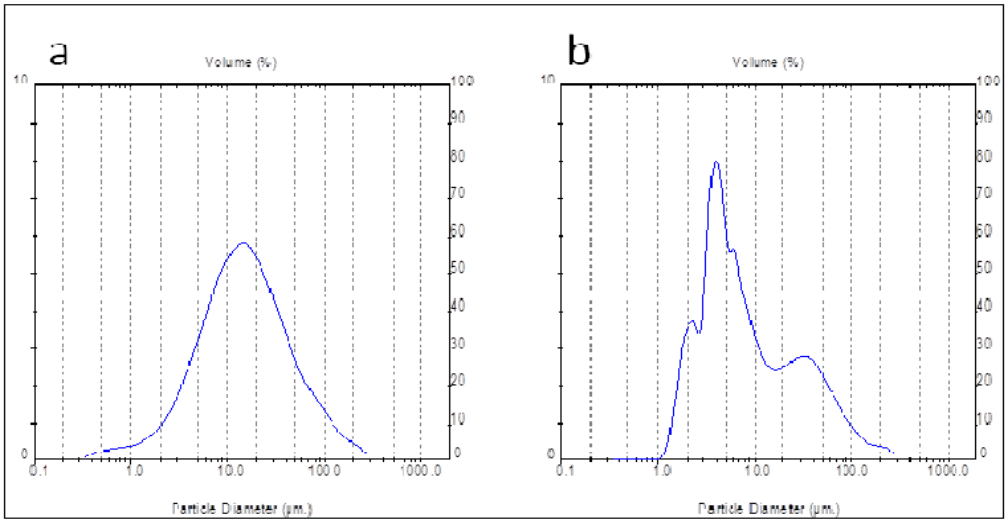

Figure 4.1. Particle size distribution graphs of perlite (a) and bentonite (b).

SEM images of the surface of raw bentonite and perlite were presented in Figures 4.2 and 4.3 respectively. Moreover, EDS mapping of the surfaces showed the signals from Cs and Co atoms at the surface of natural bentonite and perlite prior to adsorption experiments. The amount of signals (Figure 4.2 and Figure 4.3) implied that either bentonite and or perlite had few amounts of cesium and cobalt.

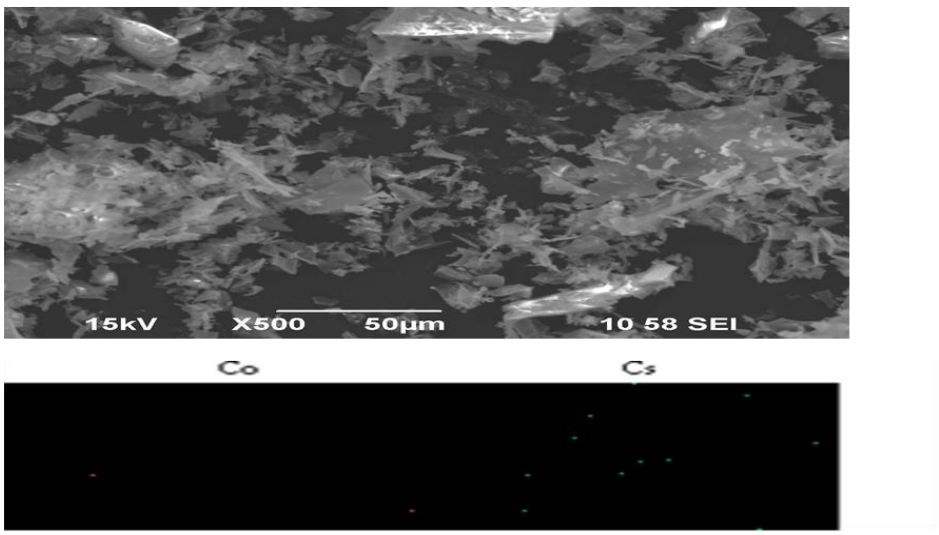

Figure 4.2. The typical SEM and EDS mapping images of the surface of bentonite.

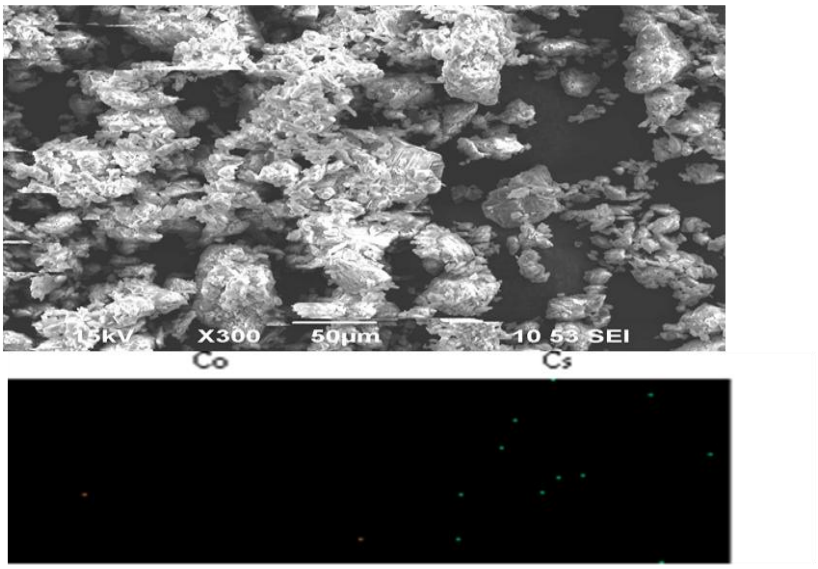

Figure 4.3. The typical SEM and EDS mapping images of the surface of perlit.

SEM and EDS mapping images of the surface of Co or Cs loaded bentonite or perlite were presented in Figure 4.4 and 4.5.

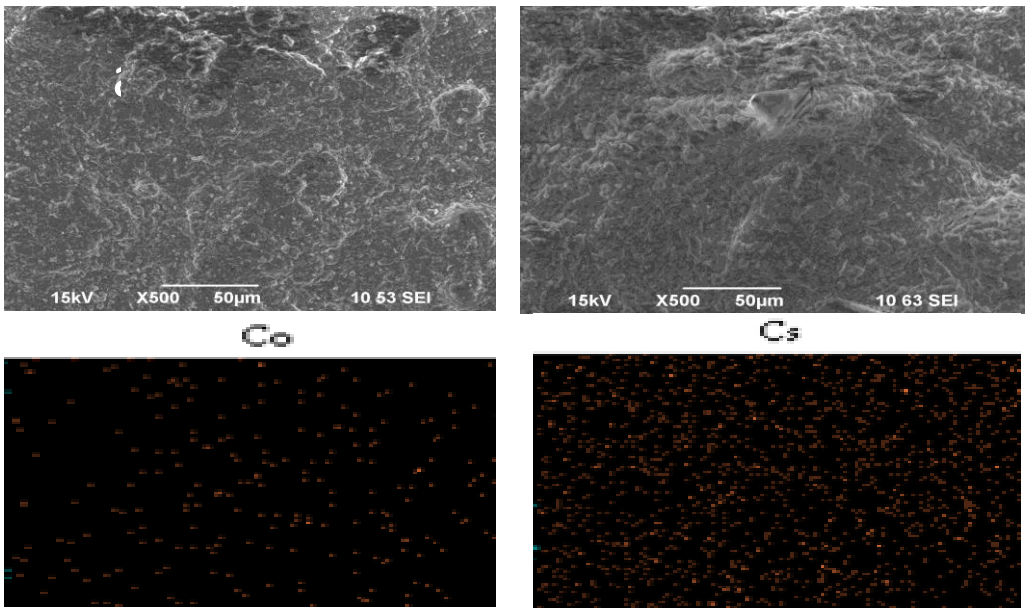

Figure 4.4. SEM images of Co^{2+} loaded bentonite surface (a) and Cs^{+} loaded bentonite surface (b) and at the following their EDS mapping images that contain spots from adsorbed Co^{2+} and Cs^{+} signals.

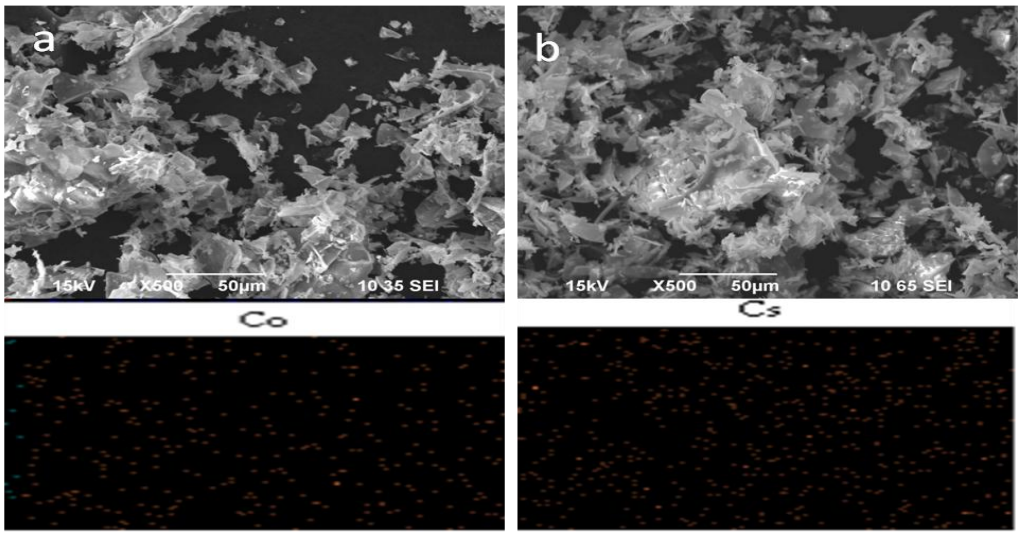

Figure 4.5. SEM images of Co^{2+} loaded perlite surface (a) and Cs^{+} loaded perlite surface (b) and at the following their EDS mapping images that contain spots that illustrate adsorbed Co^{2+} and Cs^{+} signals.

With respect to Figures 4.2, 4.3, 4.4 and 4.5, it can be stated that both bentonite and perlite surfaces were exposed to change upon adsorption of Cs^{+} and Co^{2+}. Moreover, when comparing EDS mapping images displayed in Figures 4.4 and 4.5 with the images given in Figures 4.2 and 4.3, it can be easily concluded that bentonite and perlite surfaces form a preferable sink for Cs^{+} or Co^{2+} during the adsorption.

Shahwan and co-workers studied characterization of the adsorption of the aqueous Co^{2+} onto natural bentonite. Spot EDS analysis has shown that montmorillonite fractions in natural bentonite are more effective in Co^{2+} fixation than cristobalite fractions, and the localization of the signal of adsorbed Co^{2+} was also verified by EDS mapping (Shahwan et al., 2006). Moreover, Zhang and colleagues examined the adsorption characteristics of Pb^{2+} on alkaline Ca- bentonite. The SEM graphs were utilized in order to compare the surface structure of alkaline Ca-bentonite with the Pb^{2+} adsorbed surface structure of alkaline Ca-bentonite. Alkaline Ca-bentonite has a leafy sheet surface structure with loose and porous structure. After Pb^{2+} adsorption, the leafy sheet surface of alkaline Ca-bentonite disappeared and was covered with many small fragments (Zhang et al., 2012). Removal of basic dye Rhodamine-B from aqueous solution by the adsorption onto natural perlite was also investigated (Vijayakumar et al., 2012). SEM micrographs were used in order to

characterize the surface of the natural perlite before and after adsorption. With respect to SEM images, it was revealed that before adsorption surface of the perlite was rough and porous, but after adsorption the surface was covered by dye and consequently became smooth. This situation showed the clear evidence for the change of the surface of the natural perlite upon adsorption of the dye.

4.2. Adsorption of Cesium and Cobalt onto Bentonite and Perlite

The results of the adsorption experiments of Cs^+ and Co^{2+} onto either bentonite or perlite were evaluated and presented in this part. Adsorption of either Cs^+ or Co^{2+} onto bentonite were presented first followed by the results of the adsorption experiments obtained for either Cs^+ or Co^{2+} adsorption onto perlite.

4.2.1. Adsorption Studies of Cesium onto Bentonite

Adsorption behavior of Cs^+ onto bentonite was investigated under varying experimental conditions such as pH, contact time, initial Cs^+ concentration, ionic strength, the concentration of humic acid and temperature. Adsorption equilibrium data were fitted to Freundlich, Langmuir and Dubinin-Radushkevich isotherms to calculate the maximum adsorption capacity of the bentonite and the energy of adsorption. Also, these data were used to comprehend the mechanism of the adsorption. Moreover, the equilibrium data obtained by changing temperature were used to evaluate the thermodynamic parameters.

4.2.1.1. Effect of pH. pH is one of the most important parameter assessing the adsorption capacity of an adsorbent. The pH can affect the adsorption system by changing surface properties of the adsorbent or the ionic forms of the metal in the aqueous suspension. Figure 4.6 shows the effect of pH on the adsorption of Cs^+ onto bentonite, where the percentage of adsorbed Cs^+ equals to C_s/C_i*100.

The lowest adsorption of Cs^+ onto bentonite is 35 % under very acidic condition i.e. pH 2. Cs^+ adsorption onto bentonite displays an increasing trend in acidic conditions

reaching a maximum value of 73 % at pH 8. Increasing pH to alkaline region, a decreasing trend is attained reaching a 55 % adsorption at pH 12.

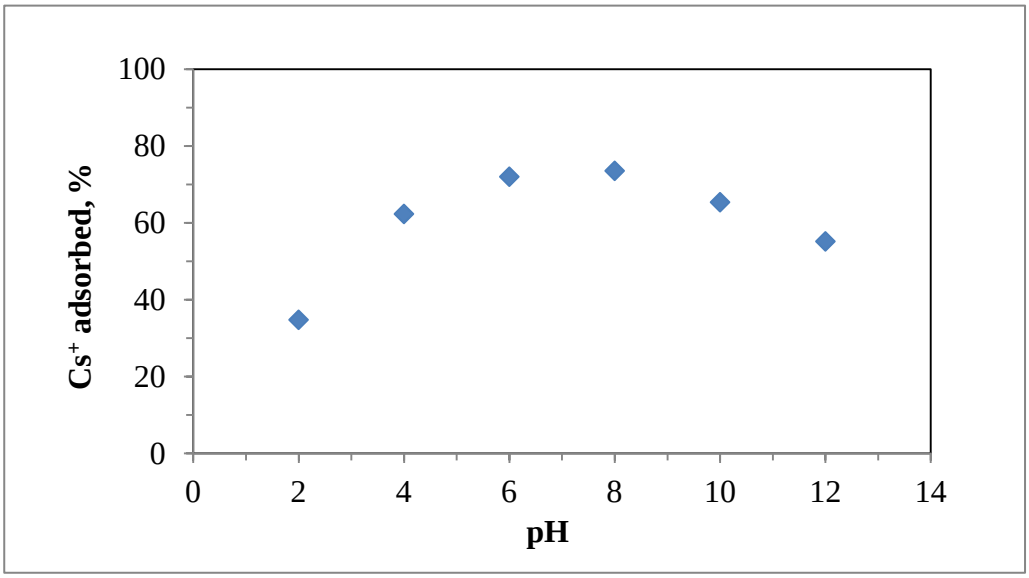

Figure 0.6. Influence of pH on adsorption of Cs^+ onto bentonite (Initial Cs^+ concentration:500 mgL^{-1}, Bentonite dosage:2.5 gL^{-1}, T:298 K, Contact time:30 min).

4.2.1.2. Effect of Contact Time. The adsorption of Cs ions was investigated as a function of shaking time and the result shows that the adsorption was reached immediately to equilibrium after mixing (Figure 4.7). The adsorption efficiency was found as 44 % in 30 min and there is a negligible change in adsorption efficiency after that time as seen in the Figure 1.2. Therefore, a period of 30 min is chosen as the contact time for the further experiments of Cs^+ ions adsorption onto bentonite.

Galambos and colleagues stated that the adsorption of Cs^+ ions onto bentonite, taken from Slovak deposits, was very fast and equilibrium was reached almost within 1 min (Galambos et al., 2010).Khan also reported that the uptake of the cesium ions onto bentonite, collected from different types of localities in Pakistan, was very fast and equilibrium was reached instantaneously (Khan, 2003). Therefore, 30 min was selected as optimum contact time during the experiments.

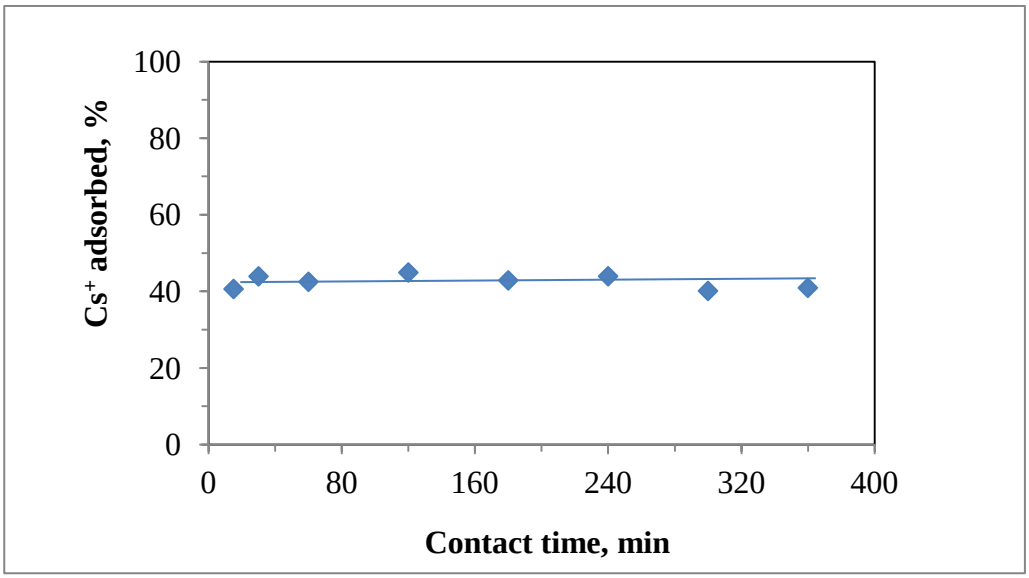

Figure 4.7. Effect of contact time on adsorption of Cs^+ onto bentonite (Initial Cs^+ concentration:500 mgL^{-1}, Bentonite dosage:2.5 gL^{-1}, T:298 K).

Kinetic studies of adsorption can give some elucidative information about adsorption mechanism. Tsai and co-workers claimed that adsorption of Cs^+ and Sr^{2+} onto bentonite is rapid and this situation indicates that ion-exchange mechanism may be the dominant mechanism controlling the adsorption process (Tsai et al., 2001). In aqueous medium exchangeable cations on bentonite surface moves to interlayer by leaving surface permanently negative and Cs^+ firstly diffuse towards active surface sites and can give nonspecific interactions with negative surface. Therefore, short interaction time period can be accepted as sufficient for nonspecific interactions.

4.2.1.3. Effect of Initial Cesium Concentration. Effect of initial concentration of Cs^+ on the adsorption profile of Cs^+ onto bentonite was presented in Figure 4.8. The amount of adsorbed (q_A) Cs^+ increased from 7.82 mgg^{-1} to 89.43 mgg^{-1} for initial Cs^+ concentration range of 20 to 600 mgL^{-1} respectively. On the other hand, the percentage of adsorbed Cs^+ decreased from 98 % to 37 % for initial Cs^+ concentration range of 20 to 600 mgL^{-1}, respectively.

When the initial concentration of Cs^+ in solution was increased beyond 500 mgL^{-1}, q_A value remained almost constant at 2.5 gL^{-1} of bentonite dosage (Figure 4.8).

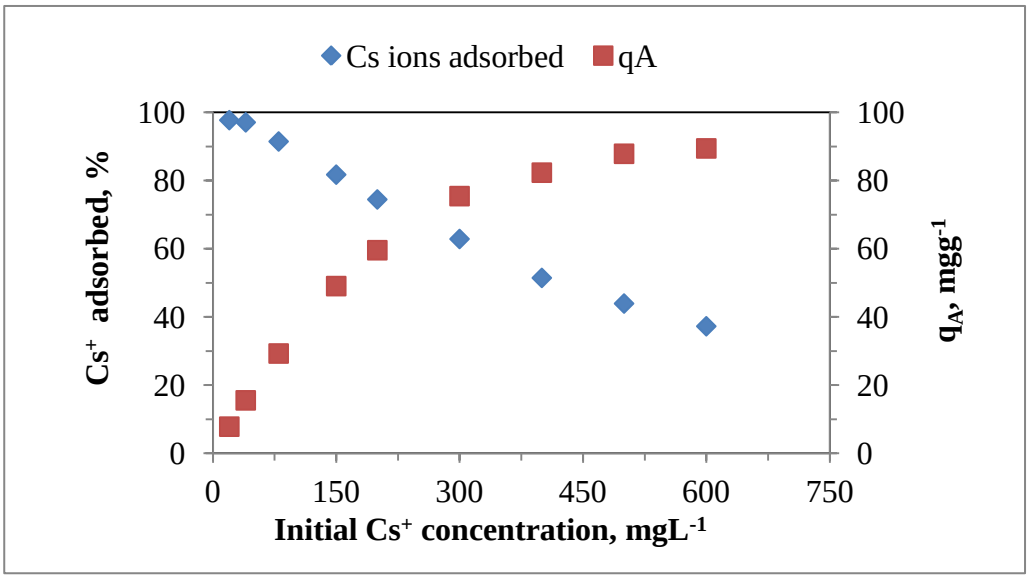

Figure 4.8. Effect of initial concentration on adsorption of Cs^+ onto bentonite (Initial Cs^+ concentration range:20-600 mgL^{-1}, Bentonite dosage:2.5 gL^{-1}, T:298 K, Contact time:30 min, pH:8.0±0.2).

During the investigation of adsorption of Cu^{2+} and Cd^{2+} onto bentonite modified by binary mixture of goethite and humic acid, Olu-Owalabi and co-workers pointed out that the amount of Cu^{2+} and Cd^{2+} ions increased with the increase in metal ion concentration, while the percentage of metal ion adsorbed decreased with the increase in metal ion concentration with Cu^{2+} being more adsorbed than Cd^{2+} (Olu-Owalabi et al., 2010). Smaller ionic radius of Cu^{2+} than Cd^{2+} and higher selectivity of Cu^{2+} than Cd^{2+} by bentonite were presented as possible reasons for this trend. Furthermore, they also stated that the decrease in percentage of metal ion adsorbed is due to the decrease in active sites on the adsorbent as more metal ions adsorbed, while the increasing adsorption capacity is due to increasing driving force of metal ions towards the active sites. The role of humic acid that could be prevailing through complexation mechanism on the adsorption of the metal ions should also be taken into consideration. Donat and colleagues studied the adsorption of Pb^{2+} and Ni^{2+} onto natural bentonite from aqueous solutions. It was stated that adsorption capacity increased as a function of initial metal concentration at 303K and the maximum value was not reached when the concentration exceeded 200 mgg^{-1}. It was explained by the fact that increasing initial metal concentration may hinder the adsorption on the bentonite surface (Donat et al., 2005).

4.2.1.4. Effect of Ionic Strength. Ionic strength of the medium was changed by introducing varying the concentrations of NaCl to the reaction solution. The percentage of the adsorption displayed decreasing trend where the efficiency values of were 72.5 %, 60.4 % and 32.3 % when adding $1x10^{-3}$ M, $1x10^{-2}$ and $1x10^{-1}$ M concentration of NaCl to the solution, respectively. Furthermore, the corresponding q_A values changed as 55.4, 48.3 and 26.0 mgg^{-1}, respectively (Table 4.2).

Table 4.2. Adsorption of Cs^+ onto bentonite with the change of ionic strength.

	Concentration of NaCl in metal solution			
	Absence of NaCl	$1x\ 10^{-3}$	$1x\ 10^{-2}$	$1x\ 10^{-1}$
Adsorption, %	74	72.5	60.4	32.3
$q_{A,}$ mgL^{-1}	59.6	55.4	48.3	26.0

This downward trend is consistent with the previously reported studies. Once Olu-Owulabi and colleagues studied the adsorption of Cu^{2+} and Cd^{2+} onto bentonite, it was found that the increase in ionic strength decreased the percentage of Cu^{2+} and Cd^{2+} adsorption (Olu-Owulabi et al., 2010). The possible reason submitted for that decreasing trend is that the increase in ionic strength reduces the negative charge on the surface of the bentonite, so the potential in the plane of the adsorption is getting positive and hence decreased the adsorption. In other words, it can be said that excess cation ions coming from electrolyte solution give a competition with the adsorbate metal ions for the active site of adsorbent decreasing the adsorption (Pathak and Choppin, 2006).

4.2.1.5. Adsorption Isotherm Modeling of Cesium Adsorption onto Bentonite . Adsorption isotherm relates the adsorbate concentration in the solution and the concentration of the adsorbate on solid phase at equilibrium and constant temperature (Sposito, 2004). Adsorption isotherm of Cs^+ was obtained at optimum pH and contact time by changing initial concentration range 20-600 mgL^{-1} and by keeping bentonite dosage constant as 2.5 gL^{-1} (Figure 4.9). It should be noted that adsorbent dosage should be kept constant because the concentration of exchangeable cations released to aqueous media can change with the amount of adsorbent and thereby decrease efficiency of the adsorption

Equilibrium concentrations i.e. C_e values varied between 0.46-376 mgL^{-1} depending on the initial concentration of Cs^+ in solution. The values of q_A calculated were in the range of 7.89-89.4 mgg^{-1} for the corresponding C_e values. Adsorption isotherm (Figure 4.9) of Cs^+ onto bentonite shows L-type isotherm shape which usually concave to concentration axes. It suggests the progressive saturation of bentonite surface with increase of Cs^+ concentration in solution.

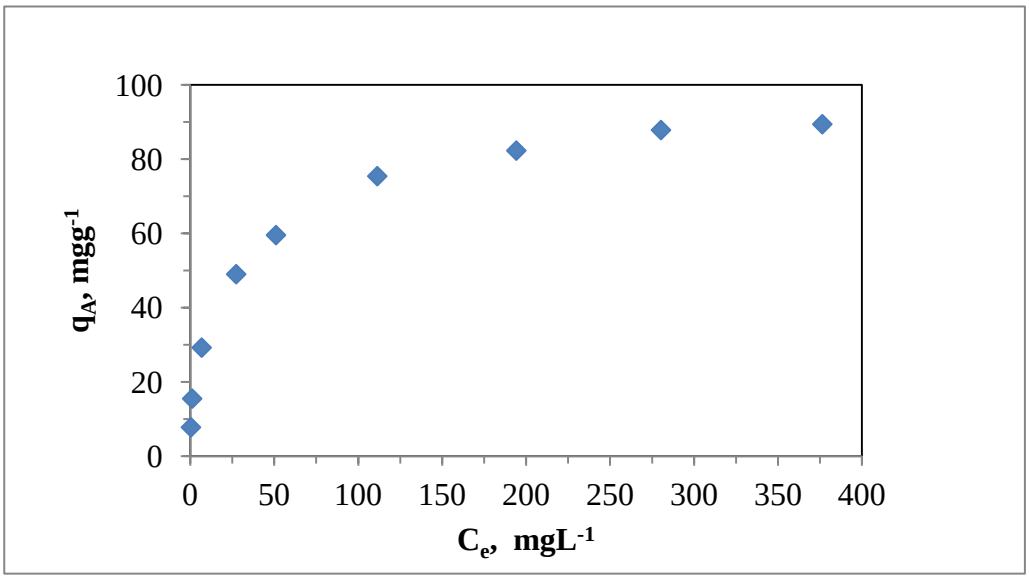

Figure 4.9. Adsorption isotherm of Cs^+ onto bentonite (Initial Cs^+ concentration range:20-600 mgL^{-1}, Bentonite dosage:2.5 gL^{-1}, T:298 K, Contact time:30 min, pH:8.0±0.1).

The equilibrium data were fitted to Langmuir isotherm equation (Equation 2.2) and a linear plot was obtained when $1/q_A$ was plotted against $1/C_e$ over the entire concentration range studied by giving regression coefficient of R^2 = 0.975 (Figure 4.10). The Langmuir adsorption model parameters and statistic fits of the adsorption data were calculated. The values for q_{max} and K_a were 83.3 mgg^{-1} and 9.60x 10^{-2} Lmg^{-1} respectively. The R^2 value (0.975) of the Langmuir isotherm model indicated that the model effectively describes the equilibrium data and the high maximum adsorption capacity (q_{max}) implies that bentonite as an adsorbent can be effectively used for the cesium removal from a radioactive liquid waste.

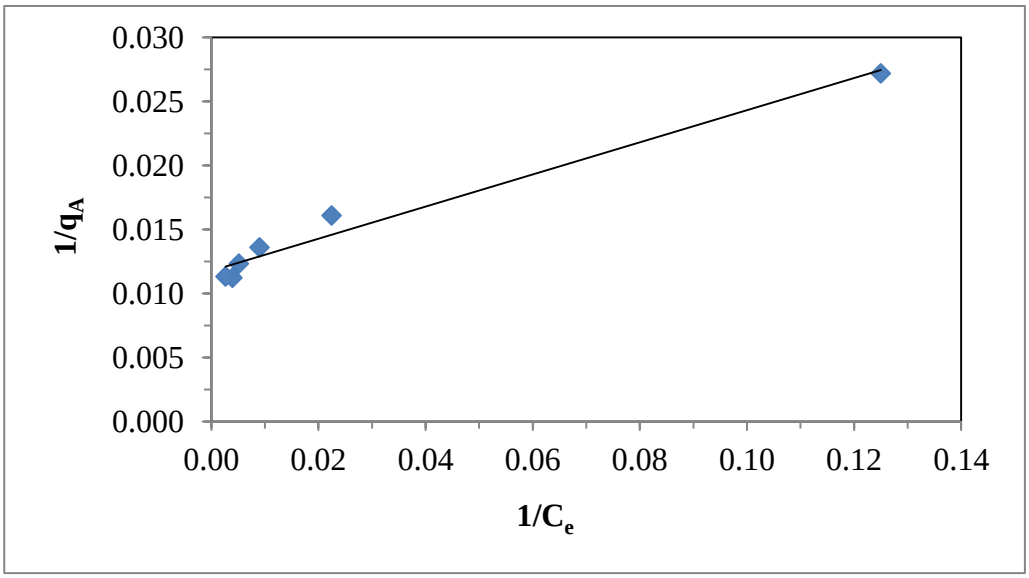

Figure 4.10. Langmuir isotherm model for Cs^+ adsorption onto bentonite (Initial Cs^+ concentration range:100-600 mgL^{-1}, Bentonite dosage:2.5 gL^{-1}, T:298 K, Contact time:30 min, pH:8.0±0.1).

Galambos and co-workers investigated the adsorption of radioactive $^{137}Cs^+$ ions onto various bentonite samples provided from different deposit site of Slovak. The equilibrium data was fitted to Langmuir model and highest adsorption capacity, q_{max}, was found as 126 $mgg^{-1}$for bentonite provided from Kopernica deposit site. Therefore, they supposed that bentonite sample is proper for the use of sealing barrier in a deep geological repository for high level of radioactive waste and spent nuclear fuel (Galambos et al., 2010).

The equilibrium data were also fitted to Freundlich isotherm equation (Equation 2.4) and the linear plot of the $logq_A$ against $logC_e$ would give the slope as 1/n and intercept as logk with a regression coefficient of R^2= 0.973 (Figure 4.11). Freundlich adsorption isotherm model parameters were calculated according to data obtained from statistic fit. The values for K_F and 1/n were 23.8 Lg^{-1} and 0.233, respectively. K_F is a constant related with adsorption capacity and the value of K_F demonstrated that bentonite was a good adsorbent for Cs adsorption and 1/n value was between 0 and 1 indicating that adsorption of Cs onto bentonite was favorable at studied conditions. The values of R^2 for Freundlich and Langmuir, which were 0.973 and 0.975, respectively were so close, so it was concluded that the equilibrium data fitted well either Freundlich or Langmuir models.

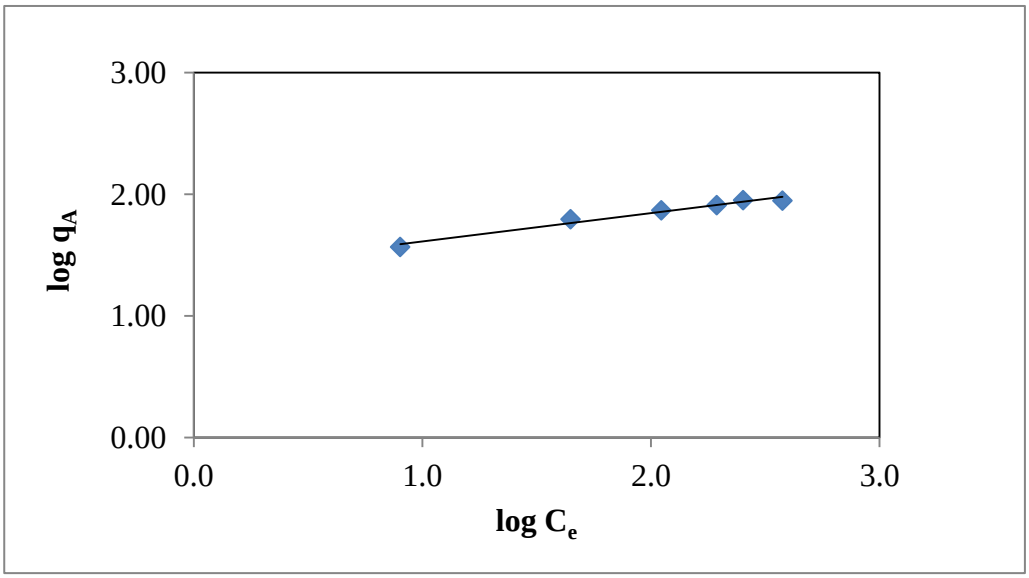

Figure 4.11. Freundlich isotherm model for Cs^{+} adsorption onto bentonite (Initial Cs^{+} concentration range:100-600 mgL^{-1}, Bentonite dosage:2.5 gL^{-1}, T:298 K, Contact time:30 min, pH:8.0±0.1).

Donat and coworkers fitted the experimental data obtained the adsorption of Pb^{2+} and Ni^{2+} onto natural bentonite into Freundlich and Langmuir model equations and It was found that the models fitted the data well. Similar results have been reported for the adsorption of zinc on the natural and Na-exchanged bentonite (Kaya and Ören, 2005) and for the sorption of Cu^{+2}, Zn^{+2} and Co^{+2} onto natural bentonite (Kubilay et al., 2007). Moreover, it was emphasized that 1/n and K_F values were the indicators for the adsorption intensity and adsorption capacity, respectively. A relatively slight slope, hence a high value of n, indicated that adsorption is good over entire range of concentrations studied, while a steep slope, hence small n, indicated that adsorption is good at high concentration but much less at low concentration. A higher value of K_F indicated higher adsorption capacity. It was concluded from that explanation bentonite had a higher capacity for Pb^{2+} than for Ni^{2+} (Donat et al., 2005).

The equilibrium data obtained from batch adsorption studies performed at 298 K was also fitted to Dubinin-Radushkevich isotherm equations (Equation 2.6). The linear plot of the $\ln q_A$ against to ε^2 was given at Figure 4.12. The model constants q_{max}, β and E were calculated as 156 mgg^{-1}, 2.46 x 10^{-9} and 14.3 $kJmol^{-1}$, respectively.

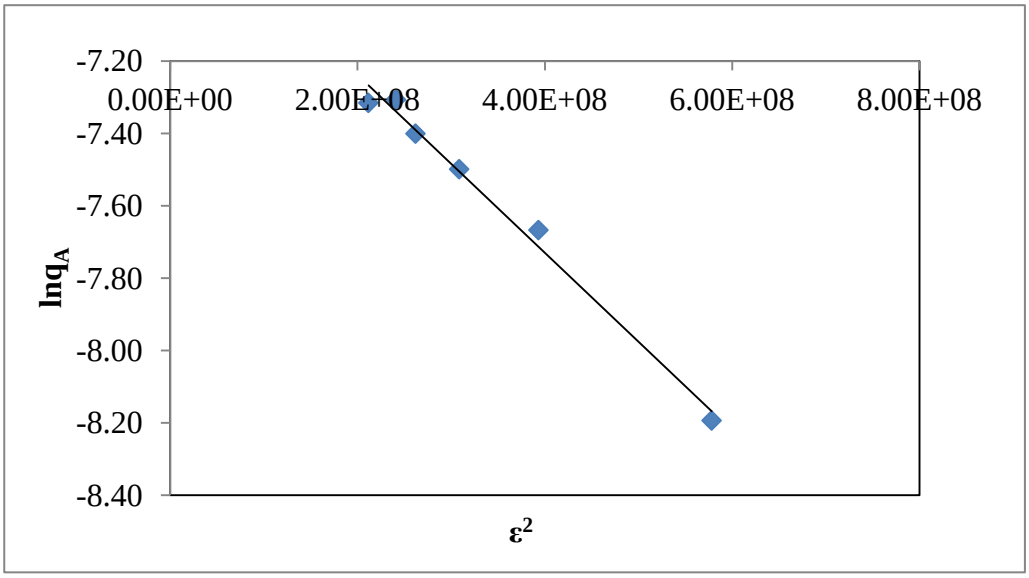

Figure 4.12. Dubinin-Radushkevich isotherm model for adsorption of Cs^+ onto bentonite (Initial Cs^+ concentration range:100-600 mgL^{-1}, Bentonite dosage:2.5 gL^{-1}, T:298 K, Contact time:30 min, pH:8.0±0.1).

The value of E, free energy change of adsorption, indicates that the main adsorption mechanism was ion exchange (Shahwan and Erten, 2002; Xu et al., 2008; Özeroğlu et al., 2011). The difference of q_{max} obtained from Langmuir and D-R models is quite large. The difference may be stemmed from separate definitions of q_{max} in two models. In Langmuir model, q_{max} represents the monolayer coverage, while in D-R model it represents the maximum adsorption of metal ions at the total specific micropore volume of the adsorbent Xu and co-workers studied the adsorption of Pb^{2+} onto bentonite and they fitted the equilibrium data to D-R model and Langmuir model (Xu et al., 2008). The achieved value of q_{max} at Langmuir model was lower than one at D-R model.

4.2.1.6. Effect of Temperature and Thermodynamic Data. The effect of temperature on the adsorption of Cs^+ onto bentonite is displayed in Figure 4.13. As displayed in Figure 4.13, adsorption of Cs^+ onto bentonite decreased with increasing in temperature. K_d (Equation 2.9) values decreased from 1705 mLg^{-1} to 1169 mLg^{-1} with respect to increasing temperature to 338 K from 288 K.

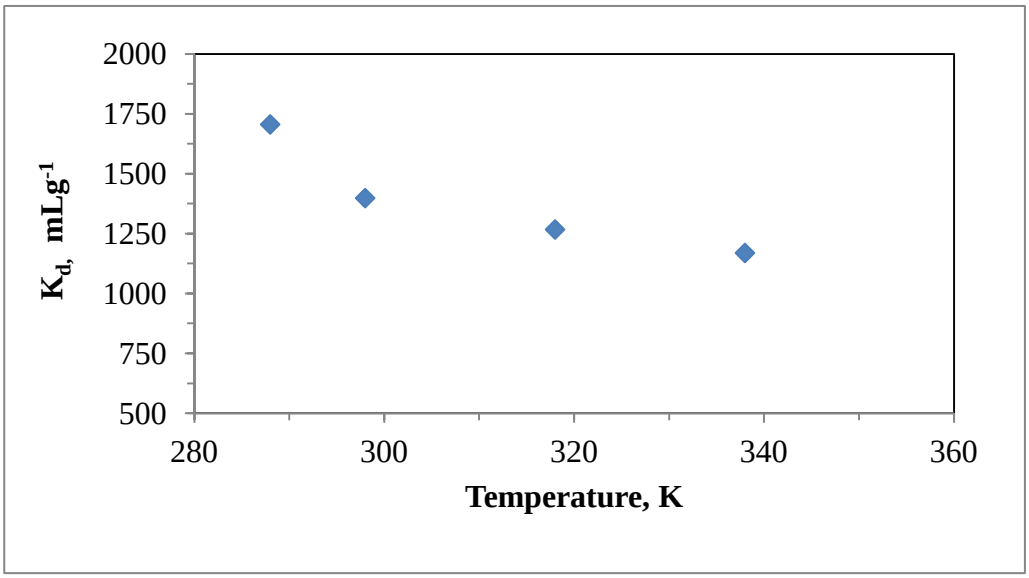

Figure 4.13. Effect of temperature on the adsorption of Cs^+ onto bentonite (Initial Cs^+ concentration: 200 mgL^{-1}, Bentonite dosage: 2.5 gL^{-1}, Contact time: 30 min, pH: 8.0±0.1).

Decreasing tendency in K_d values was observed and even reaching a almost constant condition after 298 K could be stated. Figure 4.14 shows a representative graph of $\ln K_d$ versus 1/T obtained by using experimental data only for initial 200 mgL^{-1} concentration.

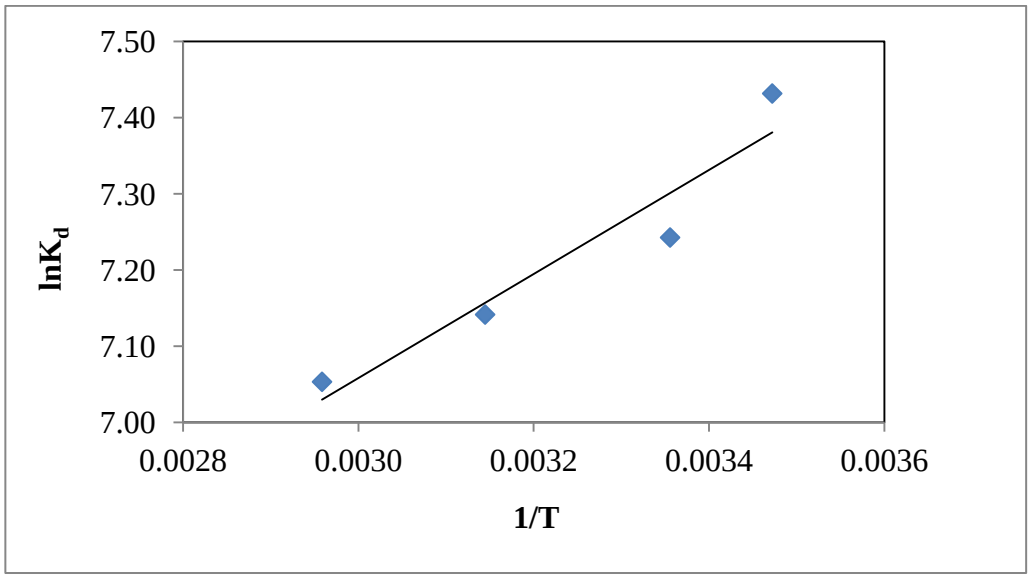

Figure 4.14. Representative plot of $\ln K_d$ against 1/T for adsorption of Cs^+ onto bentonite at different temperatures (Initial Cs^+ concentration: 200 mgL^{-1} Bentonite dosage: 2.5 gL^{-1}, Contact time: 30 min, pH: 8.0±0.1).

The mean values of ΔH^o ($kJmol^{-1}$) and ΔS^o ($J(mol\ K)^{-1}$) or Cs^+ adsorption onto bentonite were obtained by fitting experimental data to Equation 2.14 for initial concentration range from 100 mgL^{-1} to 597 mgL^{-1}. ΔG^o ($kJmol^{-1}$) values were calculated by using equation 2.13 for the specified temperature conditions (Table 4.3).

Table 4.3. Thermodynamic parameters for Cs^+ adsorption onto bentonite (Initial Cs^+ concentration range:100-597 mgL^{-1}).

ΔH^o $kJmol^{-1}$	ΔS^o $J(molK)^{-1}$	ΔG^o, $kJmol^{-1}$			
		288 K	298 K	318 K	338 K
-4.65	39.5	-16.0	-16.4	-17.2	-18.0

The negative value of ΔH^o indicates that the binding of cesium ions onto bentonite surface is exothermic and that lower temperatures enhanced the adsorption of the cesium ions onto bentonite surface. The exothermic behavior of cesium ions adsorption on other solids was reported by various researchers (Shahwan et al., 1998; Bayülken et al., 2011). Positive ΔS^o implies that the adsorption process occurs spontaneously at either high temperature or low temperature, but it indicates an instable arrangement of Cs^+ on the bentonite surface (Shahwan and Erten, 2002; Shahwan, et al., 2006). Positive ΔS^o was obtained during the adsorption of other ions onto bentonite (Rauf and Tahir, 2000; Tahir and Rauf, 2003). Donat and coworkers found that entropy of the adsorption processes of the Pb^{2+} and Ni^{2+} onto bentonite was positive and it indicated that adsorption was irreversible and also positive entropy favors the complexation and stability of the adsorption (Donat et al., 2005).

The negative values of $\Delta G^{\mathbf{o}}$ show the spontaneity of the adsorption process. Both the negative value of ΔH^o and the increase in ΔG^o with an increase in temperature imply that the adsorption process is more favorable at higher temperatures. Furthermore, it must be noted that the difference in sign between E obtained from the D-R isotherms and ΔG^o values is because of definition of E. The magnitudes of both indicate an ion exchange type of sorption mechanism (Shahwan and Erten, 2002).

4.2.2. Adsorption Studies of Cobalt onto Bentonite

Adsorption behavior of Co^{2+} onto bentonite was searched in terms of changing conditions such as pH, contact time, initial Co^{2+} concentration, ionic strength and temperature. The adsorption equilibrium data were fitted to Freundlich, Langmuir and Dubinin-Radushkevich isotherms to calculate the maximum adsorption capacity of the bentonite and the energy of adsorption. Also, these data were used both understanding the mechanism of the adsorption and finding the thermodynamic parameters of the adsorption.

4.2.2.1. Effect of pH. pH is one of the most crucial factors affecting the adsorption capacity of an adsorbent. The pH can affect the adsorption system by changing surface of the adsorbent or the ionic forms of the metal in the suspension. Figure 4.15 shows the effect of the pH on the adsorption of Co^{2+} onto bentonite where the percentage of adsorbed Co^{2+} equals to C_s/C_i*100.

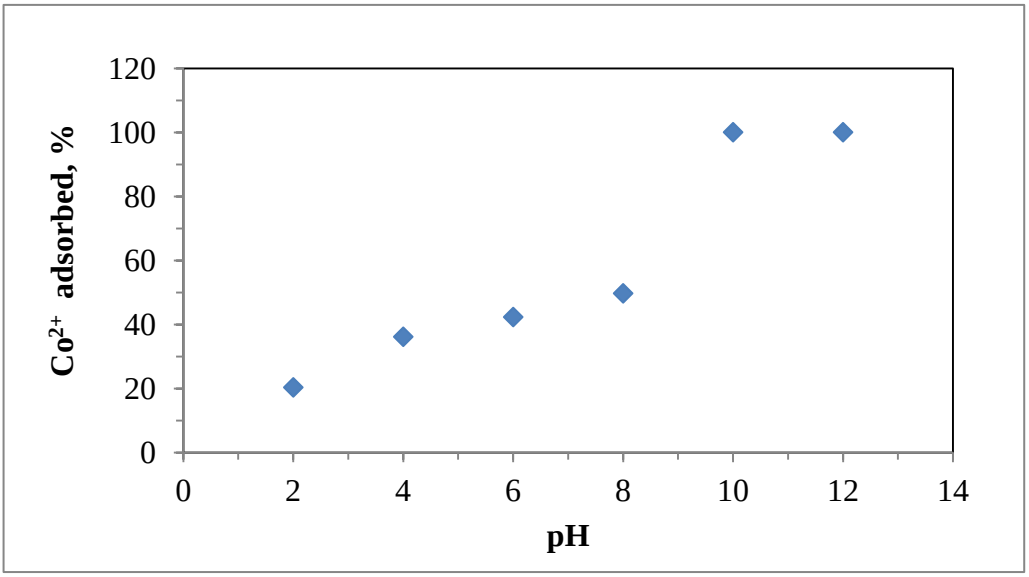

Figure 4.15. Influence of pH on adsorption of Co^{2+} onto bentonite. (Initial Co^{2+} concentration:98 mgL^{-1}, Bentonite dosage:2.5 gL^{-1}, T:298 K, Contact time:30 min).

Increasing pH from 2 to 8 raised the percentage of adsorbed Co^{2+} from 20 % to 50 %, but in alkaline conditions i.e. pH>8, the adsorption steeply increased to 100 %. Khan gives meaningful interpretation to that increase by mentioning precipitation of Co^{2+} as

$Co(OH)_2$ beyond pH 8 (Khan, 2003). Moreover, it was mentioned that after pH 8 distinguishing the adsorption and precipitation was so difficult. Therefore, pH 8 was selected as optimum pH for further experiments during the adsorption of Co^{2+} onto bentonite.

4.2.2.2. Effect of Contact Time. Adsorption of Co^{2+} was investigated as a function of shaking time and Figure 4.16 shows that the adsorption was reached immediately to equilibrium after immediate mixing. Therefore, 30 min was selected as optimum contact time for the adsorption experiments. Similar results were also reported by Kubilay and co-workers in their study performed on the adsorption of Co^{+2}, Zn^{+2} and Cu^{+2} onto bentonite at different pH values (Kubilay et al. 2007).

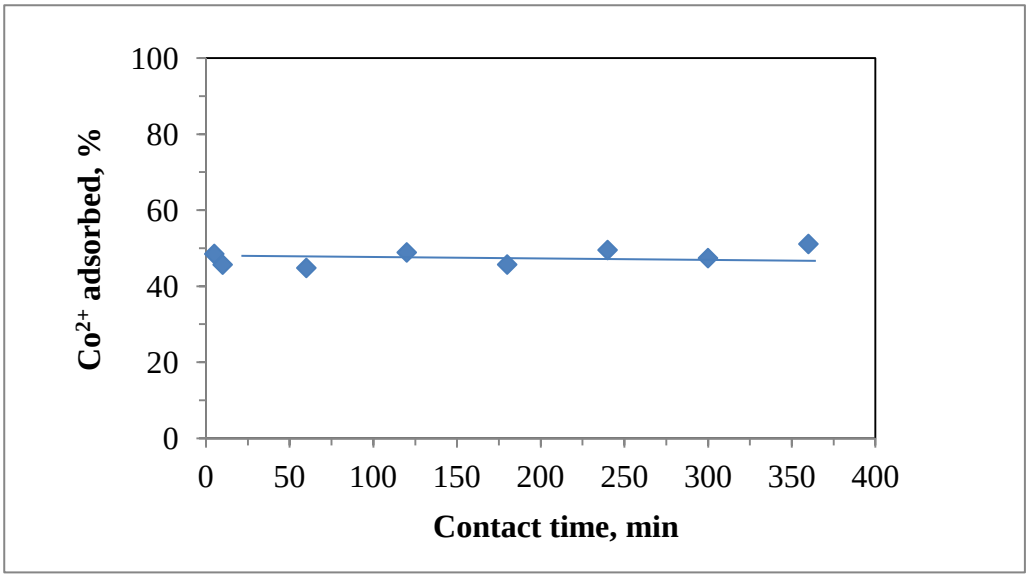

Figure 4.16. Effect of contact time on adsorption of Co^{2+} onto bentonite (Initial Co^{2+} concentration:99.6 mgL^{-1}, Bentonite dosage:2.5 gL^{-1}, T:298 K)

Kinetic studies of adsorption can give some valuable information about adsorption mechanism. Like adsorption of Cs^{+} onto bentonite in that study, cobalt ions accumulate on the surface of the bentonite by the mechanism of the ion-exchange or outer surface complex reactions dominantly.

4.2.2.3. Effect of Initial Cobalt Concentration. Effect of initial concentration on the adsorption of Co^{2+} onto bentonite was investigated while keeping the amount of bentonite constant i.e. 2.5 gL^{-1} (Figure 4.17). The amount of adsorbed Co^{2+} (q_A) increased from 1.84 mgg^{-1} to 20.2 mgg^{-1} for initial Co^{2+} ion concentration range of 5-300 mgL^{-1}. When the initial concentration of Co^{2+} in solution was increased beyond 100 mgL^{-1}, qA value displayed a stationary phase being almost constant as 18 mgg^{-1} at 2.5 gL^{-1} of bentonite dosage. On the contrary, percentage of adsorbed Co^{2+} changed from 92 % to 17 % showing a decreasing profile for respective initial Co^{2+} range as 5-300 mgL^{-1} respectively. In a similar manner, the sharp decrease in adsorbed Co^{2+} amount coincided well with the q_A saturation condition at which the initial Co^{2+} concentration was 100 mgL^{-1}.

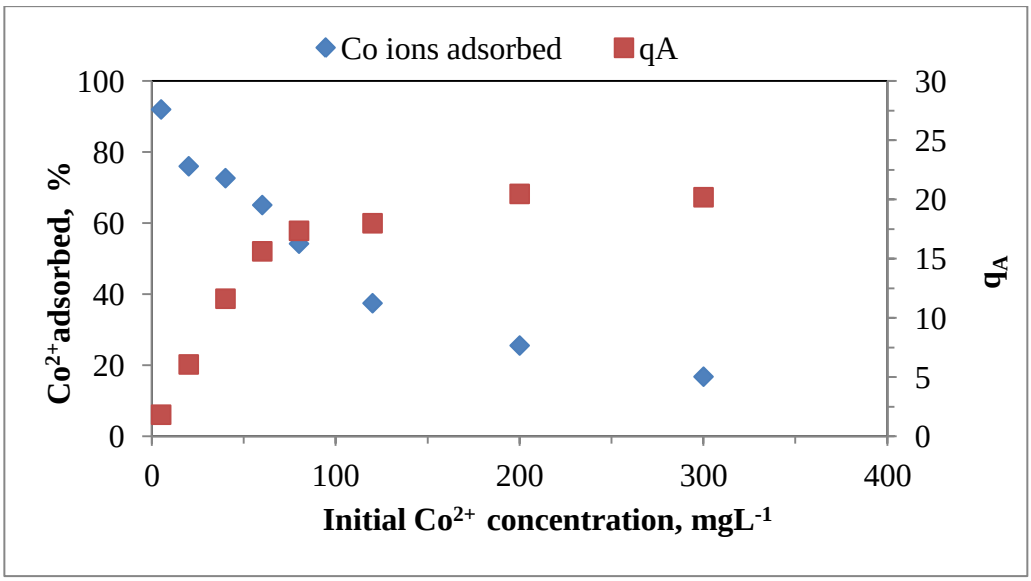

Figure 4.17. Effect of initial Co^{2+} concentration on adsorption of Co^{2+} onto bentonite (Initial Co^{2+} concentration range:5-300 mgL^{-1}, Bentonite dosage:2.5gL^{-1}, T:298 K, Contact time:30 min, pH:8.0±0.1).

It was also emphasized that energetically less favorable sites of the adsorbent become involved in adsorption with increasing the concentrations of the metal ion (Khan, 2003; Kubilay et al., 2007). Kubilay and colleagues also stated that the pores of clay minerals filled after a certain time and later increasing metal concentration did not make a considerable effect on adsorption (Kubilay et al., (2007).

4.2.2.4. Effect of Ionic Strength. Like that of Cs^+ ions, adsorption pattern of Co^{2+} ions onto bentonite with increasing the concentration of electrolyte in the solution was downward. Ionic strength of the medium was changed by varying the concentration of NaCl of the solution. The percentage of the adsorption displayed decreasing trend where the values of were 43.4 %, 36.5 % and 10.2 % when adding $1x10^{-3}$ M, $1x10^{-2}$ and $1x10^{-1}$ M concentration of NaCl to the solution, respectively. Furthermore, the corresponding q_A values changed as 16.5, 13.7 and 3.90 mgg^{-1}, respectively (Table 4.4).

Table 4.4. Adsorption of Co^{2+} onto bentonite with the change of ionic strength.

	Concentration of NaCl in metal solution			
	Absence of NaCl	$1x\ 10^{-3}$	$1x\ 10^{-2}$	$1x\ 10^{-1}$
Adsorption, %	46.2	43.4	36.5	10.2
$q_{A,}$ mgL^{-1}	17.7	16.5	13.7	3.90

The downward tendency of the adsorption implies that the adsorption mechanism was dominantly ion-exchange, whereas Yu and colleagues reported that ionic strength has no remarkable effect on the adsorption of Co^{2+} onto bentonite and it was concluded from that the dominant mechanism should be surface complexation (Yu et al., 2006). One can draw the following conclusion from above results that basal plane, permanently negatively charged, is the active site for ion-exchange adsorption and edge surface can be active site for surface complexation adsorption mechanism. Krapiel and his collaboraters gave the support to this conclusion by stating that bentonites could adsorb the metals via two different mechanisms, firstly by cation exchange in the interlayers resulting from the interactions between ions and negative permanent basal plane charge and secondly by the formation of inner sphere complexes through $Si\text{-}O^-$ and $Al\text{-}O^-$ groups at the clay particle edges (Krapiel et al., 1999).

Ren and his coworkers investigated the effect of the ionic strength on the adsorption of Pb^{2+} onto bentonite, Al_2O_3 and SiO_2. Ionic strength had a very weak or no influence on Pb^{2+} adsorption on all samples. It was stated that the competition between Pb^{2+} and Na^+ with solid surface sites was not influenced by the concentration of Na^+ in the solution. The actual colloidal state of the samples may dominate the adsorption mechanism and therefore limited the the effect of the ionic strength (Ren et al., 2007).

4.2.2.5. Adsorption Isotherm Modeling of Cobalt Adsorption onto Bentonite. The adsorption isotherm of Co^{2+} was obtained at optimum pH and contact time at room temperatures by changing the initial concentration of the cobalt ions in the range of 5-300 mgL^{-1} and by keeping bentonite dosage constant as 2.5 gL^{-1} (Figure 4.18). C_e values varied between 0.40-250 mgL^{-1} while the values of q_A calculated were in the range of 1.84-20.2 mgg^{-1} depending on the initial concentration of Co^{2+} in the solution. The shape of adsorption isotherm of Co^{2+} ions (Figure 4.18) onto bentonite was L-type isotherm shape which usually concave to concentration axes. It suggests the progressive saturation of bentonite surface with increase of Co^{2+} concentrations in the solution.

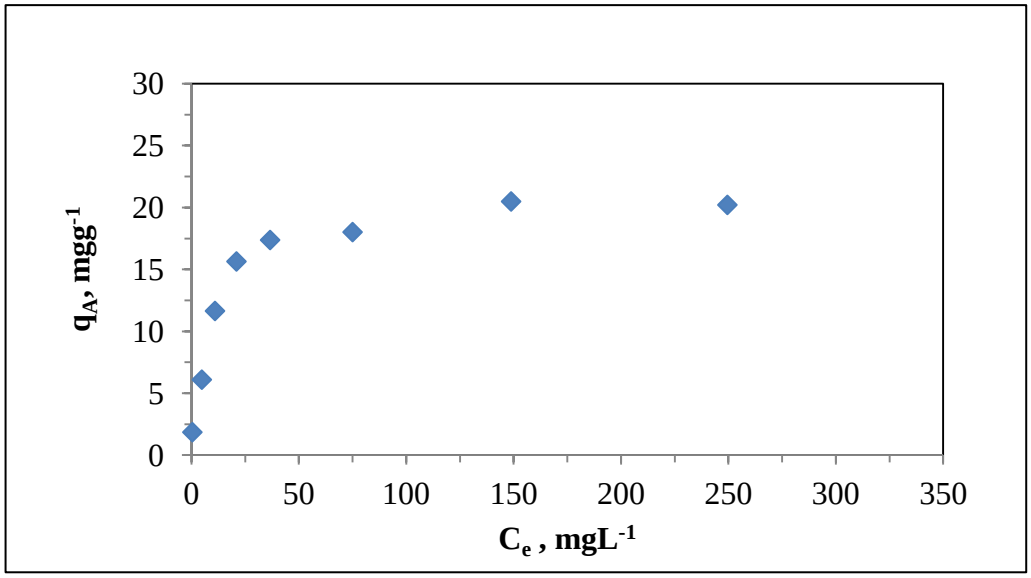

Figure 4.18. Adsorption isotherm of Co^{2+} onto bentonite (Initial Co^{2+} concentration range: 5-300 mgL^{-1}, Bentonite dosage: 2.5 gL^{-1}, T: 298K, Contact time: 30 min, pH: 8.0±0.2).

The equilibrium data were fitted to Langmuir isotherm equation (Equation 2.2) and the linear plot is obtained when $1/q_A$ is plotted against $1/C_e$ over the entire concentration range studied giving regression coefficient of R^2=0.977 (Figure 4.19). The Langmuir constant parameters and statistic fits of the adsorption data were calculated. Values for q_{max} and K_a were 15.9 $mgg^{-1}$and 3.26x 10^{-2} Lmg^{-1}, respectively. R^2 value of the Langmuir isotherm model indicated that the model efficiently describes the equilibrium data and the high maximum adsorption capacity (q_{max}) implies that bentonite can be highly usable for the cobalt removal from a radioactive liquid waste.

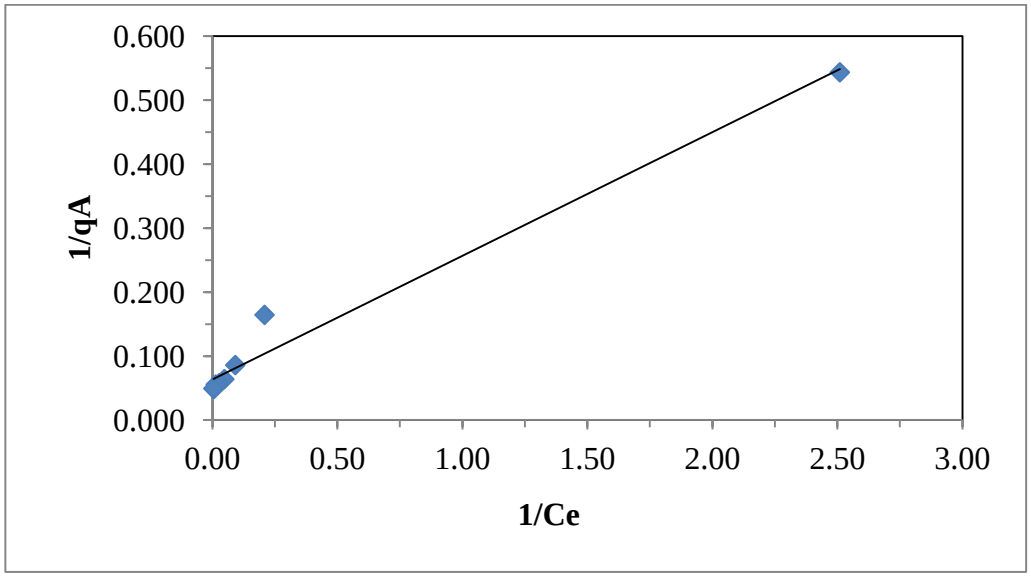

Figure 4.19. Langmuir isotherm model for Co^{2+} adsorption onto bentonite (Initial Co^{2+} concentration range:5-300 mgL^{-1}, Bentonite dosage:2.5 gL^{-1}, T:298 K, Contact time:30 min, pH:8.0±0.2).

As previously stated, Kubilay and co-workers searched the adsorption of Co^{2+}, Zn^{2+} and Cu^{2+} onto bentonite at different pH values (Kubilay et al., 2007). Langmuir model efficiently described the adsorption processes for all metals according to equilibrium data obtained. Highest adsorption capacity, q_{max}, was found as 16.9 mgg^{-1} for Co^{2+} at pH 9. This is slightly higher than the result obtained at pH 8 in this study. It may be related to simultaneously operating precipitation contributing to adsorption at higher pH conditions. Xu and colleagues studied Pb^{2+} adsorption onto bentonite and the equilibrium data was applied to Langmuir adsorption isotherm equation. The maximum adsorption capacity of the bentonite for lead ions was found as 68.5 mgg^{-1} (Xu et al., 2008).

The equilibrium data were also fitted to Freundlich isotherm equation (Equation 2.4) and the linear plot of the $logq_A$ against $logC_e$ would give the slope as 1/n and intercept as logk with a regression coefficient of R^2= 0.959 (Figure 4.19). The Freundlich constant parameters were calculated according to data obtained from statistic fit. The values for K_F and 1/n were 3.1 Lg^{-1} and 0.469, respectively. K_F is a constant related with adsorption capacity and the value of K_F demonstrated that bentonite was a good adsorbent for Co^{2+} adsorption and 1/n value was between 0 and 1 implying that adsorption of Co^{2+} onto

bentonite was favorable at studied conditions. The values of R^2 for Freundlich and Langmuir, which were 0.959 and 0.977 respectively were so close, so it was concluded that the equilibrium data fitted well either Freundlich or Langmuir models. Rauf and Tahir (2000) performed adsorption experiments using either Fe^{2+} or Mn^{2+} onto bentonite in aqeous solutions. Freundlich and Langmuir isotherm models were successfully applied to the adsorption equilibrium data. It was concluded that adsorption of both metals appeared to follow Langmuir as well as the Freundlich isotherm models.

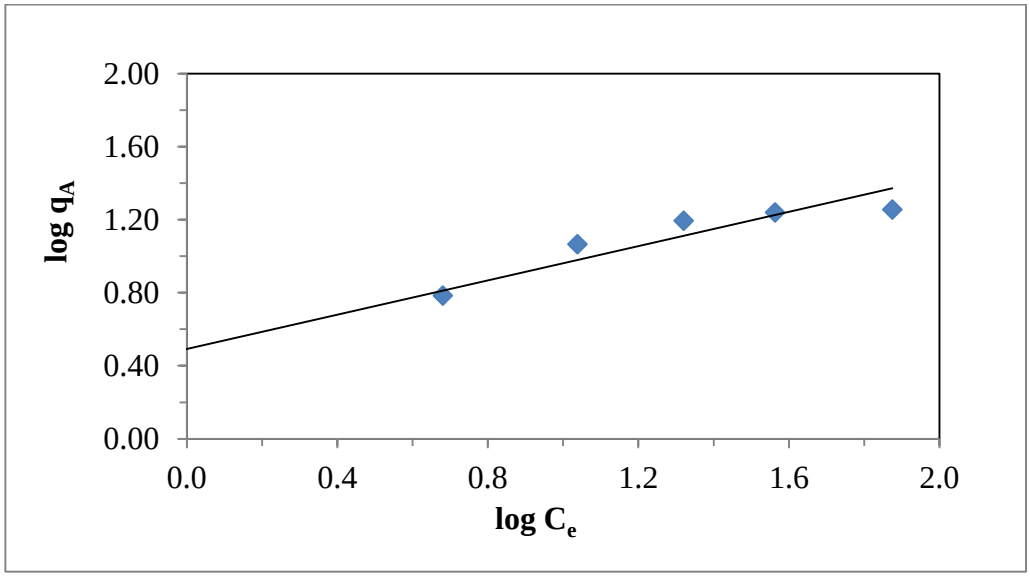

Figure 4.20. Freundlich isotherm model for Co^{2+} adsorption onto bentonite (Initial Co^{2+} concentration range:5-300 mgL^{-1}, Bentonite dosage:2.5 gL^{-1}, T:298 K, Contact time:30 min, pH:8.0±0.2).

Equilibrium data obtained from batch adsorption studies performed at 298 K was also fitted to Dubinin-Radushkevich isotherm equation (Equation 2.6). The linear plot of the lnq_A against to ε^2 was given at Figure 4.21. The model constants q_{max}, β and E were calculated as 50.7 mgg^{1-}, 3.68 x 10^{-9} and 11.7 $kJmol^{-1}$, respectively. Value of E points out that the dominant mechanism for the adsorption of cobalt onto bentonite is ion-exchange and like adsorption of the cesium onto bentonite, higher value of q_{max} was obtained than one obtained from Langmuir isotherm model because of representing total volume of micropore on the surface.

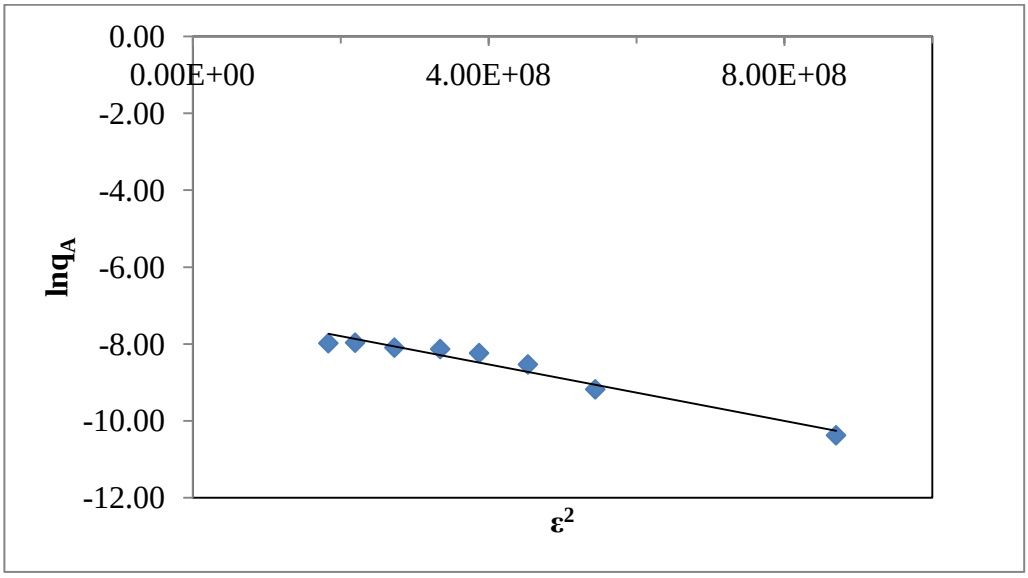

Figure 4.21. Dubinin-Radushkevich isotherm model for adsorption of Co^{2+} onto bentonite (Initial Co^{2+} concentration range:5-300 mgL^{-1}, Bentonite dosage:2.5 gL^{-1}, T:298 K, Contact time:30 min, pH:8.0±0.2).

Donat and coworkers fitted the adsorption equilibrium data obtained from the Pb^{2+} and Ni^{2+} adsorption onto natural bentonite into the D-R. q_{max} values of D-R model for the Pb^{2+} and Ni^{2+} were 49.7 mgg^{-1} and 69.3 mgg^{-1}. E values for the Pb^{2+} and Ni^{2+}, 10.80 $kJmol^{-1}$ and 10.20 $kJmol^{-1}$, respectively, were in the range of ion exchange mechanism of adsorption process (Donat et al., 2005).

4.2.2.6. Effect of Temperature and Thermodynamic Data. Distribution coefficient, K_d values were calculated according to Equation 2.9 at different temperatures. As could be seen from Figure 4.22, adsorption of Co^{2+} onto bentonite increases with increase in temperature. K_d values increased from 125 mLg^{-1} at 288 K to 272 mLg^{-1} at 338 K. This upward tendency indicates that adsorption of cobalt ion onto bentonite has endothermic nature.

Metwally and his coworkers studied the effect of temperature on the adsorption of Cs^{+}, Co^{2+} and Sr^{2+} onto hydrous titanium oxide. It was found that adsorption increased with an increase in adsorption temperature by implying a strengthening of adsorbate-adsorbent interactions at higher temperature (Metwally et al., 2007).

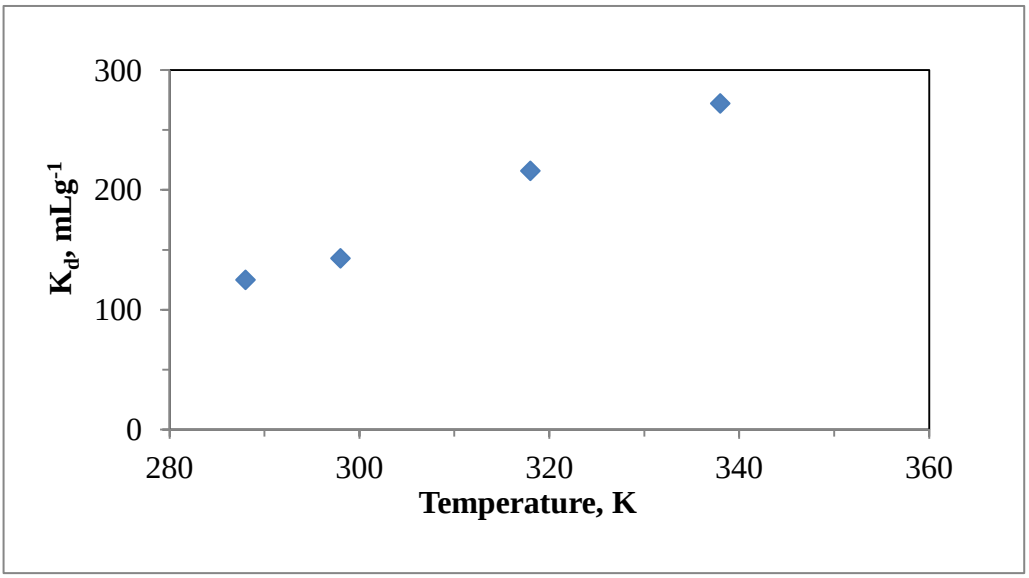

Figure 4.22. Effect of temperature on adsorption of Co^{2+} onto bentonite (Initial Co^{2+} concentration:198 mgL^{-1}, Bentonite dosage:2.5 gL^{-1}, Contact time:30min, pH:8.0±0.2).

Figure 4.23 shows a representative graph of $\ln K_d$ versus 1/T obtained by using experimental data only for initial 198 mgL^{-1} Co^{2+} concentration. Mean values of ΔH^o ($kJmol^{-1}$) and ΔS^o ($J(mol\ K)^{-1}$) of Co^{2+} adsorption onto bentonite were obtained by fitting experimental data to Equation 2.14 for initial concentration range from 26 mgL^{-1} to 205 mgL^{-1}. ΔG^o values were calculated by using Equation 2.13 for different temperatures (Table 4.5).

Table 4.5. Thermodynamic parameters for Co^{2+} adsorption on bentonite (The initial Co^{+2} concentration range:26-205 mgL^{-1}).

ΔH^o $kJmol^{-1}$	ΔS^o $J(mol\ K)^{-1}$	ΔG^o, $kJmol^{-1}$			
		288 K	298 K	318 K	338 K
13.6	39.5	-12.5	-13.4	-15.3	-17.1

Positive value of ΔH^o ($kJmol^{-1}$) as 13.6 indicates that the binding of Co^{2+} onto bentonite surface was endothermic and that higher temperatures enhanced the adsorption of the cesium ions onto bentonite surface. In a similar manner, Tahir and Rauf (2003) reported that Ni^{2+} ions adsorption onto bentonite exhibited endothermic behavior. Positive ΔS^o ($J(mol\ K)^{-1}$) as 39.5 emphasizes that the adsorption process was spontaneous. The

reason could be attributed to an instable arrangement of Co^{2+} ions on the bentonite surface under the specified pH condition. Omar and co-workers investigated the adsorption of radioactive $^{60}Co^{2+}$ onto modified bentonite. It was reported that positive ΔS^o was resulted from hydration effect and water molecules separated from hydrated metal ions or from the surface may cause an increase in entropy (Omar et al., 2009).

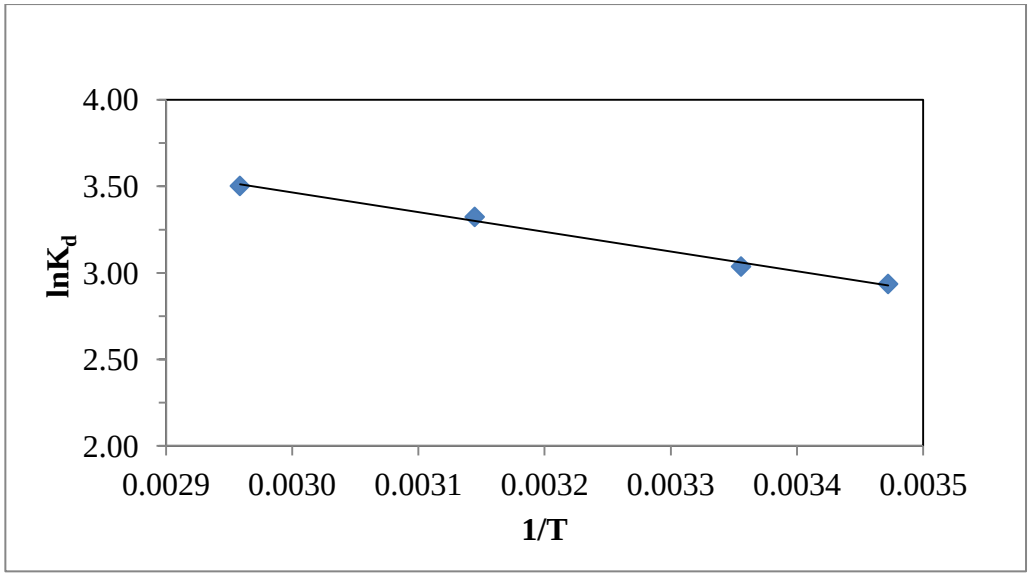

Figure 4.23. Representative plot of lnK_d against 1/T for adsorption of Co^{2+} onto bentonite at different temperatures (Initial Co^{2+} concentration:198 mgL^{-1}, Bentonite dosage:2.5 gL^{-1}, Contact time:30 min, pH 8.0±0.2).

Negative values of ΔG^o ($kJmol^{-1}$) achieved as -12.5, -13.4, -15.3 and -17.1 under temperature conditions of 288 K, 298 K, 318 K, and 338 K respectively also show the spontaneity of the adsorption process. The increase in ΔG^o with an increase in temperature implies that the adsorption process is more favorable at higher temperatures (Tahir and Rauf, 2003).

4.2.3. Adsorption Studies of Cesium onto Perlite

Adsorption behavior of Cs^+ onto perlite was investigated under varying experimental conditions such as pH, contact time, initial Cs^+ concentration, ionic strength and temperature. The adsorption equilibrium data were fitted to Freundlich, Langmuir and

Dubinin-Radushkevich isotherms to evaluate the maximum adsorption capacity of the bentonite and the energy of adsorption. Also, these data were used to assess which mechanism of the adsorption is dominant. Moreover, the equilibrium data obtained under changing temperature conditions were used to evaluate the thermodynamic parameters.

4.2.3.1. Effect of pH. The investigation in order to evaluate the effect of pH on the adsorption of Cs^+ onto perlite was performed in the range of pH 2-12. pH dependent variations in the amount of Cs^+ adsorbed onto perlite was observed at pH conditions of 4 and 8. (Figure 4.24).

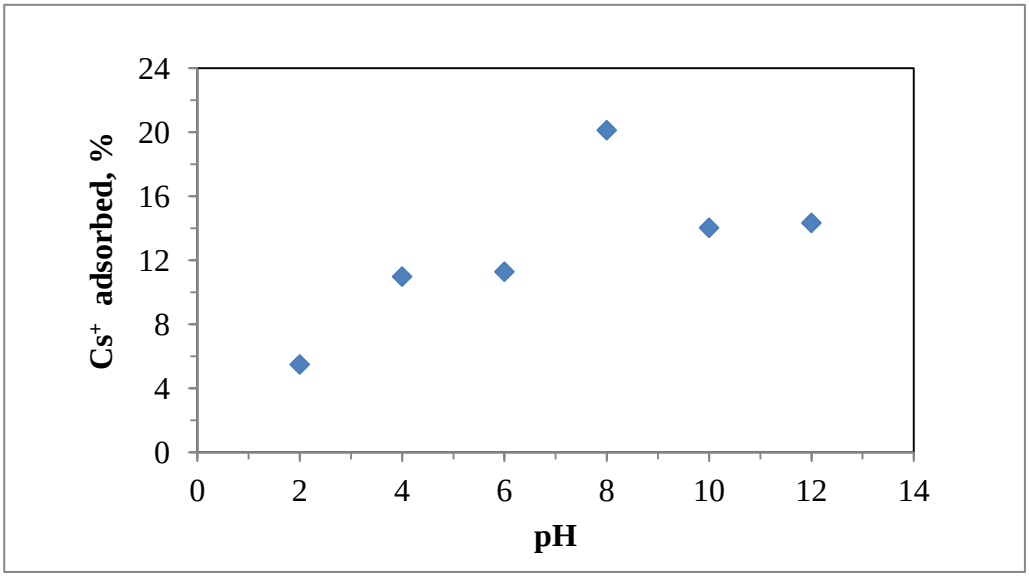

Figure 4.24. Influence of pH on adsorption of Cs^+ onto perlite. (Initial Cs^+ concentration: 32.8 mgL^{-1}, Perlite dosage: 2.5 gL^{-1}, T: 298 K, Contact time: 30 min).

Increasing the pH from 2 to 4 enhanced the percentage of adsorbed Cs^+ from 5.79 - to 11%, but above pH 4 the adsorption slightly decreased. After that, the percentage of adsorbed Cs^+ increased to 20.1 % at pH 8 and again decreased. The perlite has no net point of zero charge and exhibits negative zeta potential value at pH range of 3-11(Doğan et al., 1997). This explained the increase in the percentage of adsorption between pH 2 and 8 because aqueous cesium species is solely Cs^+ when the surface of perlite is negative at this pH range by enhancing adsorption onto perlite with the attraction forces.

4.2.3.2. Effect of Contact Time. Figure 4.25 shows the adsorption percentage of Cs^+ as a function of contact time. It can be seen that there was almost no change in adsorption during 180 min contact time after mixing and the adsorption was very fast and reached equilibrium instantaneously.

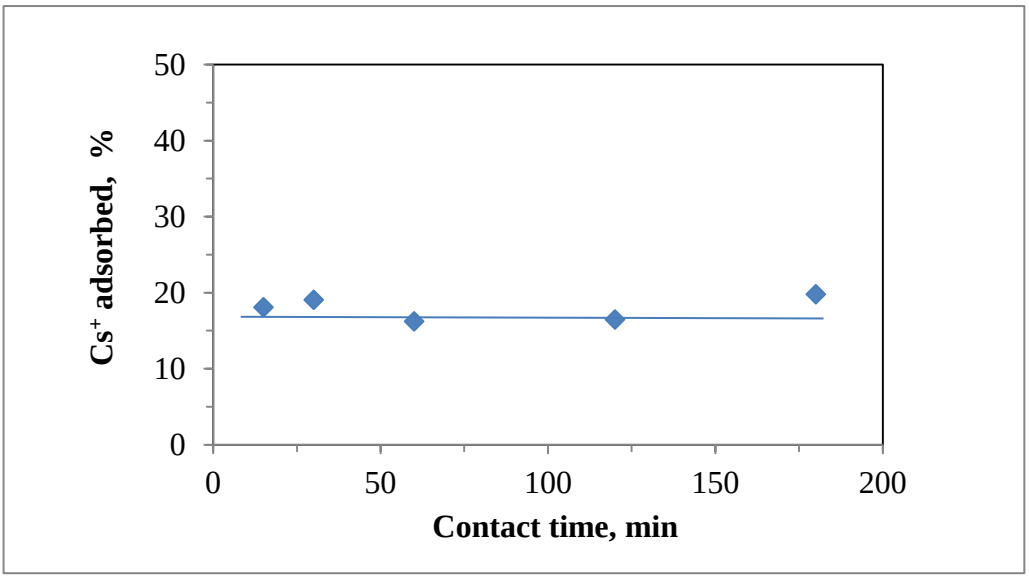

Figure 4.25. Effects contact time on adsorption of Cs^+ onto perlite (Initial Cs^+ concentration: 32.8 mgL^{-1}, Perlite dosage: 2.5 gL^{-1}, T: 298 K).

The percentage of adsorbed Cs^+ was found as 19 % and 19.8 % at 30 and 180 min, respectively. There is a negligible change in the percentage of adsorbed Cs^+ after 30 min as seen in the Figure 1.2. Therefore, a period of 30 min was chosen as contact time for the further experiments of Cs^+ adsorption onto perlite.

4.2.3.3. Effect of Initial Cesium Concentration. The amount of adsorbed Cs^+ (q_A) increased from 0.22 mgg^{-1} to 1.96 mgg^{-1} for initial Cs^+ ion concentration range 0.75-33.6 mgL^{-1}. On the other hand, the percentage of adsorbed Cs^+ decreased from 70.5 % to 14.6 %. When the initial concentration of Cs^+ in aqueous solution was increased beyond the 20 mgL^{-1}, q_A value slightly changed for perlite dosage of 2.5 gL^{-1} (Figure 4.26).

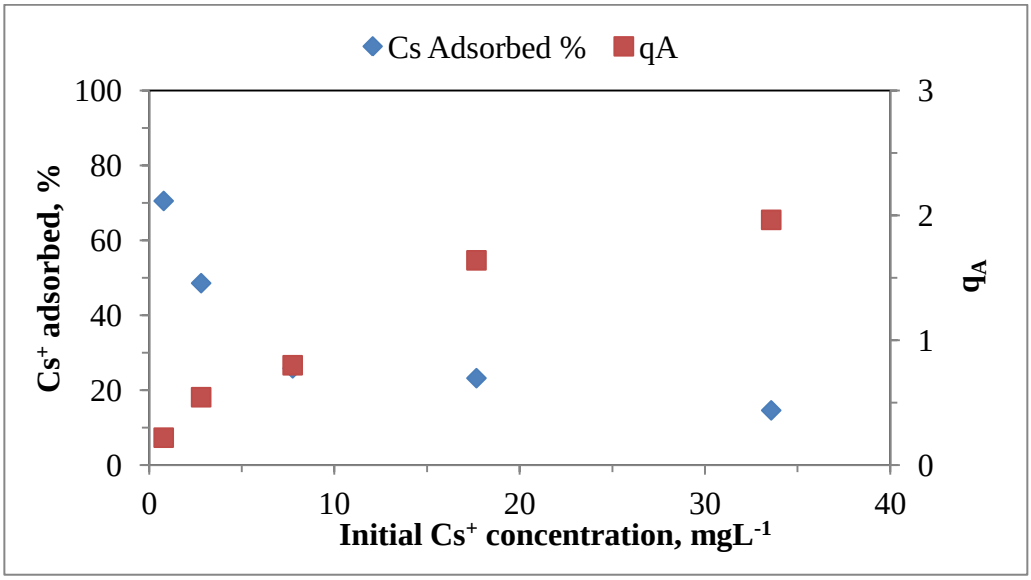

Figure 4.26. Effect of initial Cs^+ ion concentration on adsorption of Cs^+ adsorption onto perlite (Initial Cs^+ concentration range: 0.75-33.6 mgL^{-1}, Perlite dosage: 2.5 gL^{-1}, T: 298 K, Contact time: 30 min, pH: 8.0±0.2).

In the presence of an initial Cs^+ concentration of 7.4 mgL^{-1}, q_A value was 0.8 coinciding with 25.3 % adsorption of Cs^+ onto perlite. Irani and colleagues demonstrated that there was increase in lead ion adsorption capacity of perlite with raising the initial lead concentration (Irani et al., 2011). It was emphasized that that increase was solely due to an increase of the numbers of lead ions available to binding sites of adsorbents. Therefore, active sites of perlite became saturated and adsorption capacity approached a constant value.

4.2.3.4. Effect of Ionic Strength. Ionic strength of the medium was changed by varying the concentration of NaCl of the solution. The percentage of the adsorption displayed decreasing trend where the values of were 35.1 %, 12.8 % and 0.766 % when adding $1x10^{-3}$ M, $1x10^{-2}$ and $1x10^{-1}$ M concentration of NaCl to the solution, respectively. Furthermore, the corresponding q_A values changed as 0.816, 0.328 and 0.0240 mgg^{-1}, respectively (Table 4.6).

Table 4.6. Adsorption of Cs^+ onto perlite with the change of ionic strength.

	Concentration of NaCl in metal solution			
	Absence of NaCl	1x 10^{-3}	1x 10^{-2}	1x 10^{-1}
Adsorption, %	35.9	35.1	12.8	0.766
$q_{A,}$ mgL^{-1}	0.843	0.816	0.328	0.0240

Doğan and co-workers stated that as the concentration of electrolyte increases the surface of the perlite becomes less negative (Doğan et al., 1997). By acting as indifferent electrolytes which are defined as counterions adsorbed by electrolytic attraction and thereby by compressing the double layer, electrolytic solutions render the solid surface less negative. The above statement is in a good agreement with the result of this study. The increase in the concentration of NaCl in the solution gives rise to the decrease of the adsorption of Cs ions onto perlite due to weak interaction between less negative perlite surface and positive cesium ions.

4.2.3.5. Adsorption Isotherm Modeling of Cesium Adsorption onto Perlite. Adsorption isotherm was drawn with the equilibrium data obtained from batch adsorption experiments at pH and contact time and room temperature and by keeping bentonite dosage constant as 2.5 gL^{-1} (Figure 4.27). C_e value varied between 0.23-28.7 mgL^{-1} depending on the initial concentration of Cs^+ in the solution. The values of q_A to be calculated were in the range of 0.22-2.0 mgg^{-1} for the corresponding C_e values.

Adsorption isotherm of Cs^+ onto perlite shows L-type isotherm shape which usually concave to concentration axes. It implies the progressive saturation of perlite surface with increase of Cs^+ concentration in the solution. Adsorption data were analyzed with the aid of different adsorption isotherm models namely Langmuir, Freundlich and The Dubinin-Radushkevich (D-R).

Equilibrium data were fitted to Langmuir isotherm equation (Equation 2.2) and the linear plot is obtained when $1/q_A$ is plotted against $1/C_e$ over the entire concentration range studied giving regression coefficient of R^2=0.960 (Figure 4.28).

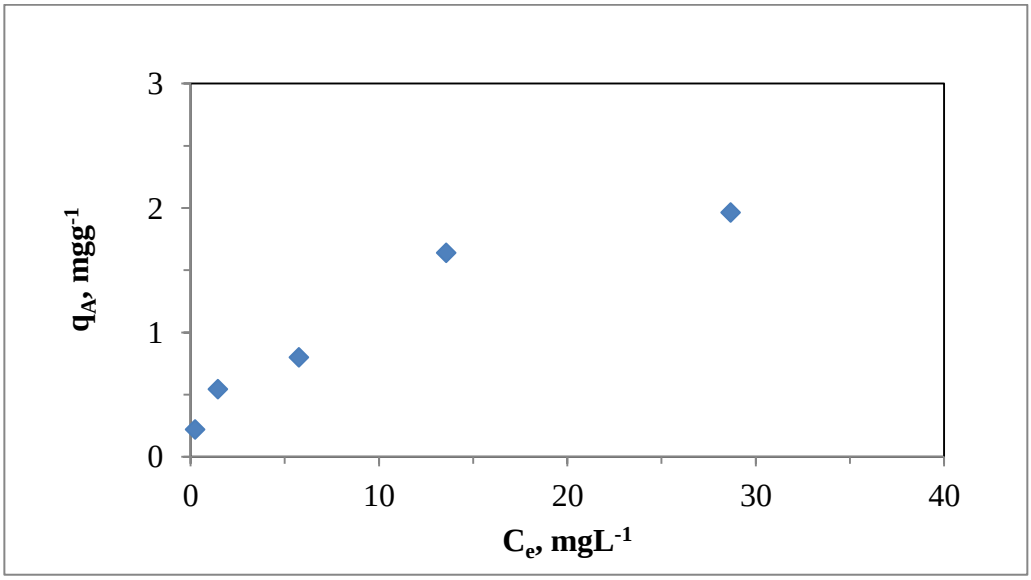

Figure 4.27. Adsorption isotherm of Cs^+ onto perlite (Initial Cs^+ concentration range:0.75-33.6 mgL^{-1}, Perlite dosage:2.5 gL^{-1}, T:298 K, Contact time:30 min, pH 8.0±0.2).

The Langmuir constant parameters and statistic fits of the adsorption data were calculated. The values for q_{max} and K_a were 1.22 $mgg^{1-}$and 0.943 Lmg^{-1}, respectively.

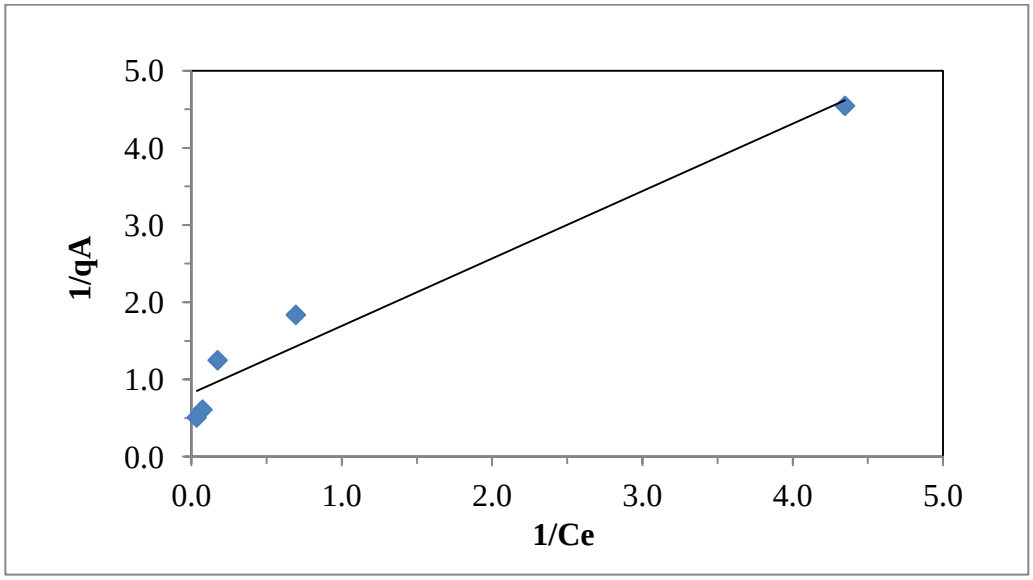

Figure 4.28. Langmuir isotherm model for Cs^+ adsorption onto perlite (Initial Cs^+ concentration range:2.8-33.6 mgL^{-1}, Perlite dosage:2.5 gL^{-1}, T:298 K, Contact time:30 min, pH:8.0±0.1).

The R^2 value of the Langmuir isotherm model indicated that the model effectively describes the equilibrium data but the value of maximum adsorption capacity of perlite for Cs^+ is less than that of bentonite. It is more likely stemmed from layered-structure of the bentonite. Ghassabzadeh and colleagues studied adsorption of Hg^{2+}, Cu^{2+} and Ag^+ onto perlite (Ghassabzadeh et al., 2010). The values of q_{max} for these ions are 0.346, 1.95 and 8.46 mgg^{-1}, respectively. Moreover, Mostaidi and co-workers found the q_{max} values as 1.79 and 2.24 for the adsorption of Cd^{2+} and Ni^{2+} onto perlite, respectively (Mostaidi et al., 2010).

Equilibrium data were fitted to Freundlich isotherm equation (Equation 2.4) and the linear plot of the $logq_A$ against $logC_e$ would give the slope as 1/n and intercept as $logK_F$ with a regression coefficient of R^2= 0.946 (Figure 4.29). The values for K_F and 1/n were 0.432 Lg^{-1} and 0.457, respectively. K_F is a constant related with adsorption capacity and the value of K_F demonstrated that perlite was a good adsorbent for Cs adsorption and 1/n value was between 0 and 1 indicating that adsorption of Cs onto perlite was favorable at studied conditions.

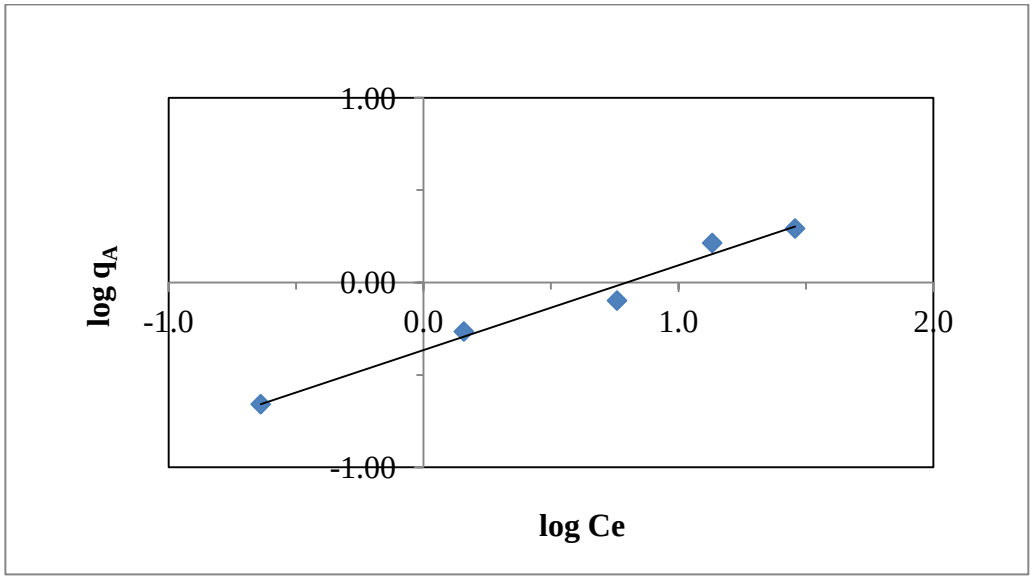

Figure 4.29. Freundlich isotherm model for Cs^+ adsorption onto perlite (Initial Cs^+ concentration range:2.8-33.6 mgL^{-1}, Perlite dosage:2.5 gL^{-1}, T:298 K, Contact time: 30min, pH 8:0±0.1).

The values of R^2 for Freundlich and Langmuir, which were 0.946 and 0.960, respectively were so close, so it was concluded that the equilibrium data followed well either Freundlich or Langmuir models.

The equilibrium data obtained batch adsorption studies performed at 298 K was also fitted to Dubinin-Radushkevich isotherm equation (Equation 2.6). The linear plot of the lnq_A against to ε^2 was given at Figure 4.29. The model constants q_{max}, β and E were calculated as 8.36mgg^{-1}, 3.41 x 10^{-9} and 12.1kJmol^{-1}, respectively.

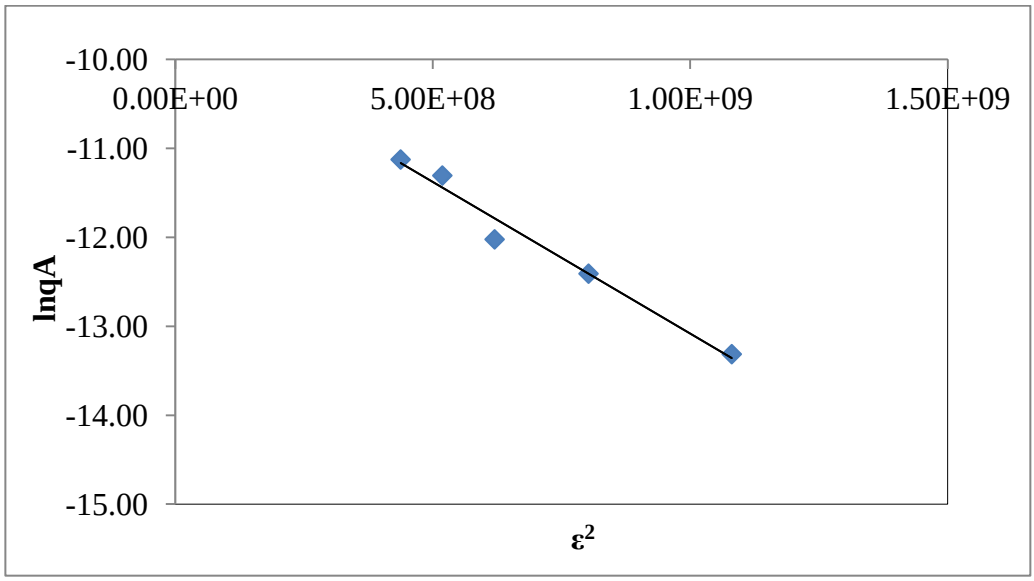

Figure 4.30. Dubinin-Radushkevich isotherm model for adsorption of Cs^+ onto perlite (Initial Cs^+ concentration range:0.75-33.6 mgL^{-1}, Perlite dosage:2.5 gL^{-1}, T:298 K, Contact time:30 min, pH:8.0±0.2).

The value of E gives information about adsorption mechanism (Xu et al., 2008). If E value lies between 8-16 kJmol^{-1}, the main adsorption process is ion exchange. The obtained E value of that study indicated that the main adsorption mechanism of Cs^+ ions onto perlite was ion exchange, like Cs^+ adsorption onto bentonite. Sarı and his coworkers studied the Sb^{3+} removal from aqueous solutions by Mn-modified expanded perlite. D-R isotherm model equation was applied to equilibrium data. The value of E was found as 6.3 kJmol^{-1} by proving that adsorption of Sb^{3+} onto Mn- modified expanded perlite occurred with the physical forces (Sarı et al., 2012).

4.2.3.6. Effect of Temperature and Thermodynamic Data. The effect of varying temperature conditions were displayed with reference to the changes calculated in K_d (mLg^{-1}) in Figure 4.31. As could be seen from Figure 4.30, adsorption of Cs^+ onto perlite expressed a slightly increasing trend with increase in temperature. K_d values rose to 180 mLg^{-1} at 338 K from 139mLg^{-1} at 288 K.

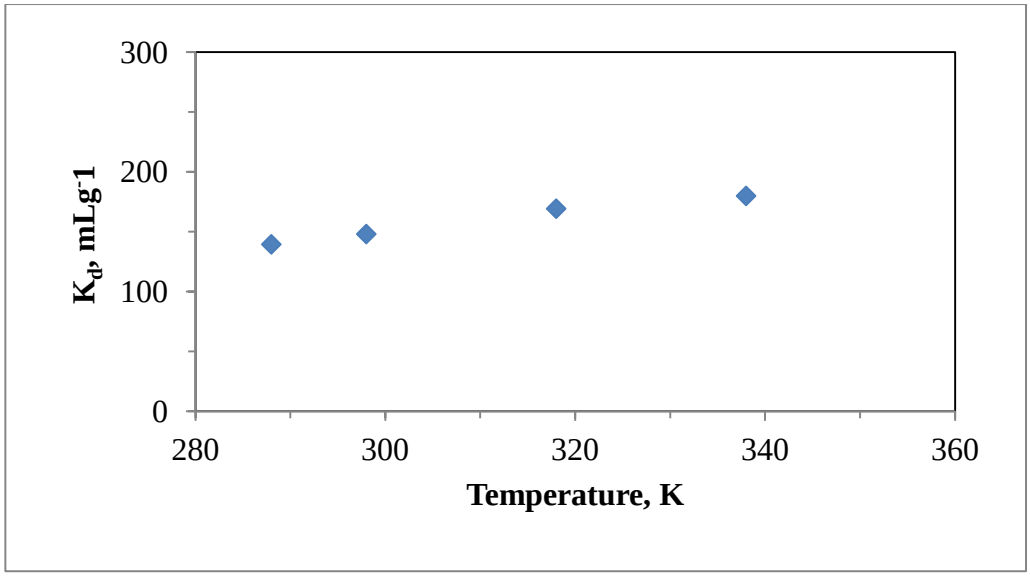

Figure 4.31. Effect of temperature on the adsorption of Cs^+ onto perlite (Initial Cs^+ concentration:7.74 mg L^{-1}, Perlite dosage:2.5 g L^{-1}, Contact time:30 min, pH:8.0±0.1).

Figure 4.32 shows a representative graph of $\ln K_d$ versus 1/T obtained by using experimental data only for initial 7.74 mgL^{-1} concentration. The mean values of ΔH^o and ΔS^o of Cs^+ adsorption onto perlite were obtained by fitting experimental data to equation 2.13 for initial concentration range from 2.8 mg L^{-1} to 33.6 mg L^{-1} (Table 4.7).

Table 4.7. Thermodynamic parameters for Cs^+ adsorption on perlite (Initial Cs^+ concentration range:2.8-33.6 mg L^{-1})

ΔH^o $kJmol^{-1}$	ΔS^o $J(mol\ K)^{-1}$	ΔG^o, $kJmol^{-1}$			
		288 K	298 K	318 K	338 K
3.5	54.7	-11.2	-11.8	-12.9	-14.0

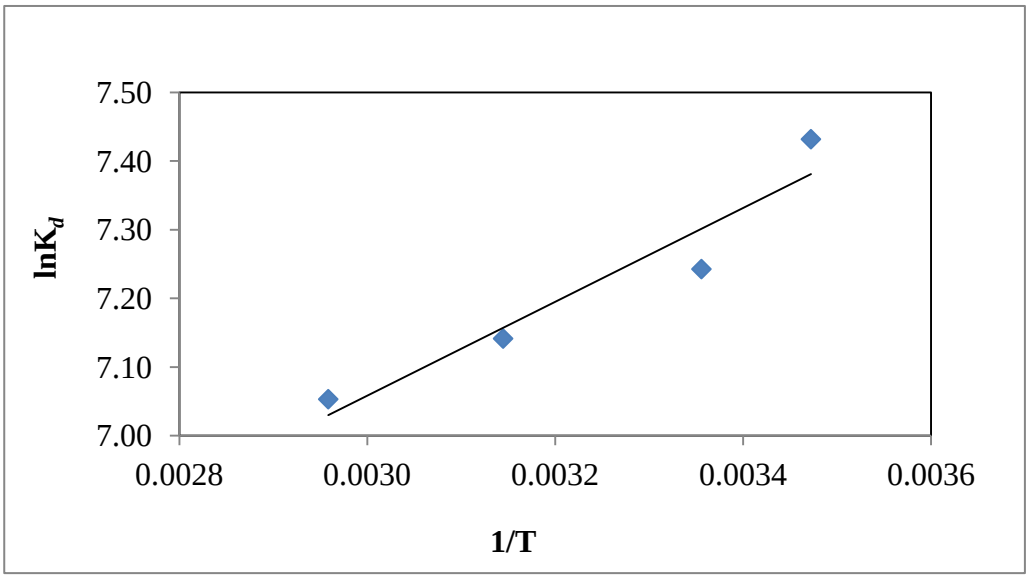

Figure 4.32. Representative plot of $\ln K_d$ against 1/T obtained during the adsorption of Cs^+ onto perlite at different temperatures (Initial Cs^+ concentration:7.74 mgL^{-1}, Perlite dosage:2.5 g L^{-1}, Contact time:30 min, pH:8.0±0.1).

Positive value of ΔH^o indicates that adsorption of cesium ions onto perlite surface is endothermic and that higher temperatures enhanced the adsorption of the cesium ions onto perlite surface. On the other hand, in the literature it was reported that some metals, like Cu^{+2}, Ag^+, Hg^{2+}, Pb^{2+}, Cd^{2+} and Ni^{2+} show the exothermic behavior during the adsorption onto perlite (Mostaedi et al., 2010; Irani, et al. 2011; Ghassabzadeh et al., 2010). Positive ΔS^o implies that the adsorption is spontaneous process and it indicates increased disorders and randomness on the surface of the perlite during adsorption.(Irani et al., 2011).

Negative values of ΔG^o show adsorption of Cs^+ onto perlite surface is thermodynamically feasible and spontaneous in nature at 288-338 K. Furthermore, feasibility of the adsorption is higher because of the increased value of ΔG^o with raising temperatures. Sari and colleagues reported that the adsorption of Cu^{2+} and Pb^{2+} onto perlite is feasible and spontaneous due to negative values of the ΔG^o at 293-323 K but the decrease in ΔG^o values with increase temperature shows a decrease in feasibility of adsorption at higher temperatures (Sari et al., 2007).

4.2.4. Adsorption Studies of Cobalt onto Perlite

Adsorption behavior of Co^{2+} onto perlite was investigated under varying experimental conditions such as pH, contact time, initial Co^{2+} concentration, ionic strength and temperature. Adsorption equilibrium data were fitted to Freundlich, Langmuir and Dubinin-Radushkevich isotherm models to evaluate the maximum adsorption capacity of the perlite and the energy of adsorption. Adsorption data were also used to assess the dominating adsorption mechanism. Moreover, the equilibrium data obtained by changing temperature were used to evaluate the thermodynamic parameters.

4.2.4.1. Effect of pH. Effect of pH on the adsorption of Co^{2+} onto perlite was evalauted by the experimets performed in the range of pH 2-12 (Figure 4.33). Adsorption of Co^{2+} onto perlite increased significantly as pH increased.

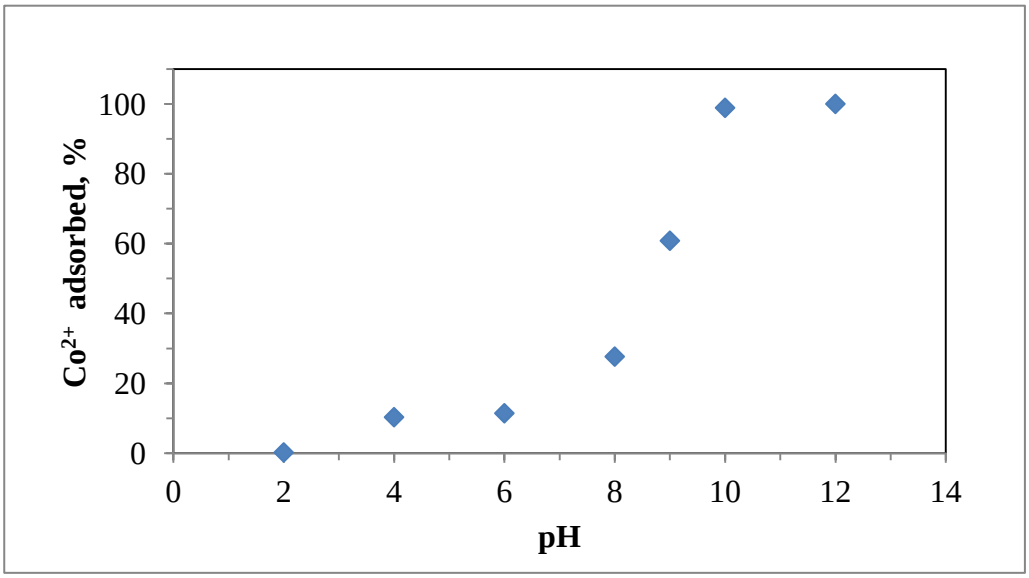

Figure 4.33. Influence of pH on adsorption of Co^{2+} onto perlite. (Initial Co^{2+} concentration: 9.8 mgL^{-1}, Perlite dosage:2.5 gL^{-1}, T:298 K, Contact time:30 min).

Increasing the pH from 2 to 8 enhanced the percentage of adsorbed Co^{2+} ions from 0.20 to 27.7 %, moreover under more alkaline conditions, i.e. pH 8-10, the percentage of adsorbed Co^{2+} increased to 98.9 % possibly due to Co^{2+} precipitation as $Co(OH)_2$ (Yuzer et al., 2008). At low pH values (pH<6), low adsorption efficiency could be explained by an

increase in positive charge density on the surface of perlite and by the presence of positively charged edge groups. As pH increases, the percentage of adsorbed Co^{2+} increases since the surface of the perlite becomes more negative and decreases the electrostatic repulsion between metal and surface. Moreover, edge surfaces of perlite also become more negatively charged leading to enhanced adsorption. Since, above pH 8 conditions, precipitation of Co^{2+} ions as hydroxide could possibly contributed to the removal of Co^{2+} ions, the subsequent adsorption studies were performed at pH 8 in order to differentiate the adsorption from precipitation during the removal of cobalt from the aqueous solution.

4.2.4.2. Effect of Contact Time. Figure 4.34 illustrates the adsorption percentage of Co^{2+} ions as a function of contact time. Adsorption was so fast at initial contact time of 5 min and no significant change was attained with respect to increasing contact time (120 min).

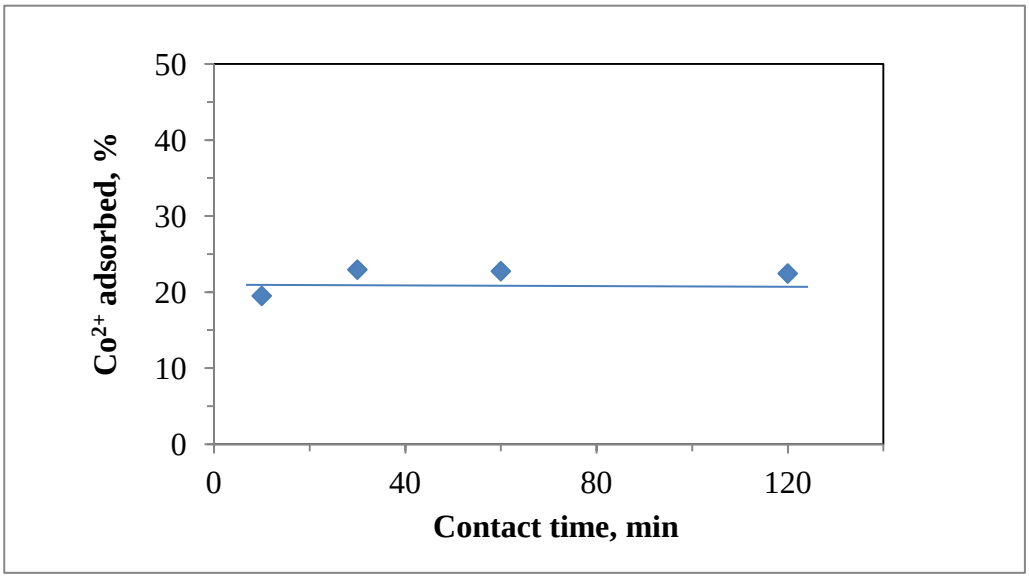

Figure 4.34. Effect of contact time on adsorption of Co^{2+} onto perlite (Initial Co^{2+} concentration:9.85 mgL^{-1}, Perlite dosage:2.5gL^{-1}, T:298K).

Percentage of adsorbed Co^{2+} was found as 22.9 and 22.4 % at contact times of 30 and 180 min, respectively. There is a negligible change in the percentage of adsorbed Co^{2+} after 30 min as seen in the Figure 4.34. Therefore, a period of 30min was chosen as contact time for the further experiments of Co^{2+}adsorption onto perlite.

4.2.4.3. Effect of Initial Cobalt Concentration. Amount of adsorbed Co^{2+} (q_A) increased from 0.22 mgg^{-1} to 2.48 mgg^{-1} for the initial Co^{2+} concentration range 0.5-38 mgL^{-1}. On the other hand, the percentage of adsorbed Co^{2+} decreased from 96.5 to 16.3 % for the same range. When the initial concentration of Co^{2+} in solution was increased beyond the around 20 mgL^{-1}, q_A value remained almost constant at 2.5 gL^{-1} of bentonite dosage (Figure 4.35).

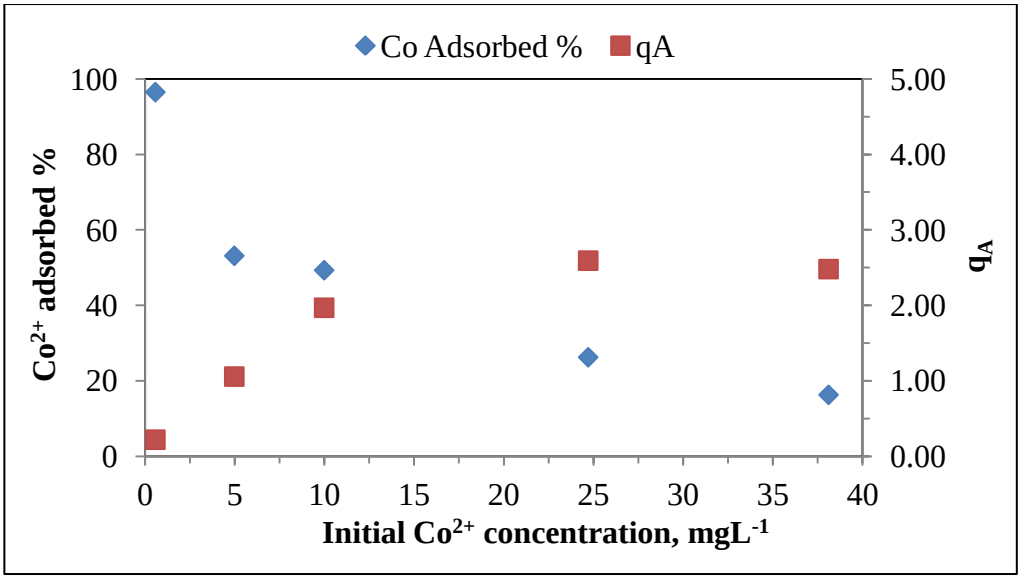

Figure 4.35. Effect of initial Co^{2+} concentration on the adsorption of Co^{2+} onto perlite (Initial Co^{2+} concentration range:0.5-38 mgL^{-1}, Perlite dosage:2.5 gL^{-1}, T:298 K, Contact time:30 min, pH:8.0±0.2).

With respect to the results attained, adsorption of Co^{2+} and Cs^{+} onto either perlite or bentonite has shown similar pattern with the change of initial metal concentration. As initial metal concentration increases, adsorption elevated towards to a constant value expressing a saturation type surface attraction. Irani and his coworkers investigated the effect of initial concentration on lead removal by perlite, dolomite and diatomite. It was reported that adsorption capacity of lead ions by studied adsorbents increased with an increase in the initial lead concentration and then approached a fixed value. This increase was mainly resulted from the increase of the numbers of lead ions available to binding sites of adsorbents. At higher lead concentration, the active sites became saturated and therefore adsorption capacity approached a constant value for studied adsorbents (Irani et al., 2011).

However, Talip and colleagues reported that thorium (20 to 250 mgL^{-1}) adsorption from aqueous solution onto perlite reached the highest value at an initial concentration of 50 mgL^{-1} and decreased rapidly after that point (Talip et al., 2009).

4.2.4.4. Effect of Ionic Strength. Ionic strength of the solution affected the adsorption of the cobalt ions onto perlite adversely. The percentage of the adsorption displayed decreasing trend where the values of were 45.1 %, 24.2 % and 7.12 % when adding $1x10^{-3}$ M, $1x10^{-2}$ and $1x10^{-1}$ M concentration of NaCl to the solution, respectively. Furthermore, the corresponding q_A values changed as 0.916, 0.496 and 0.148 mgg^{-1}, respectively (Table 4.8).

Table 4.8. Adsorption of Co^{2+} onto perlite with the change of ionic strength.

	Concentration of NaCl in metal solution			
	Absence of NaCl	$1x\ 10^{-3}$	$1x\ 10^{-2}$	$1x\ 10^{-1}$
Adsorption, %	53.1	45.1	24.2	7.2
q_A, mgL^{-1}	1.06	0.916	0.496	0.148

Silber and co workers studied the Zn^{2+} adsorption by perlite by evaluating the effects of pH, ionic strength and temperature on the adsorption. Ionic strength effect was investigated by changing the concentration of $NaClO_4$ background electrolyte as 0.001, 0.01 and 0.1 $molL^{-1}$ and by keeping pH as 7.6. It was concluded that the extent of Zn^{2+} adsorption decreases as the ionic strength increased. Furthermore, the influence of ionic strength increased as the initial Zn^{2+} concentration increased and as pH decreased (Silber et al., 2012). This result was in accordance with the results of this study because Co^{2+} and Zn^{2+} have the same oxidation state and similar chemical properties as transition metals. Positive sodium ions coming from background electrolyte solution adheres to the specific adsorption sites on the perlite as their concentration in the solution increases by preventing the adsorption of cobalt ions or zinc ions onto perlite.

4.2.4.5. Adsorption Isotherm Modeling of Cobalt Adsorption onto Perlite. Adsorption isotherm of Co^{2+} onto perlite is displayed in Figure 4.36. Adsorption isotherm of Co^{+2} onto perlite shows L-type isotherm shape which usually displays a saturation type trend following an increasing trend. As explained previously it implies the progressive saturation of perlite surface with increase of Co^{2+} concentrations in solution. C_e value varied between 0.02-31.9 mgL^{-1} depending on the initial concentration of Co^{2+} in solution. The values of q_A to be calculated were in the range of 0.22-2.48 mgg^{-1} for the corresponding C_e values.

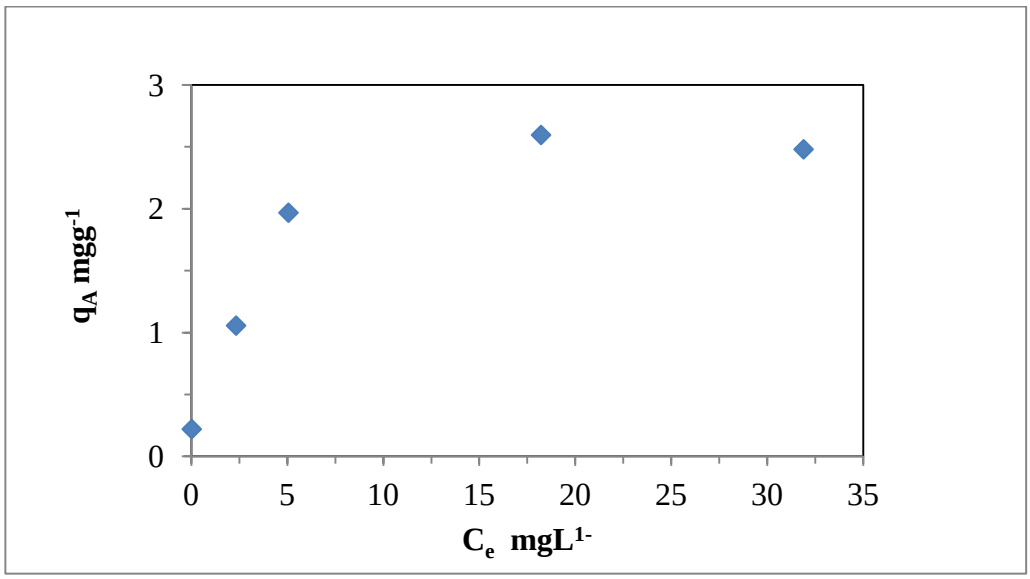

Figure 4.36. Adsorption isotherm of Co^{2+} onto perlite (Initial Co^{2+} concentration range: 0.5-38 mgL^{-1}, Perlite dosage:2.5 gL^{-1}, T:298 K, Contact time:30 min, pH:8.0±0.1).

Equilibrium data were fitted to Langmuir isotherm equation (Equation 2.2) and the linear plot is obtained when $1/q_A$ is plotted against $1/C_e$ over the entire concentration range giving a regression coefficient of R^2=0.986 (Figure 4.37). The Langmuir constant parameters and statistic fits of the adsorption data were calculated. The values for q_{max} and K_a were 1.83 mgg^{-1} and 6.83 Lg^{-1}, respectively. The R^2 value of the Langmuir isotherm model indicated that the model effectively describes the equilibrium but the value of maximum adsorption capacity for Co^{2+} ion adsorption onto perlite is more less than that of onto bentonite. It is more probably resulted from the exchangeable cations between layers of the bentonite.

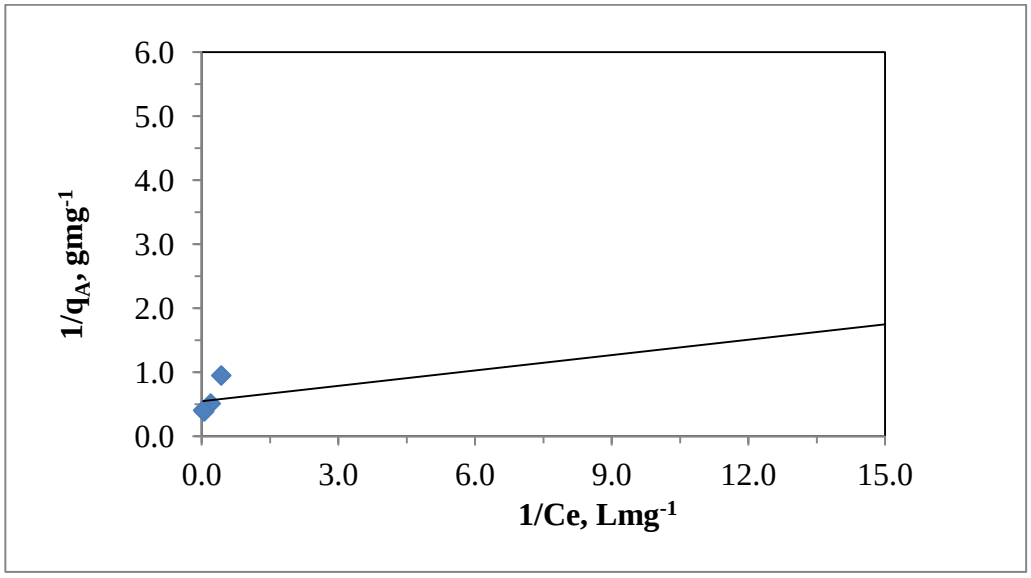

Figure 4.37. Langmuir isotherm model for Co^{2+} adsorption onto perlite (Initial Co^{2+} concentration range:0.5-38 mgL^{-1}, Perlite dosage:2.5 gL^{-1}, T:298 K, Contact time:30 min, pH:8.0±0.1).

Equilibrium data were also applied to Freundlich isotherm equation (Equation 2.4) and the linear plot of the $logq_A$ against $logC_e$ would give the slope as 1/n and intercept as $logK_F$ with a regression coefficient of R^2 equals to 0.975 (Figure 4.38). The Freundlich constant parameters were calculated according to data obtained from statistic fit. The values for K_F and1/n were 0.881 Lg^{-1} and 0.348, respectively. Since K_F is a constant related with the adsorption capacity, the value of K_F (0.881 Lg^{-1}) demonstrated that perlite could be used as an adsorbent for Co^{2+}. 1/n value (0.348) is between 0 and 1 indicating that adsorption of Co^{2+} onto perlite was favorable under the specified experimental conditions.

Besides metals, adsorption of methyl violet from aqueous solution onto perlite surface was reported (Doğan and Alkan, 2003). The equilibrium data was applied to both of the adsorption models i.e. Langmuir and Freundlich models. It was stated that Langmuir model was more favorable than Freundlich model.

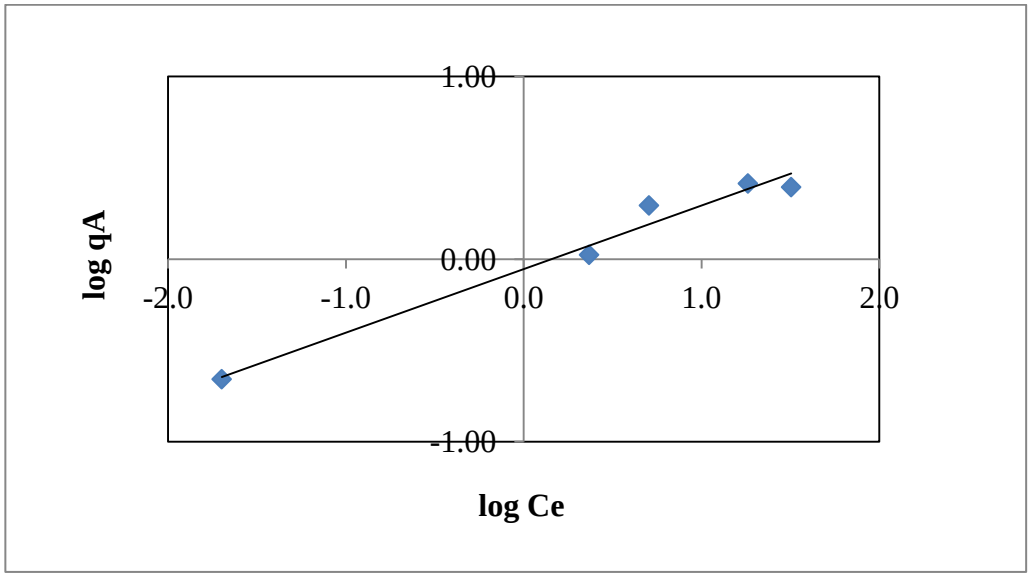

Figure 4.38. Freundlich isotherm model for Co^{2+} adsorption onto perlite (Initial Co^{2+} concentration range:0.5-38 mgL^{-1}, Perlite dosage:2.5 gL^{-1}, T:298 K, Contact time:30 min, pH:8.0±0.1).

The equilibrium data obtained batch adsorption studies performed at 298 K was also fitted to Dubinin-Radushkevich isotherm equations (Equation 2.6). The linear plot of the lnq_A against to ε^2 was given at Figure 4.39. The model constants q_{max}, β and E were calculated as 6.34 mgg^{-1}, 2.49 x 10^{-9} and 14.2 $kJmol^{-1}$, respectively.

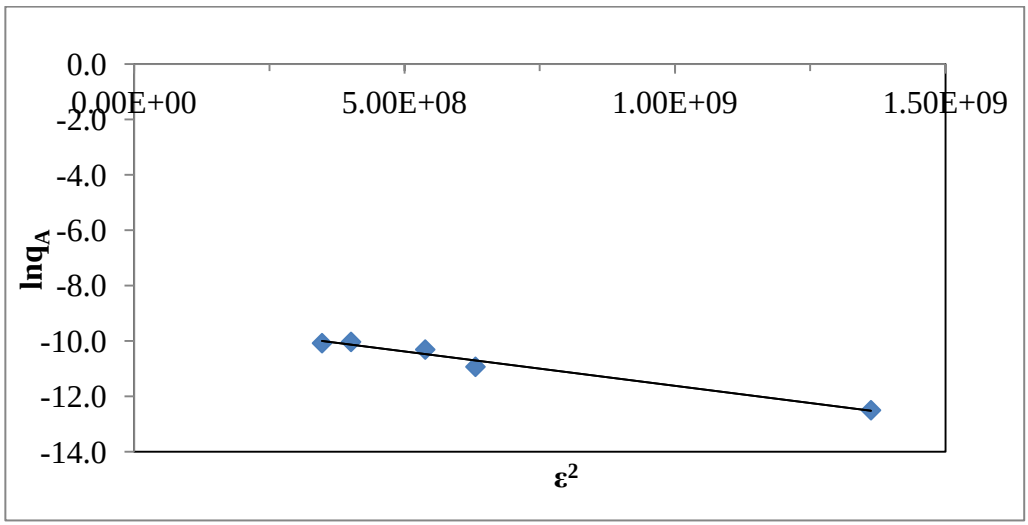

Figure 4.39. Dubinin-Radushkevich isotherm model for adsorption of Co^{2+} onto perlite (Initial Co^{2+} concentration range:0.5-38 mgL^{-1}, Perlite dosage:2.5 gL^{-1}, T:298 K, Contact time:30 min, pH:8.0±0.1).

The value of E gives valuable information about adsorption mechanism. If E value lies between 8-16 kJmol^{-1}, the main adsorption process is ion exchange. The obtained E value of that study indicated that the main adsorption mechanism of Co^{2+} ions onto perlite was ion exchange, like Co^{2+} adsorption onto bentonite.

4.2.4.6. Effect of Temperature and Thermodynamic Data. As could be seen from Figure 4.40, adsorption of Co^{2+} ions onto perlite increased with increase in temperature. K_d values rose to 303 mLg^{-1} at 338 K from 858 mLg^{-1} at 288K.

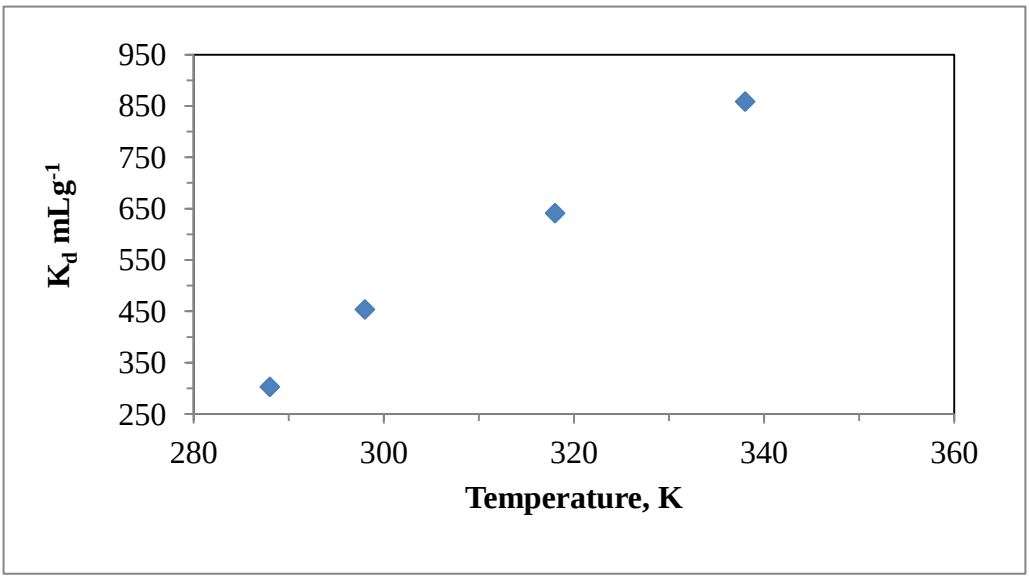

Figure 4.40. Effect of temperature on adsorption of Co^{2+} onto perlite (Initial Co^{2+} concentration:4.97 mgL^{-1}, Perlite dosage:2.5 gL^{-1}, Contact time:30 min, pH:8.0±0.1).

Figure 4.41 shows a representative graph of lnK_d versus 1/T obtained by using experimental data only for initial 4.97 mgL^{-1} concentration of Co^{2+} ions. The mean values of ΔH^o and ΔS^o of Co^{2+} adsorption onto perlite were obtained by fitting experimental data to equation 2.13 for initial concentration range from 0.5 mgL^{-1} to 25mgL^{-1}. ΔG^o values were calculated by using equation 2.12 for different temperatures. Table 4.9 includes the mean values of ΔH^o, ΔS^o and ΔG^o.

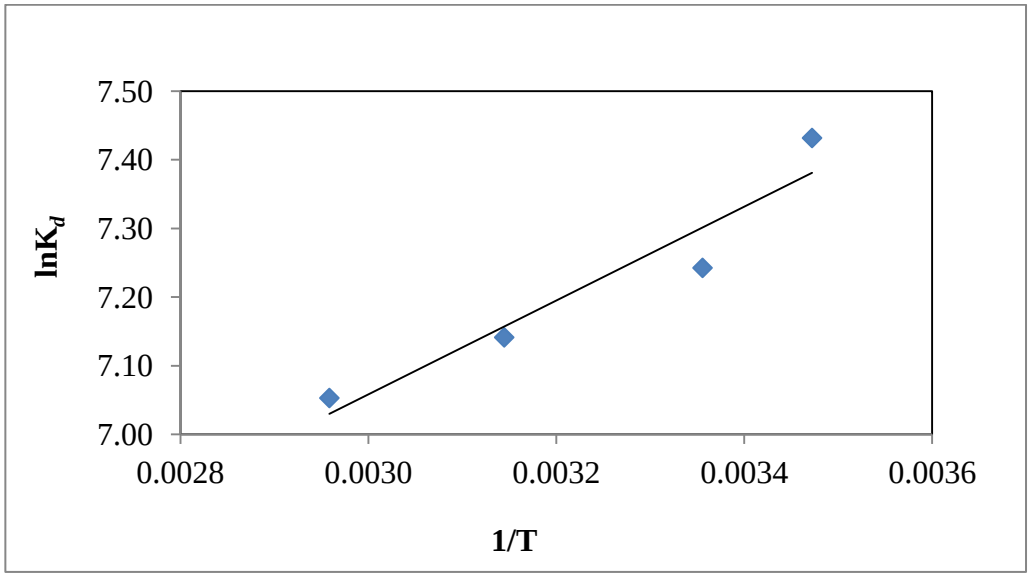

Figure 4.41. Representative plot of lnK_d against 1/T for adsorption of Co^{2+} onto perlite at different temperatures (Initial Co^{2+} concentration::4.97 mgL^{1-}, Perlite dosage:2.5 gL^{1-}, Contact time:30 min, pH:8.0±0.1).

Table 4.9. Thermodynamic parameters for Co^{2+} adsorption onto perlite (Initial Co^{2+} concentration range:5-25 mgL^{-1}).

ΔH^o $kJmol^{-1}$	ΔS^o $J(mol\ K)^{-1}$	ΔG^o, $kJmol^{-1}$			
		288 K	298 K	318 K	338 K
4.5	70	-11.6	-12.3	-13.7	-15.1

The enthalpy change during Co^{2+} ions adsorption onto perlite was positive and indicates that the nature of the adsorption was endothermic. The positive mean value of ΔS^o suggests an increase in the randomness at liquid solid interface during adsorption of Co^{2+} onto perlit. The negative ΔG^o exhibited that adsorption of Co^{2+} onto perlite surface is thermodynamically feasible and spontaneous. Ghassabzadeh and his coworkers studied the adsorption of Co^{2+} and Pb^{2+} onto expanded perlite. The values of ΔH^o were found as negative indicating the exothermic nature of adsorption for both adsorbates. Negative ΔG^o values showed that adsorption of Co^{2+} and Pb^{2+} onto expanded perlite was spontaneous and feasible (Ghassabzadeh et al., 2010).

4.3. Effect of Natural Organic Matter on the Adsorption of Cesium and Cobalt onto Bentonite and Perlite

Natural organic matter (NOM) is present throughout the ecosystem (Frimmel, 1998) and clay minerals or oxides are the important components of soils and sediments which are commonly coated with NOM as organic-clay complexes in the soil and sedimentary environments (Zhang et al., 2012). Interactions between NOM and clay or oxide minerals are expected to modify surface properties and reactivity of clay or oxide minerals, and change the mobility of pollutants bound to them (Weng et al., 2006; Ksiezopolska and Pazur, 2011). Metal adsorption onto either NOM or other adsorbents proceeds mainly through complexation mechanism.

NOM is primarily composed of humic substances of which humic acid (HA) constitutes the acid in soluble fraction. Therefore, HA was selected as the representative model compound of NOM in order to elucidate the effect of the NOM during the adsorption of cesium and cobalt onto either bentonite or perlite in this study. Varying concentrations of cesium and cobalt solutions in the presence of HA were mixed with the bentonite or perlite at the constant solid to liquid ratio as 2.5 gL^{-1} and the suspensions were shaken for 30 min at pH 8 and 298 K.

4.3.1. Adsorption of Cesium onto Bentonite in the Presence of Humic Acid

Adsorption isotherm of Cs^+ onto bentonite in the presence of 20 mgL^{-1} of HA at initial Cs^+ concentration ranging from 25 to 600 mgL^{-1} (298 K and pH 8), expressing the adsorbed amount (q_A) as a function of equilibrium concentration (C_e), was presented in Figure 4.42. C_e values varied between 0.949-398 mgL^{-1} depending on the initial concentration of Cs^+ in solution. The values of q_A calculated were in the range of 10.0-87.6 mgg^{-1} for the corresponding C_e values. HA displayed no drastic effect on the adsorption of cesium onto bentonite (Figure 4.42). When comparing the results with that obtained from adsorption of Cs^+ onto bentonite in the absence of HA, while C_e values increased, q_A values decreased in the presence of HA for the same initial concentration range (Figure 4.42).

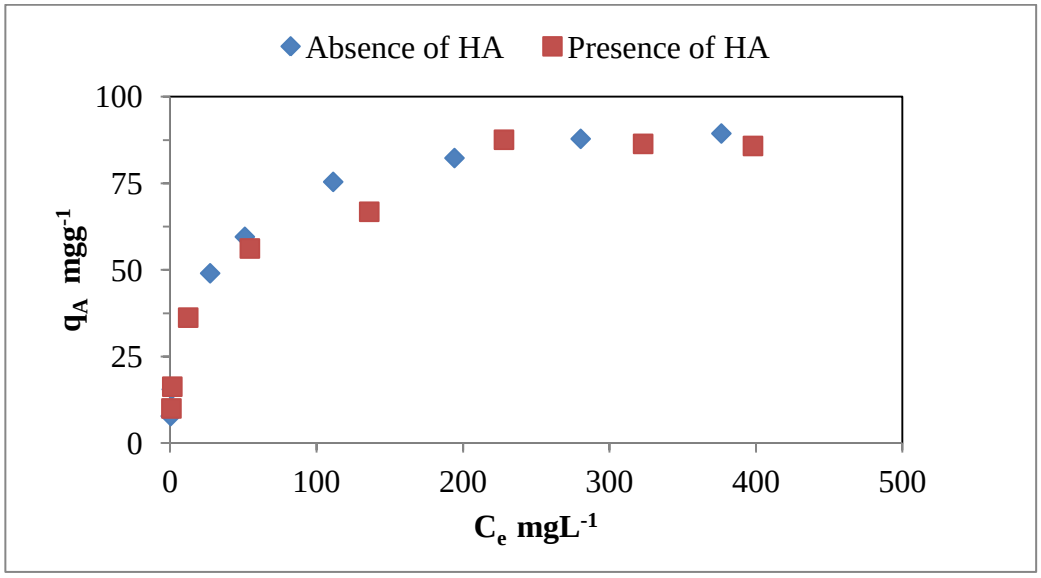

Figure 4.42. Adsorption isotherm of Cs^+ onto bentonite in the presence (■) and absence (◆) of HA. (Initial Cs^+ concentration range: 20-600 mgL^{-1}, Bentonite dosage: 2.5 gL^{-1}, T: 298 K, Contact time: 30 min, pH 8.0±0.1).

The equilibrium data displaying a Langmuiran adsorption isotherm model were fitted to Langmuir isotherm adsorption model equation (Equation 2.2) and a linear plot was obtained when $1/q_A$ was plotted against $1/C_e$ over the entire concentration range studied by giving regression coefficient of R^2 = 0.995. Langmuir adsorption isotherm model parameters, q_{max} (maximum adsorption capacity) and K_a (binding constant), were 79.4 mgg^{-1} and 0.156 Lmg^{-1} respectively. When comparing the values with that obtained from the adsorption in the absence of HA (Table 4.11), q_{max} decreased from 83.3 to 79.4 mgg^{-1} and K_a increased from 0.0960 to 0.156 Lmg^{-1} in the presence of HA in metal solution.

The equilibrium data were also fitted to Freundlich isotherm adsorption model equation (Equation 2.4) and the linear plot of $logq_A$ against $logC_e$ would give the slope as 1/n and intercept as $logK_F$ with a regression coefficient of R^2= 0.972. Freundlich adsorption isotherm model parameters, K_F and 1/n, were 12.8 Lg^{-1} and 0.342, respectively. When comparing the values with that obtained from adsorption in the absence of HA (Table 4.11), K_F significantly decreased from 23.8 to 12.8 Lg^{-1}. Moreover, the Freundlich intensity factor, 1/n increased from 0.233 to 0.342 in the presence of HA in solution.

Furthermore, the equilibrium data were fitted to Dubinin-Radushkevich isotherm adsorption model equation (Equation 2.6). The linear plot of the $\ln q_A$ against to ε^2 was drawn by giving regression coefficient of R^2= 0.987. The model parameters q_{max} (total micropore volume of adsorbent), β (adsorption coefficient related with adsorption energy) and E (free energy change of adsorption) were calculated as 179 mgg^{-1}, 3.17 x 10^{-9} and 12.6 $kJmol^{-1}$, respectively. When comparing the values with that obtained from adsorption in the absence of HA (Table 4.12), q_{max} and β increased from 156 $mgg^{-1}$and 2.46 x 10^{-9} to 179 mgg^{-1} and 3.17 x 10^{-9}, respectively. On the other hand, E value decreased from 14.3 $kJmol^{-1}$ to 12.8 $kJmol^{-1}$ in the presence of HA.

4.3.2. Adsorption of Cobalt onto Bentonite in the presence of Humic Acid

Adsorption isotherm of Co^{2+} onto bentonite in the presence of 20 mgL^{-1} of HA at initial Co^{2+} concentration ranging from 5.02 to 300 mgL^{-1} (298 K and pH 8), plotting q_A versus C_e, was presented in Figure 4.43. C_e values changed between 0.780-228 mgL^{-1} depending on the initial concentration of Co^{2+} in the solution. The values of q_A calculated varied between 1.53-27.4 mgg^{-1} for the corresponding C_e values. HA caused little increase at the q_A values (Figure 4.43). When comparing the results with that obtained from adsorption of Co^{2+} onto bentonite in the absence of HA, while C_e values decreased, q_A values increased in the presence of HA for the same initial concentration range (Figure 4.43).

The equilibrium data displaying a Langmuiran adsorption isotherm model were fitted to Langmuir isotherm adsorption model equation (Equation 2.2) and the linear plot is obtained when $1/q_A$ is plotted against $1/C_e$ over the entire concentration range studied by giving regression coefficient of R^2 = 0.996. Langmuir adsorption isotherm model parameters, q_{max} and K_a, were 29.7 mgg^{-1} and 0.102 Lmg^{-1} respectively. When comparing the values with that obtained from adsorption in the absence of HA (Table 4.11), q_{max} increased from 15.9 to 29.7 mgg^{-1} and K_a decreased from 0.326 to 0.102 Lmg^{-1} due to the presence of HA in metal solution. It can be deduced from those results HA positively affected the adsorption of Co^{2+} onto bentonite by providing with strong complexing sites for Co^{2+} in the water-solid interlayer.

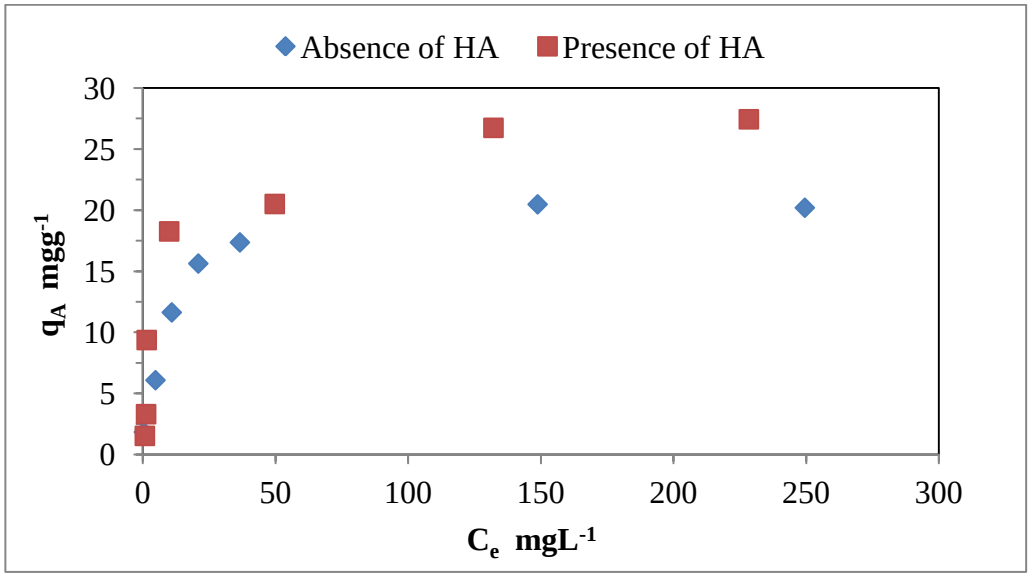

Figure 4.43. Adsorption isotherm of Co^{2+} onto bentonite in the presence (■) and the absence (◆) of HA. (Initial Co^{2+} concentration range: 5.02-300 mgL^{-1}, Bentonite dosage: 2.50 gL^{-1}, T: 298 K, Contact time: 30 min, pH 8.0±0.1).

The equilibrium data were also fitted to Freundlich isotherm adsorption model equation (Equation 2.4) and the linear plot of the $\log q_A$ against $\log C_e$ would give the slope as 1/n and intercept as $\log K_F$ with a regression coefficient of R^2= 0.774. Freundlich adsorption isotherm model parameters, K_F and 1/n, were 3.78 Lg^{-1} and 0.420, respectively. When comparing the values with that obtained from adsorption in the absence of HA (Table 4.11), K_F increased from 3.10 to 3.78 Lg^{-1}. Moreover, the Freundlich intensity factor, 1/n decreased from 0.469 to 0.420 because of the presence of HA in metal solution. Increase in K_F value indicated that HA influenced the adsorption positive. The similar results were obtained in the study performed by Olu-Owolabi and coworkers during the adsorption of the Cd^{2+} and Cu^{2+} onto bentonite in the presence of HA. It was found that K_F values for Cd^{2+} and Cu^{2+} increased from 0.820 and 0.840 to 1.89 and 1.92 Lg^{-1}, respectively when compared the results obtained in the absence of HA in metal solution (Olu-Owolabi et al., 2010).

Furthermore, the equilibrium data was fitted to Dubinin-Radushkevich isotherm adsorption model equations (Equation 2.6). The linear plot of the $\ln q_A$ against to ε^2 was drawn by giving regression coefficient of R^2= 0.814. Dubinin-Radushkevich isotherm

adsorption model parameters, q_{max}, β and E were calculated as 75.6 mgg^{-1}, 4.14 x 10^{-9} and 11.0 $kJmol^{-1}$, respectively. When comparing the values with that obtained from adsorption in the absence of HA (Table 4.12), q_{max} and β increased from 50.7 $mgg^{-1}$and 3.68 x 10^{-9} to 75.6 mgg^{-1} and 4.14 x 10^{-9}, respectively. On the other hand, E value decreased from 11.7 $kJmol^{-1}$ to 11.0 $kJmol^{-1}$ owing to the presence of HA in the metal solution.

4.3.3. Adsorption of Cesium onto Perlite in the presence of Humic Acid

Adsorption isotherm of Cs^+ onto perlite in the presence of 20 mgL^{-1} of HA at initial Cs^+ concentration ranging from 0.900 to 42.3 mgL^{-1} (298 K and pH 8), expressing q_A against C_e, was presented in Figure 4.44. C_e values varied between 0.125-35.3 mgL^{-1} depending on the initial concentration of Cs^+ in solution. The values of q_A calculated were in the range of 0.310-2.82 mgg^{-1} for the corresponding C_e values. HA displayed a drastic effect on the adsorption of cesium onto perlite (Figure 4.44). When comparing the results with that obtained from adsorption of Cs^+ onto perlite in the absence of HA, while C_e values generally decreased, q_A values increased in the presence of HA for the same initial concentration range (Figure 4.44).

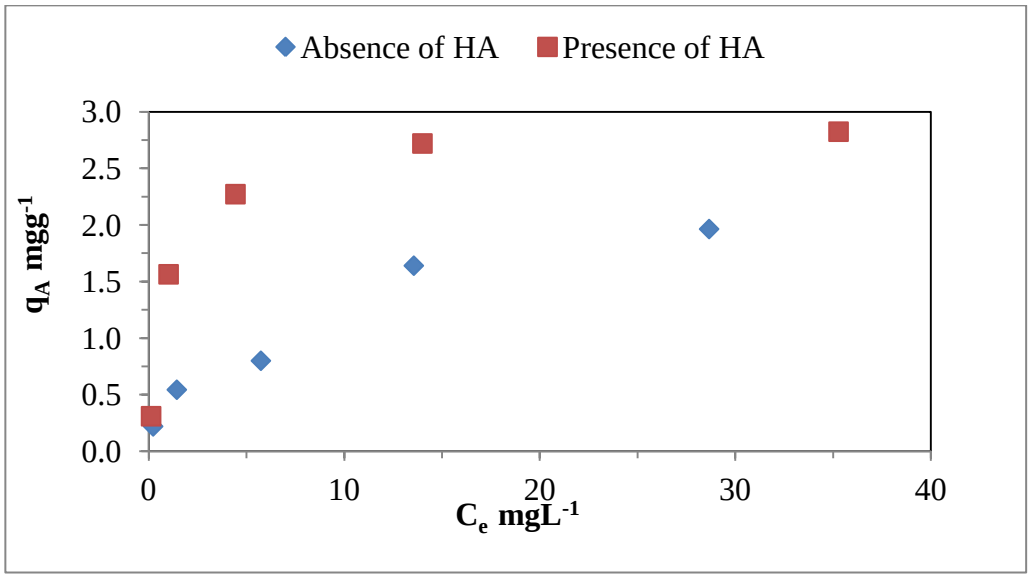

Figure 4.44. Adsorption isotherm of Cs^+ onto perlite in the presence (■) and absence (◆) of HA. (Initial Cs^+ concentration range: 0.900-42.3 mgL^{-1}, Bentonite dosage: 2.50 gL^{-1}, T: 298 K, Contact time: 30 min, pH 8.0±0.1).

The equilibrium data displaying a Langmuiran adsorption isotherm model were fitted to Langmuir isotherm adsorption model equation (Equation 2.2) and the linear plot is obtained when $1/q_A$ is plotted against $1/C_e$ over the entire concentration range studied by giving regression coefficient of R^2 = 0.999. Langmuir adsorption isotherm model parameters, q_{max} and K_a, were 3.00 mgg^{-1} and 0.925 Lmg^{-1} respectively. When comparing the values with that obtained from adsorption in the absence of HA (Table 4.11), q_{max} increased from 1.22 to 3.00 mgg^{-1} in the presence of HA, but K_a values for both conditions are close to each other, 0.943 Lmg^{-1} for the absence of HA, 0.925 Lmg^{-1} for the presence of HA in metal solution.

The equilibrium data were also fitted to Freundlich isotherm adsorption model equation (Equation 2.4) and the linear plot of the $\log q_A$ against $\log C_e$ would give the slope as 1/n and intercept as $\log K_F$ with a regression coefficient of R^2= 0.932. Freundlich adsorption isotherm model parameters, K_F and 1/n, were 1.64 Lg^{-1} and 0.171, respectively. When comparing the values with that obtained from adsorption in the absence of HA (Table 4.11), K_F increased from 0.432 to 1.64 Lg^{-1}. Moreover, the Freundlich intensity factor, 1/n decreased from 0.458 to 0.171 in the presence of HA in metal solution. The large increase at the K_F value which indicates the relative adsorption capacity of adsorbent showed that HA caused the cesium ions more affinity towards to perlite surface.

Moreover, the equilibrium data was fitted to Dubinin-Radushkevich isotherm adsorption model equations (Equation 2.6). The linear plot of the $\ln q_A$ against to ε^2 was drawn by giving regression coefficient of R^2= 0.900. The model constants q_{max}, β and E were calculated as 12.0 mgg^{-1}, 2.88 x 10^{-9} and 13.2 $kJmol^{-1}$, respectively. When comparing the values with that obtained from adsorption in the absence of HA (Table 4.12), q_{max} and E increased from 8.36 $mgg^{-1}$and 12.1 $kJmol^{-1}$ to 12.0 mgg^{-1} and 13.2 $kJmol^{-1}$, respectively. On the other hand, β value decreased from 3.41 x 10^{-9} to 2.88 x 10^{-9} in the presence of HA. Irani and co-workers studied the lead adsorption onto perlite at 298 K. D-R isotherm model was applied to equilibrium data by giving q_{max} and E values which are 8.29 $mgg^{-1}$and 9.18 $kJmol^{-1}$, respectively (Irani et al., 2011).

4.3.4. Adsorption of Cobalt onto Perlite in the presence of Humic Acid

Adsorption isotherm of Co^{2+} onto perlite in the presence of 20 mgL^{-1} of HA at initial Co^{2+} concentration ranging from 0.900 to 48.5 mgL^{-1} (298 K and pH 8), plotting q_A against C_e, was presented in Figure 4.45. C_e values varied between 0.740-45.5 mgL^{-1} depending on the initial concentration of Co^{2+} in solution. The values of q_A calculated were in the range of 0.064-1.19 mgg^{-1} for the corresponding C_e values. HA adversely affected the adsorption of the Co^{2+} onto perlite (Figure 4.45). When comparing the results with that obtained from adsorption of Co^{2+} onto perlite in the absence of HA, while C_e values increased, q_A values substantially decreased in the presence of HA for the same initial concentration range (Figure 4.45).

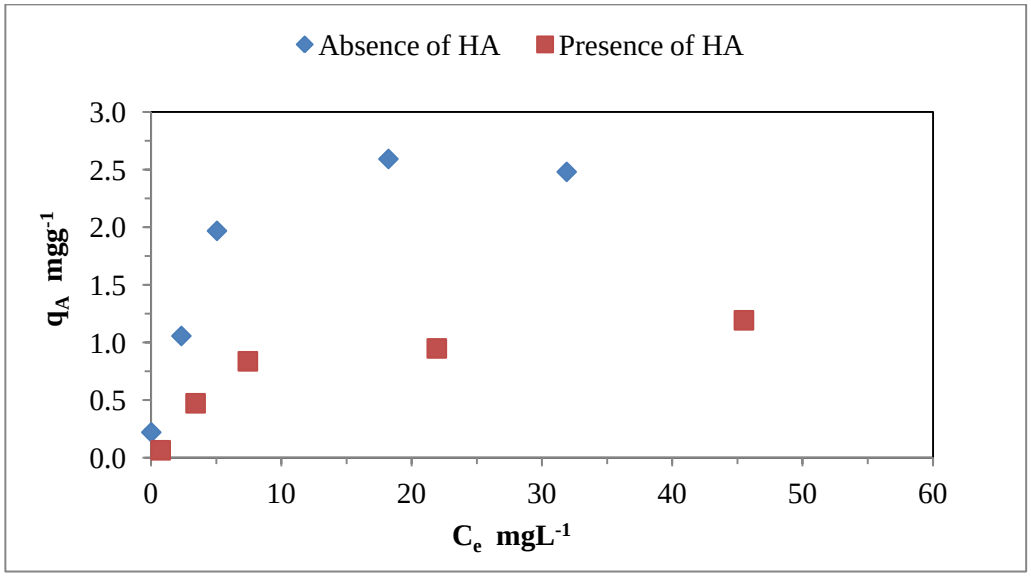

Figure 4.45. Adsorption isotherm of Co^{2+} onto perlite in the presence (■) and the absence (◆) of HA. (Initial Co^{2+} concentration range: 0.900-48.5 mgL^{-1}, Bentonite dosage: 2.5 gL^{-1},T: 298 K, Contact time: 30 min, pH 8.0±0.1).

The equilibrium data displaying a Langmuiran adsorption isotherm model were fitted to Langmuir isotherm adsorption model equation (Equation 2.2) and a linear plot was obtained when $1/q_A$ is plotted against $1/C_e$ over the entire concentration range studied by giving regression coefficient of R^2 = 0.960. Langmuir adsorption isotherm model parameters, q_{max} and K_a, were 1.34 mgg^{-1} and 0.165 Lmg^{-1} respectively. When comparing

the values with that obtained from adsorption in the absence of HA (Table 4.7), q_{max} decreased from 1.83 to 1.34 mgg^{-1} in the presence of HA. K_a value also decreased from 6.83 to 0.165 Lmg^{-1} in the presence of HA.

The equilibrium data were also fitted to Freundlich isotherm equation (Equation 2.4) and the linear plot of the $logq_A$ against $logC_e$ would give the slope as 1/n and intercept as $logK_F$ with a regression coefficient of R^2= 0.847. Freundlich isotherm model parameters, K_F and 1/n, were 0.129 Lg^{-1} and 0.680, respectively. When comparing the values with that obtained from adsorption in the absence of HA (Table 4.7), K_F decreased from 0.881 to 0.129 Lg^{-1}. Moreover, the Freundlich intensity factor, 1/n increased from 0.348 to 0.680 in the presence of HA in metal solution. Decrease in K_F value indicated that adsorption affinity toward to perlite surface for Co^{2+} substantially decreased.

The equilibrium data was finally fitted to Dubinin-Radushkevich isotherm equations (Equation 2.6). The linear plot of the lnq_A against to ε^2 was drawn by giving regression coefficient of R^2= 0.892. The model parameters, q_{max}, β and E were calculated as 11.4 mgg^{-1}, 6.14 x 10^{-9} and 9.00 $kJmol^{-1}$, respectively. When comparing the values with that obtained from adsorption in the absence of HA (Table 4.12), q_{max} and β increased from 6.34 $mgg^{-1}$and 2.49 x 10^{-9} to 11.4 mgg^{-1} and 6.14 x 10^{-9}, respectively. On the other hand, E value decreased from 14.2 to 9.00 $kJmol^{-1}$ in the presence of HA.

In conclusion, Langmuir isotherm model best described the all equilibrium data obtained from the adsorption of representative metals onto adsorbents during the presence of HA in metal solutions. q_{max} values obtained from Dubinin-Radushkevich isotherm model equation increased for all adsorption of representative metals onto adsorbents during the presence of HA in metal solutions. It may be resulted from increased surface area due to HA bound to the surface of the adsorbents.

4.4. Overall Discussion

Enthalpy of hydration of an ion means energy released upon attachment of water molecules to ion. ΔH_{hyd} is the symbol of the enthalpy of hydration. The hydration energies of studied cations are listed in Table 4.6. The table illustrates the point that Cs^+ has higher ionic size and lower absolute value of enthalpy of hydration than Co^{2+} has.

Table 4.10. Ion radius and enthalpy of hydration of studied cations

Ion	$r_{ion,}$ A^0	ΔH_{hyd}, $kJmol^{-1}$
Cs^+	1.67	-276
Co^{2+}	0.745	-1996

In the results of the experiments which were indicated at Table 4.11, it is obvious that the adsorption of Cs^+ onto bentonite is higher than that of Co^{2+}. There is a possible cause for that situation. Cs^+ has large ionic size and its enthalpy of hydration is low (Table.4.10). Therefore, Cs^+ likes to be adsorbed rather than be hydrated. On the other hand, Co^{2+} prefers be hydrated by water molecules which are around itself. Yıldız (2007) stated that alkali cation exchange selectivity is controlled by selectivity of the solution phase for the more strongly hydrated cation. In other words, the cation with the least negative heat of hydration has more chance to be specifically adsorbed to the surface because the more weakly hydrated ions are easier to dehydrate (Teppen and Miller, 2006).

The other result obviously shown in Table 4.11 is that bentonite is higher adsorption capacity for the studied cations than that of perlite. The possible causes for that situation can be cited as bentonite has higher surface area (57.8 m^2g^{-1}) than perlite has (2.12 m^2g^{-1}) and the bentonite structure is very different from the perlite structure. Bentonite contains montmorillonite as main mineral which has layers contained three sheets. There is one octahedral sheet between two tetrahedral sheets in bentonite structure. The layers are hold by weak van der Waals forces to each other, so there are not so close. Between the layers there are spaces for ion exchange. The ions can pass in these regions easily to exchange with cations, especially Ca^{2+} and Na^+ neutralized the permanent negative charge of the bentonite surface (Yıldız, 2007).

Table 4.11. Langmuir and Freundlich Adsorption Model Parameters.

Adsorbent - Adsorbate	Langmuir Isotherm Model Parameters			Freundlich Isotherm Model Parameters		
	$q_{max,}$ mgg^{-1}	K_a	R^2	$K_{F,}$ Lg^{-1}	1/n	R^2
Bentonite-Cs^+	83.3	0.096	0.975	23.8	0.233	0.973
Bentonite-Co^{2+}	15.9	0.033	0.977	3.10	0.469	0.959
Perlite-Cs^+	1.22	0.943	0.960	0.432	0.457	0.946
Perlite-Co^{2+}	1.80	6.83	0.985	0.880	0.345	0.975

Furthermore, Kraepiel and colleagues stated that adsorption models for clays like bentonite usually involve two distinct types of surface sites at the interface between solid and the solution (Krapiel et al., 1999). One of them is symbolized as $\equiv X^-$ groups bearing a permanent charge which account for cation exchange part of the adsorption. The other is shown as amphoteric $\equiv SOH$ groups that are present on the edge surface of the bentonite. Surface charge of the edge surface of bentonite is controlled by the protonation/deprotonation of the $\equiv SOH$ groups.

$$\equiv XNa + H^+ \Leftrightarrow \equiv XH + Na^+ \quad (4.1)$$

$$\equiv XNa + M^+ \Leftrightarrow \equiv XM + Na^+ \quad (4.2)$$

Above reactions 4.1 and 4.2 take place between layers as ion exchange reaction. $\equiv X^-$ represents permanent negative surface charge of the bentonite and behaves like a solid exchanger. Sodium ion is represented as exchangeable cation in bentonite $\equiv XNa$ and M^+ is represented as absorbable metal cation, Cs^+ and Co^{2+} in this study. Both reactions 4.1 and 4.2 show that a competition between H^+ and M^+ for adsorption active sites increases at low pH value and that lowers the adsorption capacity of the bentonite. This is compatible with the results of that study in which low metal adsorption was observed at low pH value for both bentonite and perlite.

Second type of active groups is present at the edge surface of the bentonite, namely ≡SOH hydroxyl active group. Some possible reactions taking place at edge surface of the bentonite are presented at the following for both Cs^+ and Co^{2+}

$$\equiv SOH + Cs^+ \Leftrightarrow \equiv SOCs + H^+ \quad (4.3)$$

$$\equiv SOH + Co^{2+} \Leftrightarrow \equiv SOCo^+ + H^+ \quad (4.4)$$

$$2 \equiv SOH + Co^{2+} \Leftrightarrow \equiv SOCo + H^+ \quad (4.5)$$

$$\equiv SOH_2^+ + Cs^+ \Leftrightarrow \equiv SOCs + 2H^+ \quad (4.6)$$

$$\equiv SOH_2^+ + Co^{2+} \Leftrightarrow \equiv SOCo^+ + 2H^+ \quad (4.7)$$

$$\equiv SOH + Na^+ \Leftrightarrow \equiv SONa + H^+ \quad (4.8)$$

$$\equiv SONa + Cs^+ \Leftrightarrow \equiv SOCs + Na^+ \quad (4.9)$$

$$\equiv SONa + Co^{2+} \Leftrightarrow \equiv SOCo^+ + Na^+ \quad (4.10)$$

$$2 \equiv SONa + Co^{2+} \Leftrightarrow \equiv SOCo + H^+ \quad (4.11)$$

Na ions represent the cation coming from the electrolyte solution. The charge of the edge surface hydroxyl group is pH-dependent. With increasing of pH value, the concentrations of surface groups, uncharged surface group as ≡SOH, positively charged group as $\equiv SOH_2^+$ and negatively charged surface group as $\equiv SO^-$, become different. $\equiv SOH_2^+$ decreases, whereas $\equiv SO^-$ increases with increasing pH (Xu, et al., 2008). The reactions between 4.3 and 4.11 can be presented as either ion exchange reactions between metal cations and hydronium ions in the solution or surface complexation reactions in which O atom in surface hydroxyl group bears electrons with metal cation.

As for perlite structure, the silicon atoms at the surface tend to maintain their tetrahedral coordination by attaching to a number of hydroxyl groups (Figure 2.6). Furthermore, perlite shows negative zeta potential and has no isoelectrical point in the pH range of 3 and 11 because of its permanent negative charge due to isomorphic substitution and structural defects that may occur as broken edges during expansion procedure of the

natural perlite (Alkan et al., 2005). The effect of the pH on the negative surface charge of the perlite is that increasing of the pH raises the negativity of the surface and therefore positive ion adsorption on the surface increases. Both studied cations, Co^{2+} and Cs^{+} have exhibited a similar tendency on the adsorption of perlite surface when changing of pH.

$$\equiv SiOH + H^{+} \Leftrightarrow \equiv SiOH_2^{+} \quad (4.12)$$

$$\equiv SiOH + OH^{-} \Leftrightarrow \equiv SiO^{-} + H_2O \quad (4.13)$$

The fact that perlite has no isoelectrical point and negative surface charge at pH between 3 and 11 has shown that main reaction reasonable for the surface charge of the perlite is the reaction 4.13 (Alkan et al., 2005). Studied cations, Co^{2+} and Cs^{+} can give some surface complex reactions with the negative surface of the perlite as the following.

$$\equiv SiO^{-} + Cs^{+} \Leftrightarrow \equiv SiOCs \quad (4.14)$$

$$\equiv SiO^{-} + Co^{2+} \Leftrightarrow \equiv SiOCo^{+} \quad (4.15)$$

$$2 \equiv SiO^{-} + Co^{2+} \Leftrightarrow \equiv 2SiOCo \quad (4.16)$$

Alkan and coleagues stated that monovalent cations have usually non-specific and weak interactions whereas divalent cations like Co^{2+}, Cu^{2+} and Pb^{2+} have specific and strong interactions with surface of the perlite (Alkan et al., 2005). In the light of this expression, the reaction 4.14 and 4.15 may be described as outer surface complex reaction due to weak interactions with the surface and the reaction 4.16 are also described as inner surface complex reactions which form strong interactions with the surface.

To sum up, perlite solely has adsorption sites on the edge surface as hydroxyl groups whereas bentonite has either layered structure that gives more adsorption sites or hydroxyl groups on the edge surface. Therefore, adsorption capacity of the bentonite is higher than that of perlite for studied cations.

R^2 value given in Table 4.7 which is equal or higher than 0.95 demonstrated that Langmuir and Freundlich models fit adsorption equilibrium data reasonably well for all experiments. The magnitude of constant K_F gives some valuable information about relative adsorption affinity towards adsorbed cations, and the magnitude of constant 1/n is an indicator of linearity of adsorption. The high values of K_F given in Table 4.7 indicate that bentonite has higher affinity towards cations than perlite. The values of 1/n also indicate that nonlinear adsorption takes place for all experiment.

D-R isotherm describes adsorption on a single type of uniform pores. In this respect, the D-R isotherm is an analogue of Langmuir type but it is more general because it does not assume a homogeneous surface or constant adsorption potential (Ibrahim et al., 2008). The magnitude of E can be related to reaction mechanism. If E is in the range of 8-16kJmol^{1-}, adsorption is governed by ion exchange mechanism (Helfferich, 1962). It can be reported that ion exchange mechanism was the main mechanism for all adsorption processes due to E values given in Table 4.12.

Table 4.12. Dubinin-Radushkevich Adsorption Model Parameters.

Adsorbent-Adsorbate	q_{max}, mgg^{-1}	β, 10^{-9}	E, kJmol^{-1}
Bentonite-Cs^+	156	2.46	14.3
Bentonite-Co^{2+}	50.7	3.68	11.7
Perlite-Cs^+	8.36	3.41	12.1
Perlite-Co^{2+}	6.34	2.49	14.2

Furthermore, surface complexation reaction can play some roles during adsorption because given E values is not so high for a chemical reaction. q_{max} values for D-R isotherm are more higher than Langmuir ones for all adsorption experiments because q_{max} represents monolayer coverage in Langmuir model, whereas it represents total specific micropore coverage in D-R model

The ΔH^o values reported in Table 4.9 stand for observed enthalpy change, ΔH^o_{obs}, which includes the contribution of intrinsic enthalpy change, ΔH^o_{int}, and the hydration

enthalpy of adsorbed cation, ΔH^{o}_{hyd}, given in Table 4.5. Shahwan and co-workers related them with an equation as presented below (Shahwan et al., 2006).

$$\Delta H^{o}_{obs} = \Delta H^{o}_{int} - \Delta H^{o}_{hyd} \quad (4.17)$$

The intrinsic enthalpy change is associated with the fixation reaction of Co^{2+} on the adsorption sites and is always exothermic, and hydration enthalpy reflects the strength of interaction between the naked cation and its hydration sphere. Hence for the intrinsic adsorption reaction to take place, the cation must first undergo partial dehydration in a way that facilitates its migration through the solution to the sites on the surface of adsorbent (Shahwan et al., 2006). It was concluded from above explanations that the cations with relatively low hydration enthalpies, so low charge to size ratio, will demonstrate observed exothermic adsorption behavior, while the cations of higher charge to size ratio will generally show observed endothermic behavior.

Table 4.13. Thermodynamic parameters at different temperatures.

Adsorbent-Adsorbate	ΔH^{o} $kJmol^{-1}$	ΔS^{o} $J(mol\ K)^{-1}$	ΔG^{o} $kJmol^{-1}$
Bentonite-Cs^{+}	-4.65	9.16	-16.9
Bentonite-Co^{2+}	13.6	39.5	-14.5
Perlite-Cs^{+}	3.5	54.7	-12.5
Perlite-Co^{2+}	4.5	70.0	-13.2

The values of ΔH^{o} given in Table 4.13 is generally consistent with the above conclusion for Co^{2+} adsorption onto both bentonite and perlite but Cs^{+} adsorption onto perlite is endothermic, in place of exothermic. It may be concluded that Cs^{+} interaction with the surface of bentonite should be stronger than that of the surface of perlite. The values of ΔS^{o} are positive for all adsorption studies by indicating more disordered form after adsorption. Released water molecules from the hydrated metal ions or from the surface may be reasons for entropy increase. The negative values of ΔG^{o} as shown in Table 4.13 indicate the feasibility and their spontaneous nature for all adsorption processes.

HA represents a major fraction of dissolved NOM in freshwaters. Because of the high functionality due to the presence of carboxylic and phenolic groups, HA can strongly complex with metal ions and thereby modify the retention, adsorption, migration and bioavailability of metal ions in the natural environment. As a result of pH dependent deprotonation, HA enhances the cation adsorption at low pH values, but reduces the adsorption at high pH values (Montavon et al., 2002). Whether HA exerts a mobilizing or retarding effect depends on the complex behavior of metal ions in the ternary system metal solution-HA-oxide surface (Xu et al., 2008). The increase of adsorption can be explained by the adsorption of HA on oxide surface followed by the interaction of metal ions with surface adsorbed HA, whereas the reduction of adsorption at high pH can be interpreted by the formation of soluable metal-HA complexes in solution (Montavon et al., 2002).

Batch adsorption experiments were also performed in the presence of HA for the elucidation of adsorption behavior of Cs^{+} and Co^{2+} onto either bentonite or perlite . The adsorption data attained under the specified conditions were further modelled to Langmuir, Freundlich and Dubinin-Radushkevich isotherm adsorption models (Table 4.14).

Table 4.14. Adsorption isotherm parameters for the adsorption of Cs^{+} and Co^{2+} onto bentonite or perlite in the presence of HA or absence of HA conditions.

System	Adsorption isotherm models						
	Langmuir		Freundlich		Dubinin-Radushkevich		
	q_{max}	K_a	K_F	1/n	q_{max}	$\beta x10^{-9}$	E
	Bentonite						
Cs	83.3	0.0960	23.8	0.233	156	2.46	14.3
Cs and HA	79.4	0.156	12.8	0.342	179	3.17	12.6
Co	15.9	0.326	3.10	0.469	75.6	4.14	11.0
Co and HA	29.7	0.102	3.78	0.420	50.7	3.68	11.7
	Perlite						
Cs	1.22	0.943	0.432	0.458	8.36	3.41	12.1
Cs and HA	3.00	0.925	1.64	0.171	12.0	2.88	13.2
Co	1.83	6.83	0.881	0.348	6.34	2.49	14.2
Co and HA	1.34	0.165	0.129	0.680	11.4	6.14	9.00

Referring to the previously reported results (Tables 4.11 and 4.12) for comparison purposes the adsorption data attained in the absence of HA were also presented in the Table 4.14.

With respect to q_{max} values of Langmuir model, HA had no drastic effect on the adsorption capacity of bentonite for Cs^+ (Table 4.14), whereas it substantially influenced the adsorption capacity of bentonite for Co^{2+} (Table 4.14). Furthermore, HA increased the adsorption capacity of the perlite for Cs^+ (Table 4.14), but decreased for Co^{2+} (Table 4.14). It can be concluded from these results that HA gave little interactions with the surface of bentonite and Cs^+ at the solid-liquid interface. Moreover, HA and Cs^+ interaction in the solution could play role on the minimal decrease for the adsorption capacity of bentonite for Cs^+. Cs^+ and Co^{2+} have distinct chemical characteristics. While Cs^+ is an alkali metal that does not make easily complex with any ligands or the surface of clay or minerals in the solution, Co^{2+} is a transition metal that gives easily complex interactions with the any ligands or the surface of clay or mineral. Furthermore, HA and the surface of bentonite and perlite are negative and common species of the cesium and cobalt ions are Cs^+ and Co^2 at the studied pH 8 (Yuzer et al., 2008; Bayulken et al., 2011). As for bentonite, negative surface of bentonite and negative active sites of HA gave very little interaction with each other, but ternary interaction of Co^{2+}-surface of bentonite-HA could occur by stabilizing cobalt on the surface, but Cs^+ was not efficient to make such a ternary interactions with the surface of bentonite and HA. Therefore, it can be said that Cs^+-HA interaction in the solution is common than Cs^+-bentonite interaction at the surface. For perlite, Cs^+ adsorption commonly increased when Co^{2+} adsorption decreased at the presence of HA. It can be possible explanation for Co^{2+} adsorption decrease onto negative perlite surface is that Co^{2+} can make stronger complexation with the HA in the solution than with perlite surface. Increase in Cs^+ adsorption onto perlite surface at the presence of HA can be clarified by the contribution of HA on the stabilizing of Cs^+ on the surface of perlite, namely Cs^+-HA interaction in the solution was not efficient as HA-Cs^+-perlite interaction at the solid liquid interface.

Freundlich parameters, K_F and 1/n, show the relative adsorption capacity and adsorption intensity, respectively. With respects to results in the Table 4.14, the values of K_F were in accordance with the Langmuir parameter, q_{max} in terms of decreasing and increasing trend of the adsorptions during the presence of HA. K_F value of Cs^+ adsorption onto bentonite in the absence of HA was lower than that of Cs^+ adsorption onto bentonite in the presence of HA. Moreover, K_F value for the adsorption of Co^{2+} onto bentonite increased at the condition of the presence of HA in the solution. When comparing the K_F

values obtained from different adsorbents, Cs^+ and Co^{2+} adsorptions onto bentonite had much more K_F values than that onto perlite. 1/n values between 0 and 1 signify that adsorption is good at the studied conditions. 1/n values were compared for different adsorption experiments. Co^{2+} adsorption onto perlite in the presence of HA had the highest value of 1/n, while Cs^+ adsorption onto perlite in the presence of HA had the lowest value of 1/n. HA significantly decreased the 1/n value during the adsorption of Cs^+ onto perlite in the presence of HA. However, HA did not affect the 1/n values for the adsorption of adsorbate onto bentonite substantially.

D-R isotherm model parameters, q_{max} and E, indicated the micropore volume of the adsorbent and mean value of free energy of the adsorption, respectively. With respects to values in the Table 4.14, HA increased q_{max} values for Cs^+ adsorption onto bentonite, but decreased the values for Co^{2+} adsorption onto bentonite. As for perlite, HA increased the q_{max} values during both Cs^+ adsorption and Co^{2+} adsorption onto perlite. Cs^+ adsorption onto bentonite in the presence of HA had the highest value of q_{max}, while Co^{2+} adsorption onto perlite in the absence of HA had the lowest value of q_{max}. When comparing the q_{max} values obtained from different adsorbents, Cs^+ and Co^{2+} adsorptions onto bentonite have much more q_{max} values than that onto perlite. E values stayed in the range of 8-16 $kJmol^{-1}$ during the adsorption of Cs^+ and Co^{2+} onto bentonite or perlite at the presence or absence of HA by implying that the adsorption mechanisms of HA-metals-adsorbents ternary system or metals-adsorbents binary system can be ion-exchange or outer sphere complex interactions.

5. CONCLUSION

In this study, potential usage of bentonite and perlite during the removal of Cs^+ and Co^{2+} from aqueous solutions was evaluated by using batch adsorption technique. Percentage of adsorption and quantity of adsorbed metals on the surface (q_A) was evaluated as a function of time, pH, temperature, ionic strength, initial metal concentration and humic acid concentration. Furthermore, adsorption isotherm data was interpreted by Langmuir, Freundlich and D-R adsorption isotherm models and thermodynamic parameters, ΔH^o, ΔS^o and ΔG^o, were determined. At the following, some conclusive remarks on the whole study were given.

- Cs^+ and Co^{2+} adsorptions onto bentonite or perlite occurred rapidly and reached to the equilibrium in 30 min.
- The adsorptions of Cs^+ and Co^{2+} onto bentonite or perlite were strongly pH-dependent and ionic strength dependent.
- The adsorption of Cs^+ onto bentonite decreased with increase at temperature, but the adsorption of Cs^+ onto perlite increased slightly with the increase at temperature. The adsorptions of Co^{2+} onto bentonite or perlite increased with the increase at temperature.
- Cs^+ had more affinity to the surface of bentonite than the surface of perlite and monolayer adsorption capacity of bentonite for Cs^+ was higher than for Co^{2+}.
- Co^{2+} had more affinity to the surface of bentonite than the surface of perlite.
- E values derived from D-R isotherm adsorption models were in the range of 8-16 $kJmol^{-1}$ that indicates the ion-exchange mechanism for all adsorption experiments in the study.
- When the adsorption of Cs^+ onto bentonite was exothermic, other adsorptions were endothermic nature. After all adsorption experiments, solid-liquid interface and the surface of adsorbents became more disordered. Furthermore, all adsorption reactions in the study were feasible and spontaneous.

- HA had little influence on the adsorption of Cs+ onto bentonite, whereas it affected the adsorption of Co^{2+} onto bentonite. Furthermore, HA significantly increased the adsorption of Cs^{+} onto perlite, but it decreased the adsorption of Co^{2+} onto perlite.

In conclusion, bentonite can be used as decontaminant more efficiently for the removal of Cs^{+} and Co^{2+} from the radioactive wastewater or as backfill material during the construction of deep geological repository that resides the high activity radioactive waste than the perlite can be. Therefore, in order to increase the adsorption capacity of bentonite and perlite for the radioactive elements, some treatment techniques for the surface of bentonite or perlite can be developed in further researches.

REFERENCES

Abollino, O., Aceto, M., Malandrino, M., Sarzanini, C., Mentasti, E., 2003. Adsorption of heavy metals on Na-montmorillonite. Effects of pH and organic substances. Water Research, 37, 1619-1627.

Akkaya, R., 2012. Synthesis and characterization of a new low-cost composite for the adsorption of rare earth ions from aqueous solutions. Chemical Engineering Journal, 200-202, 186-191.

Akkaya, R., 2013a. Effects of pH, concentration and temperature on radionuclides sorption onto polyhydroxyethyl methacrylate-expanded perlite composite. Journal of Radioanalytical and Nuclear Chemistry, 295, 351-355.

Akkaya, R., 2013b. Removal of radioactive elements from aqueous solutions by adsorption onto polyacrylamide-expanded perlite: Equilibrium, kinetic, and thermodynamic study. Desalination, 321, 3-8.

Aksoyoglu, S., 1989. Sorption of U(VI) on granite. Journal of Radioanalytical and Nuclear Chemistry, 134, 393-403.

Alihosseini, A., Taghikkani, V., Safekordi, A.A., Bastani, D., 2010. Equilibrium sorption of crude oil by expanded perlite using different adsorption isotherms at 298.15 K. International Journal of Environmental Science and Technology, 7, 591-598.

Alkan, M., Dogan, M., 2001. Adsorption of copper(II) onto perlite. Journal of Colloid and Interface Science, 243, 280-291.

Alkan, M., Demirbaş, Ö., Dogan, M., 2005. Zeta potential of unexpanded and expanded perlite samples in various electrolyte media. Microporous and Mesoporous Materials, 84, 192-200.

Azizi, S.N., Asemi, N., 2012. A Box-Behnken design for determining the optimum experimental condition of fungicide (Vapam) sorption onto modified with perlite.Journal of Environmental Science and Health, Part-B, 47, 692-699.

Badii, K., Amini, F.L., Rasoli Ahari, S.S., 2011. Effect of surface morphology of macro-scale perlite particles on adsorption process of Malachite Green dye. Desalination and Water Treatment, 28, 12.

Bayülken, S., Başçetin, E., Güçlü, K., Apak, R., 2010. Investigation and modeling of cesium (I) adsorption by Turkish clays: Bentonite, Zeolite, Sepiolite, and Kaolinite. Enviromental Progress and Sustainable Energy, 30, 70-80.

Bostick, B.C., Vairavamurthy, M.A., Karthikeyan, K.G., Chorover, J., 2002. Cesium adsorption on clay minerals: An EXAFS spectroscopic investigation. Environmental Science and Technology, 36, 2670-2676.

Butterman, W.C., Brooks, W.E., Reese, R.G., 2005. Cesium. Open-File Report, 2004-1432, U.S. Geological Survey, Virginia.

Chang, F.R.C., Sposito, G., 1996. Electrical double layer of a disk-shaped clay mineral particle: Effects of electrolyte properties and surface of charge density. Journal of Colloid and Interface Science, 178, 555-564.

Chen, Y., He, Y., Ye, W., Lin, C., Zhang, X., Ye, B., 2012. Removal of chromium (III) from aqueous solutions by adsorption on bentonite from Gaomiazozi, China. Enviromental Earth Science, 67, 1261-1268.

Chen, Y., Wang, J., 2012. Removal of radionuclide Sr^{2+} ions from aqueous solution using synthesized magnetic chitosan. Nuclear Engineering and Design, 242, 445-451.

Christidis, G.E., Scott, P.W., Dunham, A.C., 1997. Acid activation and bleaching capacity of bentonites from the islands of Milos and Chios, Aegean, Greece. Applied Clay Science, 12, 329-347.

Christidis, G., Huff, D.H., 2009. Geologic aspects and genesis of bentonites. Elements 5, 93-98.

Corami, A., Mignardi, S., Vincenzo, F., 2008. Cadmium removal from single- and multi-metal (Cd+ Pb+ Zn+Cu) solutions by sorption on hydroxyapatite. Journal of Colloid and Interface Science, 317, 402-408.

Debnath, S., Ghosh, U.C., 2009. Nanostructured hydrous titanium (IV) oxide: Synthesis, characterization and Ni (II) adsorption behavior. Chemical Engineering Journal, 152, 480-491.

Dogan, M., Alkan, M., 2003. Removal of methyl violet from aqueous solution by perlite. Journal of Colloid and Interface Science, 267, 32-41.

Dogan, M., Alkan, M., Çakır, Ü., 1997. Electrokinetic properties of perlite. Journal of Colloid and Interface Science, 192, 114-118.

Dogan, M., Alkan, M., Onganer, Y., 2000. Adsorption of methylene blue from aqueous solution onto perlite. Water Air Soil Pollution, 120, 229-248.

Donat, R., Akdogan, A., Erdem, E., Cetisli, H., 2005. Thermodynamics of Pb^{2+} and Ni^{2+} adsorption onto natural bentonite from aqueous solutions. Journal of Colloid and Interface Science, 286, 43-52.

Doulia, D., Leodopoulos, C., Gimouhopoulos, K., Rigas, F., 2009. Adsorption of humic acid on acid-activated Greek bentonite. Journal of Colloid and Interface Science, 340, 131-141.

Fike, W.B., 2001. Sorption of cadmium, copper, lead, and zinc as influenced by ionic strength, pH, and selected soil components, Ph. D. Dissertation, Virginia Polytechnic Institute and State University.

Frimmel, F.H., 1998. Characterization of natural organic matter as major constituents in aquatic systems. Journal of Contaminated Hydrology, 35, 201-216.

Galambos, M., Kufcakova, J., Rosskopfova, O., Rajec, P., 2010. Adsorption of cesium and strontium on natrified bentonite. Journal of Radioanalytical and Nuclear Chemistry, 283, 803-813.

Galambos, M., Paucova, V., Kufcakova, J., Rosskopfova, O., Rajec, P., Adamcova, R., 2010. Cesium sorption on bentonites and montmorillonite K10. Journal of Radioanalytical and Nuclear Chemistry, 284, 55-64.

Ghassabzadeh, H., Mohaddespour, A., Mostaedi, M.T., Zaheri, P., Maragheh, M.G., Taheri, H., 2010. Adsorption of Ag, Cu and Hg from aqueous solutions using expanded perlite. Journal of Hazardous Materials, 177, 950-955.

Ghassabzadeh, H., Mostaedi, M.T., Mohaddespour, A., Maragheh, M.G., Ahmadi, S.J., Zaheri, P., 2010. Characterizations of the Co (II) and Pb (II) removal process from aqueous solutions using expanded perlite. Desalination, 261, 73-79.

Giannakopoulou, F., Haidouti, C., Chronopoulou, A., Gasparatos, D., 2007. Sorption behavior of cesium on various soils under different pH levels. Journal of Hazardous Materials, 149, 553-556.

Giles, C.H., McEvsan, T.H., Nakhwa, S.N., Smith, D., 1960. A system classification of solution adsorption isotherm and its use in diagnosis of adsorption and in measurement of specific surface areas of solids. Journal of Chemical Society, 33, 3973-3993.

Greenwood, N.N., Earnshaw, A., 1984. Chemistry of the Elements. Pergamon Press, Oxford.

Hayes, K.F., Leckie, J.O., 1987. Modelling ionic strength effects on cation adsorption at hydrous oxide/solution interfaces. Journal of Colloid and Interface Science, 115, 564-572.

Heydartaemeh, M.R., Ardejani, F.D., Khashayar, B., Shabani, K.S., Mousavi, S.E., 2014. $FeCl_2$/ $FeCl_3$ perlite nanoparticles as a novel magnetic material for adsorption of green malachite dye. Arabian Journal for Science and Engineering, 39, 3383-3392.

Ibrahim, H.A., El-Kamash, A.M., Hanafy, M., Abdel-Monem, N.M., 2008. Examination of the use of synthetic zeolite NaA-X blend as backfill material in a radioactive waste disposal facility: Thermodynamic approach. Chemical Engineering Journal, 144, 67-74.

International Atomic Energy Agency, 1994. Classification of radioactive waste. Safety Series No. 111-G-1.1, IAEA, Vienna.

Irani, M., Amjadi, M., Mousamian, M.A., 2011.Comparative study of lead sorption onto natural perlite, dolomite and diatomite. Chemical Engineering Journal, 178, 317-323.

Karakaya, M.Ç., Karakaya, N., Bakır, S., 2011. Some properties of potential applications of the Na- and Ca-bentonite of Ordu (N.E Turkey). Applied Clay Science, 54, 159-165.

Karapiel, A.M.L., Keller, K., Morel, F.M.M., 1999. A model for metal adsorption on montmorillonite. Journal of Colloid and Interface Science, 210, 43-54.

Kaya, A., Ören, A.H., 2005. Adsorption of zinc from aqueous solutions to bentonite. Journal of Hazardous Materials, 125, 18.

Khan, S.A., 2003. Sorption of the long-lived radionuclides ^{134}Cs, ^{85}Sr and ^{60}Co on bentonite. Journal of Radioanalytical and Nuclear Chemistry, 258, 3-6.

Ksiezopolska, A., Pazur, M., 2011. Surface properties of bentonite and illite complexes with humic acids. Clay Minerals, 46, 149-156.

Kubilay, Ş., Gürkan, R., Savran, A., Şahan, T., 2007. Removal of Cu (II), Zn (II) and Co (II) ions from aqueous solutions by adsorption onto natural bentonite. Adsorption, 13, 41-51.

Leroy, P., Revil, A., 2004. A triple-layer model of the surface electrochemical properties of clay minerals. Journal of Colloid and Interface Science, 270, 371-380.

Li, D., Huang, S., wang, W., Peng, A., 2001. Study on the kinetics of cerium (III) adsorption-desorption on different soils of China. Chemosphere, 44, 663-669.

Lima, E.J., Bosch, P., Bulbulian, S., 1998. Modification of the structure of natural bentonite and study on the sorption of Cs^{+}. Journal of Radioanalytical and Nuclear Chemistry, 237, 41-45.

Ma, B., Sanghwa, O., Shin, W.S., Choi, S.J., 2011. Removal of Co^{2+}, Sr^{2+} and Cs^{+} from aqueous solution by phosphate-modified montmorillonite (PMM). Desalination, 276, 336-346.

Makrlik, E., Vanura, P., 2010. Extraction of strontium and barium into nitrobenzene by using synergistic mixture of hydrogen dicarbollylcobaltate and polyethylene glycol PEG 1000. Journal of Radioanalytical and Nuclear Chemistry, 283, 497-501.

Malakootian, M., Jaafarzadeh, N., Hossaini, H., 2011. Efficiency of perlite as a low cost adsorbent applied to removal of Pb and Cd from paint industry effluent. Desalination and Water Treatment, 26, 243-249.

Metwally, E., Abdel Rahman, R.O., Ayoub, R.R., 2007. Modelling batch kinetics of cesium, cobalt and strontium ions adsorption from aqueous solutions using hydrous titanium oxide. Radiochimica Acta, 95, 409-416.

Montavan, G., Markai, S., Andres, Y., Grambow, B., 2002. Complexation studies of Eu(III) with alumina-bound polymaleic acid: effect of organic polymer loading and metal ion concentration. Environmental Science and Technology, 36, 3303-3309.

Mostaedi, T.M., Ghassabzadeh, M., Maragheh, G., Ahmadi, S.J., Taheri, H., 2010. Removal of cadmium and nickel from aqueous solution using expanded perlite. Brazillian Journal of Chemical Engineering, 27, 299-308.

Mostafa, M.G., Chen, Y., Jean, J., Liu, C., Lee, Y., 2011. Kinetics and mechanism of arsenate removal by nanosized iron oxide-coated perlite. Journal of Hazardous Materials, 187, 89-95

Moussavi, G., Bagheri, A., 2012. Removal of petroleum hydrocarbons from contaminated groundwater by combined technique of adsorption onto perlite followed by the O_3/H_2O_2 process. Environmental Technology, 33, 1905-1912.

Moyer, B.A., Bazelaire, E., Bonnesen, P.V., 2005. Next generation extractants for cesium separation from high level waste: From fundamental concepts to site implementation. Annual Report, Environmental Management Science Program, Project no: 73803.

Nowack, B., Sigg, L., 1996. Adsorption of EDTA and metal-EDTA complexes onto goethite. Journal of Colloid and Interface Science, 177, 106-121.

Okumura, T., 2003. The material flow of radioactive cesium-137 in the U.S. 2000. http://www.epa.gov/rpdweb00/docs/source-management/csfinallongtakeshi.pdf

Olu-Owolabi, B.I., Popoola, D.B., Unuabonah, E.I., 2010. Removal of Cu^{2+} and Cd^{2+} from aqueous solution by bentonite clay modified with binary mixture of goethite and humic acid. Water Air Soil Pollution, 211, 459-479.

Omar, H., Arida, H., Daifullah, A., 2009. Adsorption of ^{60}Co radionuclides from aqueous solution by raw and modified bentonite. Applied Clay Science,44, 21-26.

O'Reilly, S.E., Hochella, M. F., 2003. Lead sorption efficiencies of natural and synthetic Mn and Fe-oxides. Geochimica et Cosmochimica Acta, 67, 4471-4487.

Ozcan, A., Oncu, E.M., Ozcan, A.S., 2006. Kinetics, isotherm and thermodynamic studies of adsorption of acid blue 193 from aqueous solutions onto natural sepiolite. Colloids and Surfaces Adsorption, 277, 299-305.

Ozeroglu, C., Dogan, E., Keceli, G., 2011. Investigation of Cs (I) adsorption on densely crosslinked poly(sodium methacrylate) from aqueous solutions. Journal of Radioanalytical and Nuclear Chemistry, 289, 577-586.

Pathak, P.N., Choppin, G.R., 2006. Kinetic and thermodynamic studies of cesium (I) sorption on hydrous silica. Journal of Radioanalytical and Nuclear Chemistry, 270, 299-305.

Rafatullah, M., Sulaiman, O., Hashim, R., Ahmad, A., 2010. Adsorption of methlene blue on low-cost adsorbents: A review. Journal of Hazardous Materials, 177, 70-80.

Rao, S.V.S., Paul, B., Lal, K.B., Narasimhan, S.V., Ahmed, J., 2000. Effective removal of cesium and strontium from radioactive waste using chemical treatment followed by utra filtration. Journal of Radioanalytical and Nuclear Chemistry, 246, 413-418.

Rauf, N., Tahir, S.S., 2000. Thermodynamics of Fe(II) and Mn(II) adsorption onto bentonite from aqueous solutions. The Journal of Chemical Thermodynamics, 32, 651-658.

Ren, A., Yu, S., Han, J., Chang, P., Chen, C., Chen, J., Wang, X., 2007. A Comparative Study of Pb^{+2} Sorption onto MX-80 bentonite, LA bentonite, γ-Al_2O_3 and SiO_2. Journal of Radioanalytical and Nuclear Chemistry, 272, 3-10.

Sarı, A., Tuzen, M., Cıtak, D., Soylak, M., 2007. Adsorption characteristics of Cu (II) and Pb (II) onto expanded perlite from aqueous solutions. Journal of Hazardous Materials, 148, 387-394.

Sarı, A., Sahinoglu, G., Tuzen, M., 2012. Antimony (III) adsorption from aqueous solutions using raw perlite and Mn-modified perlite: Equilibrium, thermodynamic, and kinetic studies. Industrial and Engineering Chemistry Research, 51, 6877-6886.

Shahwan, T., Erten, H.N., 2002. Thermodynamic parameters of Cs^+ sorption on natural clays. Journal of Radioanalytical and Nuclear Chemistry, 253, 115-120.

Shahwan, T., Erten, H.N., Unugur, S., 2006. A characterization study of some aspects of the adsorption of aqueous Co^{2+} on a natural bentonite clay. Journal of Colloid and Interface Science, 300, 447-452.

Shahwan, T., Suzer, S., Erten, H.N., 1998. Sorption of studies of Cs^+ and Ba^{2+} cations on magnesite. Applied Radiation Isotopes, 49, 915-921.

Silber,A., Bar-Yosef, B., Suryano, S., Levkovitch, I., 2012. Zinc adsorption by perlite: Effcts of pH, ionic strength, temperature, and pre-use as growth substrate. Geoderma, 170, 159-167.

Singh, S., Eapen, S., Thorat, V., Kaushik, C.P., Roj, K., D'Souza, S.F., 2008. Phytoremediation of ^{137}cesium and ^{90}ctrontium from solutions and low-level nuclear waste by *Vetiveria Zizanoides*. Ecotoxicology and Environmental Safety, 69, 306-311.

Snoeyink, V.L., Summers, R.L., 1999. Adsorption of Organic Compounds, Chapter 13. In Letterman, R.D., (Ed.) Water Quality and Treatment, AWWA, Fifth Ed., McGrow Hill, Inc., USA, 13.1-13.76.

Sposito, G., 2004. Surface Chemistry of Natural Particles, Oxford University Press, Inc., USA.

Suphandag, S.A., 2006. Evaluation of NOM-metal oxide adsorption system under influential structural concepts, Ph.D. Thesis, Bogazici University.

Tahir, S.S., Rauf, N., 2003. Thermodynamics studies of Ni(II) adsorption onto bentonite from aqueous solution. The Journal of Chemical Thermodynamics, 35, 2003-2009.

Talip, Z., Eral, M., Hiçsönmez, Ü., 2009. Adsorption of thorium from aqueous solutions by perlite. Journal of Environmental Radioactivity, 100, 139-143.

Tekin, N., Dincer, A., Demirtaş, Ö., Alkan, M., 2010. Adsorption of cationic polyacrylamide (C-PAM) on expanded perlite. Applied Clay Science, 50, 125-129.

Teppen, B.J., Miller, D.M., 2006. Hydration energy determines isovalent cation exchange selectivity by clay minerals. Soil Science Society of America, 70, 31-40.

Thanh, D.N., Singh, M., Ulbrich, P., Strnadova, N., Stepanek, F., 2011. Perlite incorporating γ-Fe_2O_3 and α-MnO_2 nanomaterials: Preparation and evaluation of a new adsorbent for As (V) removal. Seperation and Purification Technology, 82, 93-101.

Tsai, S., Ouyang, S., Hsu, C., 2001. Sorption and diffusion behavior of Cs and Sr on Jih-Hsing bentonite. Applied Radiation and Isotopes, 54, 209-215.

U.S. Environmental Protection Agency Radiation Protection Home Page, http://www.epa.gov/radiation/radionuclides/ (accessed July 2013).

Valsala, T.P., Joseph, A., Sonar, N.L., Sonavane, M.S., Shah, J.G., Raj, K., Venugopal, V., 2010. Separation of strontium from low level radioactive waste solutions using hydrous manganese dioxide composite materials. Journal of Nuclear Materials, 404, 138-143.

Vejsada, J., 2006. The uncertainties associated with the application of batch technique for distribution coefficient determination: A case study of cesium adsorption on four different bentonites. Applied radiation and Isotopes, 64, 1538-1548.

Vijayakumar, G., Tamilarasan, R., Dharmendirakumar, M., 2012. Adsorption, kinetic, equilibrium abd thermodynamic studies on the removal of basic dye Rhodamine-B from aqueous solution by the use of natural adsorbent perlite. Journal of Material and Environmental Science, 3, 157-170.

Wang, X., Xu, D., Chen, L., 2011. Sorption and complexation of Eu (III) on alumina: Effects of pH, ionic strength, humic acid and chelating resin on kinetic dissociation study. Applied Radiation and Isotopes, 64, 414-421.

Weng, L.P., Van Riemsdijk, W.H., Koopal, L.K., Hiemstra, T., 2006. Adsortion of humic substances on goethite: comparision between humic acid and fulvic acids. Environmental Science and Technology, 40, 7494-7500.

Xu, D., Tan, X.L., Chen, C.L., Wang, X.K., 2008. Adsorption of Pb (II) from aqueous solution to MX-80 bentonite: Effect of pH, ionic strength, foreign ions and temperature. Applied Clay Science, 41, 37-46.

Yıldız, B., 2007. Investigation of the adsorption kinetics of some radioisotopes on clay minerals in Turkey and evaluation of thermodynamic parameters of adsorption, Ph.D. Thesis, Hacettepe University.

Yu, S.M., Ren, A.P., Chen, C.L., Chen, Y.X., Wang, X., 2006. Effect of pH, ionic strength and fulvic acid on the sorption and desorption of cobalt to bentonite. Applied Radiation and Isotopes, 64, 455-461.

Yuzer, H., Kara, M., Sabah, E., Celik, M.S., 2008. Contribution of cobalt ion precipitation to adsorption in ion exchange dominant system. Journal of Hazardous Materials, 151, 33-37.

Zhang, H., Tong, Z., Wei, T., Tang, Y., 2012. Sorption characteristics of Pb(II) on alkaline Ca-bentonite. Applied Clay Science, 65, 21-23.